

# University of Naples Federico II



**DI**  
**C**  
**Ma**  
**PI**

Dipartimento  
di Ingegneria Chimica,  
dei Materiali e della  
Produzione Industriale  
Università degli Studi  
di Napoli Federico II

**Department of Chemical, Materials and Production  
Engineering (DICMaPI)**

**XXXIII Cycle - PhD Program**

**Industrial Product and Process Engineering**

***Structured Functionalized Active Carbon Sorbents  
for the Purification of Gas Streams***

**Tutor:**

**Prof. Domenico Caputo**

**Scientific Committee:**

**Dr. Luciana Lisi**

**Dr. Stefano Cimino**

**Candidate:**

**Elisabetta Maria Cepollaro**



## **Acknowledgments**

The last three years have been very intense, full of work and of new goals to achieve.

I would like to thank my tutor, prof. Domenico Caputo, for giving me the opportunity to continue my PhD after a not so easy start.

I am infinitely grateful to Dr. Luciana Lisi, who trusted me, even though she didn't know anything about me, and I didn't know which way to take and she has been my constant guide on this journey. Thank you for always being on my side and supporting me day by day. I will treasure all the advices, knowledge and skills.

Extremely grateful also to Dr. Stefano Cimino, always present in my activities. His charisma and his passion for research encouraged me to always go further and to do better and better.

Thanks to Dr. Nicola Gargiulo for his help in carrying out a part of my work.

## Abstract

Energy demand is constantly increasing as the world population and rapid industrial development grow fast. The main source of energy is represented by fossil fuels, responsible for greenhouse gas emissions into the atmosphere, global warming and climate change. In order to foster sustainable development, renewable sources are gaining great interest. However, the use of both fossil fuels and renewable sources requires purification processes of the gas streams from the energy production plants. Hydrogen sulphide ( $H_2S$ ), from natural gas processing, oil refining, biogas production and coal gasification, is a highly toxic compound for humans, it represents a poison for many catalysts and downstream fuel treatment devices and it is responsible for acid rains.

A valid solution in industrial practice for the abatement of this pollutant is represented by the adsorption technique which can be considered an economic process combined with versatility, simplicity and high efficiency. Among the various adsorbent materials, activated carbons are widely used to remove hydrogen sulphide, as they offer a high surface area, a high pore volume and a variety of organic groups on its surface. The addition of metal oxides dispersed on the activated carbons facilitates the removal of  $H_2S$  due to its high chemical affinity with metal cations.

The use of activated carbons in structured form such as monoliths or foams is required in practical application when high pressure drop must be avoided. Unfortunately, most of carbon materials are available as powders since activated carbon in structured form is difficult to obtain due to the poor adhesion properties that require the use of binders which, despite giving good mechanical properties, reduce the adsorption capacity of the activated carbon monolith compared to that of the starting carbon powder due to the partial blocking of porosity.

This thesis focus on structured activated carbon as sorbents for gas purification. In the first part of the work, the promoting effect of dispersed

metals on commercial activated carbon monoliths was studied in order to improve the absorption properties of this material which are lower than the granular activated carbon samples which do not contain a binder. The reactive adsorption of H<sub>2</sub>S on copper and/or magnesium oxides dispersed onto activated carbon monolith was investigated in the co-presence of O<sub>2</sub> and H<sub>2</sub>O in the gas stream at room temperature and in a lab-scale fixed-bed reactor. H<sub>2</sub>S capture rate and capacity of sorbents and the nature of sulphur species formed upon adsorption were analyzed using different techniques. Adsorption performance changes significantly depending on the metal although the adsorption is reactive in both cases. Two types of mechanisms were identified on the Cu-modified monolith: a faster mechanism associated to the formation of sulphates promoted by copper oxide and a slower mechanism involving the oxidation of H<sub>2</sub>S to elemental sulphur. Otherwise, a single adsorption mechanism is activated by magnesium, occurring through the dissociation of H<sub>2</sub>S into HS<sup>-</sup> and H<sup>+</sup> promoted by the basic character of MgO. Moreover, a slow transformation of elemental sulphur into additional sulphate species was identified in the presence of O<sub>2</sub> and water for saturated Cu-containing sorbents.

Thermal regeneration of the saturated AC monoliths was evaluated and it was found that for both copper and magnesium the porous structure of the AC monoliths was completely restored due to the decomposition of sulphate species at a lower temperature, especially for Cu-modified sorbents, and the evaporation of elemental sulphur at a higher temperature, prevailing for Mg-modified sorbents. No significant loss of capture capacity was detected for sorbents after the thermal treatment which can then be proposed as effective and regenerable materials for gas purification

In order to overcome concerns related to the addition of a binder, in the second part of the work, a new methodology was developed for the production of activated carbon as a three-dimensional microporous foam without any binder that does not involve the common complex multi-step procedure for obtaining foamy carbon with an open porosity including the template synthesis

using a replica technique.  $\text{ZnCl}_2$  or  $\text{CuCl}_2$  were used as Lewis acid activators for the polymerization of furfuryl alcohol, chosen as carbon precursor, directly providing a polymeric foam due to the rapid evaporation of water formed in the reaction. Various synthesis parameters as temperature of polymerization and the composition of pyrolysis gas were explored in order to produce activated carbons with different porosity and metal load. The temperature of polymerization was selected according to the Lewis acidity strength of the two metal chlorides: lower for  $\text{CuCl}_2$  and higher for  $\text{ZnCl}_2$ . The following pyrolysis of the polymer was investigated in the absence and in the presence of  $\text{O}_2$  traces at 600 or 850 °C in order to produce activated carbons with specific textural features and different metal content. Carbons with larger surface areas, also related to the presence of some mesopores, were obtained using  $\text{ZnCl}_2$  to activate the polymerization whereas  $\text{CuCl}_2$  promoted the formation of narrower micropores. Furthermore, copper was mostly preserved even at high pyrolysis temperature in contrast to zinc which was almost totally lost at 850 °C due to the much lower evaporation temperature with respect to metallic copper. The study provided a methodology to produce materials with different features for the adsorption of different molecules by suitably tuning the process parameters.

## Contents

<b>Introduction</b> .....	1
<i>List of figures</i> .....	5
<i>References</i> .....	6
<b>Chapter 1. An overview of gas purification methods: H<sub>2</sub>S adsorption on Activated Carbons</b> .....	8
<b>1.1. Gas purification techniques</b> .....	9
<b>1.2. Adsorption</b> .....	11
<b>1.2.1. Adsorption theory</b> .....	11
<b>1.2.2. Adsorption kinetics</b> .....	15
<b>1.2.3. Assessment of textural properties</b> .....	17
<b>1.2.4. Adsorbent materials</b> .....	21
<b>1.3. Activated Carbons (ACs)</b> .....	23
<b>1.3.1. Synthesis and main properties</b> .....	24
<b>1.3.2. Structured ACs</b> .....	26
<b>1.3.3. ACs Applications</b> .....	28
<b>1.4. H<sub>2</sub>S Adsorption</b> .....	30
<b>1.4.1. H<sub>2</sub>S properties</b> .....	30
<b>1.4.2. Adsorbents for H<sub>2</sub>S removal</b> .....	33
<i>List of figures</i> .....	40
<i>List of tables</i> .....	41
<i>References</i> .....	42
<b>Chapter 2. Mechanism of H<sub>2</sub>S adsorption on metal modified commercial activated carbon monoliths</b> .....	56
<b>2.1. Materials and Methods</b> .....	57
<b>2.1.1. Sorbent preparation</b> .....	57
<b>2.1.2. Sorbent characterization</b> .....	58
<b>2.1.3. H<sub>2</sub>S adsorption/desorption tests</b> .....	58
<b>2.2. Results and Discussion</b> .....	60
<b>2.2.1. Sorbent characterization</b> .....	60

2.2.2.	H <sub>2</sub> S adsorption tests .....	64
2.2.3.	Temperature Programmed Desorption tests .....	76
2.2.4.	Sorbent characterization after adsorption/desorption tests ..	83
2.2.5.	XPS analysis .....	86
2.2.6.	Sorbents regeneration .....	89
	<i>List of figures</i> .....	92
	<i>List of tables</i> .....	94
	<i>References</i> .....	95
<b>Chapter 3. Synthesis and Characterization of Activated Carbon Foam ....</b>		<b>96</b>
3.1.	Activated Carbon Foam .....	97
3.2.	ACs synthesis .....	102
3.3.	Sample Characterization .....	106
3.4.	Results and Discussion .....	107
	<i>List of figures</i> .....	123
	<i>List of tables</i> .....	125
	<i>References</i> .....	126
4.	<b>Conclusions</b> .....	<b>130</b>
	<b>Appendix</b> .....	<b>132</b>

## Introduction

Following the world population growth and the rapid industrial development, the demand for energy is ever increasing. It is estimated that the world population will reach around 9 billion by 2050 and according to the US Energy Information Administration (EIA), energy consumption will increase by almost 50%. Fossil fuels are the main source of energy but their negative impact on the environment is now well known: they are responsible for greenhouse gas emissions into the atmosphere, the cause of global warming and climate change. In order to limit the use of fossil fuels, also because of their high costs, and to facilitate sustainable development, many interests are towards the use of renewable sources. Currently, fossil fuels still remain the main source of energy, while renewables provide 14.5% of the world's energy supply (Halkos and Gkampoura, 2020).

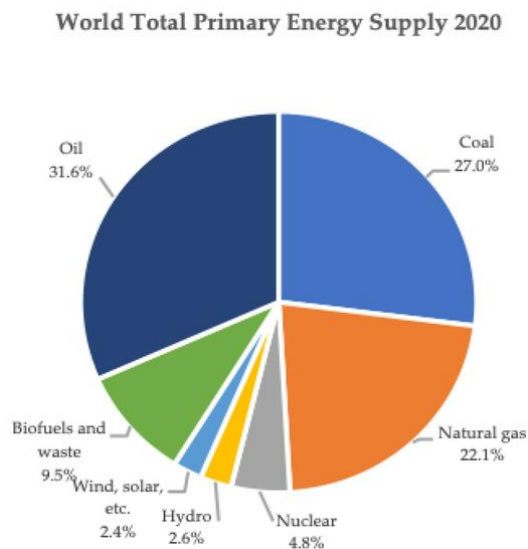


**Figure 1.** World Total Primary Energy Supply 2020 (Halkos and Gkampoura, 2020)

The use of fossil fuels (coal, oil, natural gas) or renewable sources (biogas, biomass, solid urban waste) involves purification processes of the streams outgoing from energy production plants. In a coal fired power plant energy is produced directly by burning coal whereas in the coal gasification process coal

is reacted with steam and O<sub>2</sub> or air. Finally, the so-called IGCC (Integrated gasification combined cycle) combines the coal gasification process with gas and steam turbine technologies to produce energy (Kapoor et al., 2020).

The outgoing streams contain traces of impurities, one of the most common from natural gas processing, oil refining, biogas production and coal gasification being hydrogen sulphide (H<sub>2</sub>S) which is a highly toxic compound for humans, it represents a poison for many catalysts and downstream fuel processing devices, and it is responsible for acid rain (oxidizing to SO<sub>2</sub>).

A widely used technology to remove hydrogen sulphide is the Claus process in which it is partially oxidized by oxygen in a furnace whilst the remaining hydrogen sulphide and sulphur dioxide are converted into elemental sulphur in catalytic reactors (Liu et al., 2020). Claus catalysts suffer from deactivation caused by condensation of sulphur, a key problem in many industrial processes as sulphur compounds lead to a significant loss of activity in a very short time (Liu et al., 2020; Ashrafi et al., 2008).

An alternative solution in the industrial practice is represented by the adsorption technique which can be considered an economical process coupled to versatility, simplicity and high process efficiency (Monteleone et al., 2011). Adsorbent materials generally used to remove hydrogen sulphide are zeolites, metal oxides, mesoporous silica, activated carbons (ACs). Activated Carbons are the most widely used materials as adsorbent because they offer a high surface area, high volume of pores and a variety of organic groups on its surface. ACs are cheap materials (10-20 €/kg) compared to other sorbents or inorganic catalysts (100-200 €/kg) (Monteleone et al., 2011). Physisorption of H<sub>2</sub>S on ACs generally takes place through dissociation into HS<sup>-</sup> and then, if oxygen is present, through oxidation to elemental sulphur. Sulphur is deposited in the micropores leading to the progressive deactivation of the activated carbons (Zhang et al., 2016).

The surface of the activated carbons can be suitably modified in order to increase the adsorption capacity.

The H<sub>2</sub>S removal capacity can increase if metal oxides are dispersed on the activated carbons, since hydrogen sulphide has a high chemical affinity with metal cations. Nevertheless, the use of bulk metal oxides as absorbents can negatively influence the capture process as they tend to evaporate or can lead to a loss of surface area and porosity in addition to mechanical sintering and disintegration (Montes et al., 2013). The metals introduced on the surface of sorbent can increase the life and performance of the adsorbent. Therefore, the dispersion of metal oxides on porous materials with a high surface area, as activated carbon, improves H<sub>2</sub>S removal process.

The use of activated carbons in structured form such as monoliths or foams is required in practical application when high pressure drop must be avoided. Nevertheless, most of carbon materials are obtained as powders and that limits their applicability when macroscopic morphologies are required (Taguchi et al., 2003).

However, activated carbon in a structured form is difficult to obtain as it requires the use of binders which, despite offering good mechanical properties, reduce the adsorption capacity of the AC monolith compared to that of the starting carbon material due to the partial blockage of porosity (Lozano-Castelló et al., 2002). The non-accessibility to the pores depends on the type of binder. There are commercially available activated carbon monoliths consisting of a carbon layer on a ceramic substrate with limited adhesion and a load of about 50%.

This PhD Thesis focused on the study of activated carbons in a structured form to be used as sorbents for the adsorption of H<sub>2</sub>S from natural and bio gas. The work can be divided into two main research activities.

The first part of the work is devoted to the modification of commercial activated carbon monoliths with two different metals in order to improve the H<sub>2</sub>S capture properties of carbon which were reduced by the addition of a binder. This study focused on the mechanism of H<sub>2</sub>S adsorption promoted by

the two different metal oxides (copper and magnesium oxides) and on the possible regeneration strategy to restore the original capture properties.

The second part is devoted to the development of a preparation method for activated carbons as foamy structure without using a binder starting from the polymerization of a carbonaceous precursor (polyfurfuryl alcohol) activated by  $\text{ZnCl}_2$  or  $\text{CuCl}_2$ . This was based on the idea to use as activator of the polymerization the same two active metals promoting  $\text{H}_2\text{S}$  adsorption. The research activity focused on the production of these structured carbonaceous materials avoiding the complex multi-step expensive procedures currently proposed to produce these scaffolds.

The first chapter of this thesis offers an overview of gas separation/purification methods, with particular attention to the adsorption techniques widely used for the removal of pollutants focusing on ACs and on the need to produce highly efficient structured sorbents.

The second chapter reports the characterization and adsorption tests of  $\text{H}_2\text{S}$  on commercial Activated Carbons in a structured form funzionalized by metal oxides while, in the third chapter, the innovative method of production of activated carbons as foams and their characterization has been discussed.

All tests were conducted at the Department of Chemical, Materials and Industrial Production Engineering of University of Naples Federico II (DICMAPI) and at Combustion Research Institute of the Italian National Research Council of Naples (STEMS-CNR). This work has been supervised by Dr. Luciana Lisi (STEMS-CNR), Dr. Stefano Cimino (STEMS -CNR) and Prof. Domenico Caputo (DICMAPI).

*List of figures*

**Figure 1.** World Total Primary Energy Supply 2020 (Halkos and Gkampoura, 2020) ..... 1

## References

- Ashrafi, M., Pfeifer, C., Pröll, T., Hofbauer, H. (2008). Experimental study of model biogas catalytic steam reforming: 2. Impact of sulphur on the deactivation and regeneration of Ni-based catalysts. *Energy fuels*, 22(6), 4190-4195. 4
- Halkos, G. E., Gkampoura, E. C. (2020). Reviewing Usage, Potentials, and Limitations of Renewable Energy Sources. *Energies*, 13(11), 2906. 1
- Kapoor, R., Ghosh, P., Tyagi, B., Vijay, V. K., Vijay, V., Thakur, I. S., Kamyab, H., Nguyen, D. D., Kumar, A. (2020). Advances in biogas valorization and utilization systems: A comprehensive review. *Journal of Cleaner Production*, 273, 123052. 2
- Liu, X., Zhang, Q., Ye, G., Li, J., Li, P., Zhou, X., Keil, F. J. (2020). Deactivation and regeneration of Claus catalyst particles unraveled by pore network model. *Chemical Engineering Science*, 211, 115305. 3
- Lozano-Castelló, D., Cazorla-Amorós, D., Linares-Solano, A., Quinn, D. F. (2002). Activated carbon monoliths for methane storage: influence of binder. *Carbon*, 40(15), 2817-2825. 7
- Monteleone, G., De Francesco, M., Galli, S., Marchetti, M., Naticchioni, V. (2011). Deep H<sub>2</sub>S removal from biogas for molten carbonate fuel cell (MCFC) systems. *Chemical Engineering Journal*, 173(2), 407-414. 5
- Montes, D., Tocuyo, E., González, E., Rodríguez, D., Solano, R., Atencio, R., Ramos, M. A., Moronta, A. (2013). Reactive H<sub>2</sub>S chemisorption on mesoporous silica molecular sieve-supported CuO or ZnO. *Microporous and mesoporous materials*, 168, 111-120.
- Taguchi, A., Smått, J. H., Lindén, M. (2003). Carbon monoliths possessing a hierarchical, fully interconnected porosity. *Advanced Materials*, 15(14), 1209-1211. 6

Zhang, Z., Wang, J., Li, W., Wang, M., Qiao, W., Long, D., Ling, L. (2016).  
Millimeter-sized mesoporous carbon spheres for highly efficient catalytic  
oxidation of hydrogen sulphide at room temperature. *Carbon*, 96, 608-  
615.

**Chapter 1. An overview of gas purification methods: H<sub>2</sub>S adsorption on Activated Carbons**

## 1.1. Gas purification techniques

The purification of gaseous streams leaving energy production plants, lowering the level of pollutants, is a key step for the sustainability, for the protection of the environment and to avoid damage to pipelines and corrosion of the equipment in industrial processes. The main processes used for the removal of pollutants are:

- **Gas-liquid Absorption.** One of the most important unit processes in gas purification is *absorption* which involves contact between a gas and a liquid phase. The choice of the liquid is based on the solubility of the gas to be treated in it, selectivity, volatility, high chemical stability, low cost. In industrial practice, the process takes place in an absorption column (tower) in which the two phases go countercurrent so the liquid flows down and the gas proceeds upward. The absorption process can be physical or chemical depending on whether or not chemical reactions take place between the gas to be treated and the solvent chosen. The adsorption reverse process used to recover the gas or the solvent or both is called *stripping*.
- **Gas-solid Adsorption.** The feed gas stream is brought into contact with the surface of a solid adsorbent. This process will be described more in details in Section 1.2.
- **Cryogenic Separation.** It is a low temperature distillation process that takes place at a temperature below the freezing point of gas streams. This technique is used industrially for air distillation, for the separation of commercial helium, for hydrogen recovery and for CO<sub>2</sub> capture from gas streams (Shimekit and Mukhtar, 2012). This method is the most used for the extraction of lighter liquids. Since the gas mixture is compressed and cooled a great deal of energy is required to bring the flow to sub-zero temperatures (Abu-Zahra et

al., 2016). The choice of this technique involves high economic costs.

- **Permeation through a membrane.** The membranes used for gas separation are thin films that are able to selectively transport the gases due to the difference in the permeability of the species through the membrane itself. The process is therefore influenced by the physical and chemical structure of the membrane and by the type of species that must pass through it. The key parameters of the process are therefore permeability which indicates the ability of the species to pass through the membrane, solubility which indicates the quantity of species retained by the membrane and diffusion as index of the speed to go through. The membranes used can be polymeric, glassy and rubbery, inorganic or with a mixed structure.

Absorption is essentially used for the removal of CO<sub>2</sub> and H<sub>2</sub>S, but it is not always the most appropriate choice. Physical solvents are preferred over chemical ones which cause damage to the plants, but the operating pressures required for physical solvents and consequently operating costs are too high. Cryogenic separation allows to obtain a higher degree of purity of the products, but a high energy is required for the regeneration and there is a need for special materials suitable for such low temperatures which involves too high prices.

This method is more suitable for CO<sub>2</sub> removal/separation (Ahmad et al., 2019). Membrane technology is a high purity and environmentally friendly process. However, it is widely used for the removal of CO<sub>2</sub> from biogas and the cost of this process is higher when CO<sub>2</sub> and H<sub>2</sub>S are removed together. In conclusion, adsorption appears to be the most effective technique among gas separation methods and is the widely used for the removal of hydrogen sulphide as it is a simple and highly efficient process coupled to low costs.

Adsorption of gaseous molecules is particularly important for activated carbons, both for their role as purification sorbents and because physisorption

represents the main characterization technique of highly porous materials. For this reason, a short overview of adsorption theory is reported below.

## **1.2. Adsorption**

The term *adsorption* includes the uptake of gaseous or liquid component of mixtures by the external and/or internal surface of porous solids. In chemical engineering, adsorption is the separation process of components of a fluid phase that are transferred onto the surface of a solid adsorbent (McCabe, 1993). The term *sorption* is used to describe every type of capture of a substance by the external surface of solids or liquids as well as by the internal surface of porous solids or liquids (Skoulikides, 1989). In this process only the surface of the adsorbent is involved; if the adsorptive enter the structure of bulk solid *absorption* occurs. The reverse process is called *desorption* (Inglezakis and Pouloupoulos, 2006).

### **1.2.1. Adsorption theory**

Adsorption is an enrichment of one or more components that takes place in an interfacial layer and therefore, as already mentioned, only the adsorbent surface is involved. The solid is called *adsorbent* and the gas, which can be adsorbed, is called *adsorptive*. *Adsorbate* is the fluid adsorbed (Thommes et al., 2015). *Desorption* is the opposite process in which the adsorbate molecules leave the adsorbent surface. When the adsorption and desorption curves do not coincide hysteresis loop takes place.

Depending on the type of bonds and interactions two kinds of adsorption can be distinguished: physical adsorption (or physisorption) and chemical adsorption (or chemisorption). In physisorption the adsorbate is bound to the adsorbent with Van der Waals interactions, weak electrostatic forces in which no electron exchange occurs. In this case the adsorbate molecules can be

trapped on the surface as they impact it with low energy. If the molecules hit the surface with higher energy, this cannot be dissipated by the adsorbent and therefore they bounce. The variation of enthalpy is typically less than  $20 \text{ kJ mol}^{-1}$  so that the physical bonds can easily break, and desorption can take place. The physisorption process can be multilayered; even if already covered with other molecules, the adsorbate can adhere to the surface of the adsorbent. The adsorption strength decreases as the number of adsorbate layers already attached to the surface increases (Inglezakis and Pouloupoulos, 2006; Artioli, 2008). On the other hand, chemical adsorption (or chemisorption) involves an exchange of electrons since the interactions are stronger and more stable at high temperatures because the adsorbate forms covalent chemical bonds. Generally, only a single molecular layer can be adsorbed in this process (Inglezakis and Pouloupoulos, 2006).

The amount adsorbed on a solid surface depends upon the absolute temperature  $T$ , the pressure  $P$  and the interaction potential between the adsorbate (vapor) and adsorbent (surface)  $E$ . Since adsorption is a surface process, the adsorbent with a larger surface has a greater ability to adsorb substances. Therefore, the best adsorbents are porous substances, or more generally those with the largest surface per unit of volume. Porosity is defined as the ratio of the total pore volume to the volume of the particle or agglomerate. According to size, pores can be classified into:

- micropores with widths not exceeding about  $20 \text{ \AA}$
- mesopores with a width between  $20 \text{ \AA}$  and  $500 \text{ \AA}$
- macropores with widths greater than about  $500 \text{ \AA}$

A further distinction is that between narrow micropores (also called ultra-micropores) of approximate width  $<7 \text{ \AA}$  and wide micropores (also called super-micropores) (Thommes, 2010).

The surface of porous adsorbents can be divided into an outer and an inner surface. In general, the external surface is that outside the pores, while the

internal surface is relative to all the walls of the pores; in the presence of micropores, the external surface is defined as a non-microporous surface.

The study of adsorption processes is carried out through the adsorption isotherm, experimental curves obtained by the relationship between the concentration of the adsorbate in the fluid phase and the concentration of the adsorbate in the adsorbent particles at a given temperature and under equilibrium conditions. Some types of isotherms are shown in Figure 1.1. The linear isotherm starts from the origin and adsorbs a quantity proportional to the concentration in the fluid. Convex isotherms are favourable as there is a high loading of particles captured by the adsorbent at low concentration in the fluid phase. The limiting case of the favourable isotherm is given by the irreversible adsorption which presents a constant amount of material captured whatever the concentration of the fluid phase. Finally, the unfavourable isotherm is the concave one as despite the high concentrations in the fluid phase, low solid loadings are obtained (McCabe, 1993).

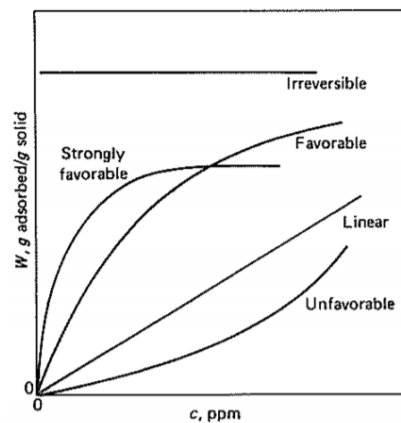
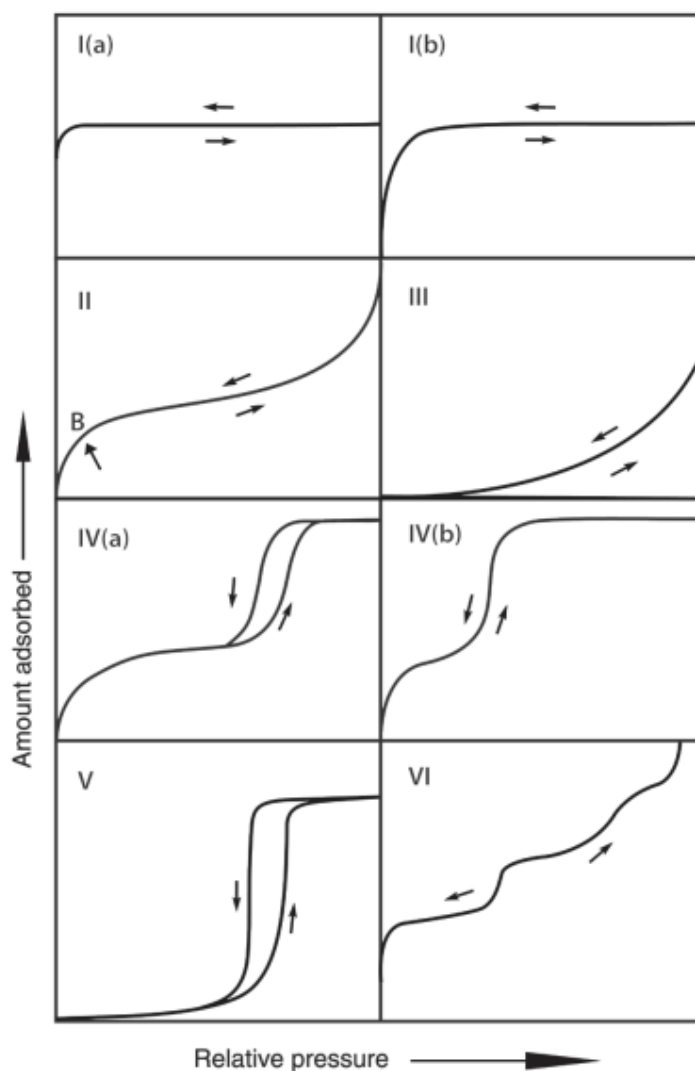


Figure 1. 1 Adsorption isotherms (McCabe, 1993)

Figure 1.2 shows another type of classification of the physisorption isotherms grouped into six types according to the IUPAC classification:



**Figure 1. 2** IUPAC classification of physisorption isotherms (Thommes et al., 2015)

Microporous solids with relatively small outer surfaces have a type I isotherm. By adsorption of nitrogen and argon at 77 K and 87 K, the Type I (a) isotherms are those of microporous materials with narrow micropores ( $< \sim 10 \text{ \AA}$  width) while those of type I (b) are related to materials having wider micropores and narrow mesopores ( $< \sim 25 \text{ \AA}$ ). Type II isotherms are typical of non-porous solids or macroporous adsorbents. In the case of a type III isotherm the adsorbent-adsorbate interactions are now relatively weak and the adsorbed molecules are clustered around the most favorable sites on the surface of a non-

porous or macroporous solid. Mesoporous adsorbents exhibit type IV isotherms with a trailing plateau characteristic of saturation. In the case of a type IVa isotherm, capillary condensation, in which a gas condenses into a liquid phase in a pore, is accompanied by hysteresis. When the mesopores are smaller in width, fully reversible type IVb isotherms are observed. Type V isotherms are attributed to relatively weak adsorbent-adsorbent interactions. Type VI reversible isotherm is representative of layer-by-layer adsorption on a uniform non-porous surface (Thommes et al., 2015).

### 1.2.2. Adsorption kinetics

The complex phenomena occurring during an adsorption process can be described as follows:

- *external transport*: through the outermost layer (film) and directly in contact with the solid particle;
- *internal diffusion*: transport within the adsorbent pores until the active site is reached
- *adsorption*: bonds formation between the adsorbent and the adsorbate.

The two opposing resistances to the motion of the adsorbate are due to molecular diffusion (which depends on the diffusivity and thickness of the film) and the movement in the pores of the solid as the molecules must pass through tortuous pores in order to reach all available sites.

In order to study the kinetics of the adsorption phenomena and the influence of the characteristic parameters of the process, a pilot scale process, for example a fixed bed column, is used. A breakthrough curve from the experiment is obtained as reported in Figure 1.3:

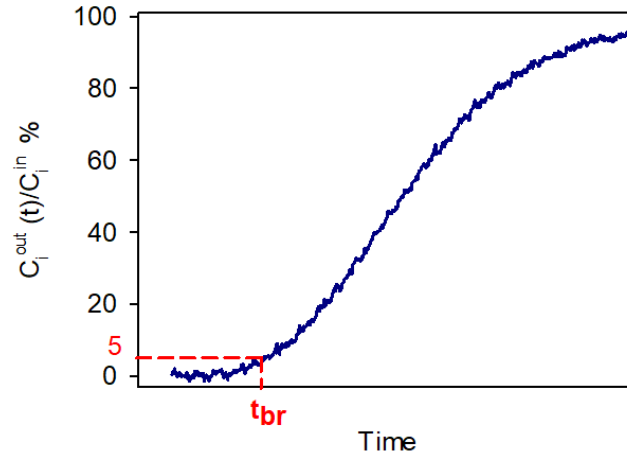


**Figure 1. 3** Breakthrough curve in a fixed bed reactor

A breakthrough curve has a sigmoidal shape and represents the concentration of the pollutant in the gas stream leaving the column as a function of time. At the beginning the pollutant is completely adsorbed, then its output concentration increases up to the initial level when the solid is completely saturated. The value of the time corresponding to the pollutant concentration in the outgoing gas approximately equal to 5% of the initial value is called the breakthrough time ( $t_{br}$ ).

The area above the breakthrough curve is proportional to the total quantity of pollutant captured by the adsorbent; in fact, the adsorption capacity of solids is evaluated by a mass balance on species  $i$  (pollutants) above the column. The solid total adsorption capacity is evaluated as follow:

$$\omega_{ads} = \frac{Q^t C_i^{in} \rho_i}{m M_i} \int_0^{t^*} \left(1 - \frac{C_i^{out}(t)}{C_i^{in}}\right) dt \quad (1.1)$$

where  $Q^t$  [ $L s^{-1}$ ] is the total gas flow rate,  $C_i^{in}$  [-] is the pollutant volumetric fraction in the gas feed,  $C_i^{out}$  [-] is the pollutant volumetric fraction at the bed outlet;  $\rho_i$  is pollutant density and  $M_i$  [ $g mol^{-1}$ ] its molecular weight;  $m$  [g] is the sorbent dose and  $t^*$ [s] represents the time required to reach 99% recovery of the initial inlet concentration of pollutant.

### 1.2.3. Assessment of textural properties

The most suitable process used for the determination of surface area is physical adsorption. Gas adsorption is a well-established tool for the characterization of porous materials.

The accessibility of the pores depends on the size and shape of the probe molecules. Nitrogen adsorption at 77 K is typically used for micro- and mesopore size analyzes. In the presence of micropores extremely low values ( $\sim 10^{-7}$ ) of relative pressures must be explored for the corresponding analysis. Unfortunately, the diffusion rate is slow in this pressure range. Furthermore, sometimes in the case of narrow micropores, the  $N_2$  molecule is trapped inside the micropores and the measurement of the adsorption isotherm is not accurate. Argon at 87 K fills the narrow micropores at higher pressures than nitrogen at 77 K but kinetic restrictions at cryogenic temperatures for the characterization of very narrow micropores are not overcome. This problem is solved by using  $CO_2$  as adsorbent at 273 K. At 273 K, the saturation vapor pressure of  $CO_2$  is very high ( $\sim 3.5$  MPa) and therefore the pressures required for micropores size analysis are in a moderate relative pressure range ( $\sim 0.1$  to 100 kPa). Diffusion is faster and pores as small as 4 Å can be accessed. However,  $CO_2$  cannot be used in the presence of microporous solids with polar surface groups (e.g. oxides, zeolites, MOFs) since the quadrupole moment of  $CO_2$  is also greater than that of  $N_2$  making it difficult to correlate pressure with size of pores (Thommes et al., 2015).

Many mathematical models have been developed based on the interpretation of adsorption isotherms to describe the mechanism involved during the process. The first successful model is Langmuir isotherm described by the following equation:

$$\omega_{eq} = \frac{\omega_{max} K_L P_{eq}}{1 + K_L P_{eq}} \quad (1.2)$$

where  $\omega_{eq}$  [mmol g<sup>-1</sup>] and  $P_{eq}$  [bar] are the adsorbent specific molar adsorption capacity and the equilibrium gas partial pressure of the adsorbate, respectively;  $K_L$  [bar<sup>-1</sup>] and  $\omega_{max}$  [mmol g<sup>-1</sup>] are the Langmuir equilibrium constant and the maximum adsorption capacity of the adsorbed species, respectively. This formulation is based on four hypotheses:

- (i) the adsorbate cannot attach indifferently to the surface but only to particular sites where a bond with the adsorbate occurs;
- (ii) adsorption occurs only in a monolayer and only one molecule can adsorb on a site;
- (iii) no adsorbate-adsorbate interaction occurs as molecules adsorbed do not interact with the other molecules of adsorbate;
- (iv) all sites are energetically equivalent.

The single-layer adsorption hypothesis is one of the more restrictive hypotheses as adsorption frequently occurs in multilayer, however this model provides an accurate description of the phenomenon when the amount adsorbed is low and there is no interaction with the solvent. the saturation is reached quite fast.

Another widely used model is the Freundlich isotherm which does not have as many limitations as the Langmuir theory. Freundlich method is not empirical but theoretically based as the Langmuir model. The equation that describes this model, reported below, does not even show an asymptote as the adsorbent would never saturate and would bind continuously to the adsorbate. This assumption does not make sense, so this model is not used when the concentration of the adsorbate is high.

$$\omega_{eq} = K_F P_{eq}^{\frac{1}{n}} \quad (1.3)$$

In which  $K_F$  [mmol g<sup>-1</sup> bar<sup>-1/n</sup>] and  $1/n$  [-] are the Freundlich constant and the heterogeneity parameter. Furthermore, according to this model, the energy

required for adsorption is not constant but exponential. The strength of the bonds is not the same as the greater the number of molecules bonded to a site, the less likely it is that another molecule will bond to that same site since (exponentially) greater energy is required (Artioli, 2008).

A new model to improve Langmuir's theory was proposed by Brunauer, Emmett and Teller (1938). The main hypothesis of this model is that multilayer adsorption, i.e. another layer can adsorb on the first adsorbate layer, and this adsorption is regulated by a Langmuir equation. The BET equation is usually expressed in linear form:

$$\frac{p/p_0}{n(1-p/p_0)} = \frac{1}{n_m c} + \frac{(c-1)}{n_m c} (p/p_0) \quad (1.4)$$

where  $p_0$  is the saturation vapor pressure,  $n$  is the molar amount adsorbed at pressure  $p$ ,  $n_m$  is the molar amount of adsorbate required for complete monolayer coverage and the parameter  $c$  is exponentially related to the energy of monolayer adsorption and gives indication of the shape of the isotherm. This method works well for mesopores but given the difficulty of finding a linear range of the BET plot, for micropores the procedure is based on the following criteria:

- (i) the quantity  $c$  should be positive;
- (ii) application of the BET equation should be restricted to the range where the term  $n(1-p/p_0)$  continuously increases with  $p/p_0$
- (iii) the  $p/p_0$  value corresponding to  $n_m$  should be within the selected BET range.

The BET method is the most widely used for estimating the surface area of porous sorbents.

In order to estimate the volume of micropores, several methods and approaches have been proposed. The micropore volume is often evaluated by macroscopic procedures as in the *t-plot method* using a standard multilayer

thickness curve (Thommes et al., 2015). This method was proposed by Lippens and de Boer and consists of a comparison of the isotherm with a reference curve obtained from data on several non-porous adsorbents with C constants (from BET method) similar to the microporous sample under test (Eddaoudi, 2005). As mentioned above BET method may not be applicable for micropores. An alternative is the  $\alpha_s$  method developed by Gregg and Sing which does not consider the capacity of the monolayer and therefore allows a more direct comparison between the test isotherm and the reference isotherm. Another popular method for evaluating the volume of micropores is based on the Dubinin-Radushkevich (DR) theory which predicts that the micropores are filled with a homogeneous liquid phase that has properties similar to bulk (Thommes, 2010). The limitation of these methods consists of not considering the effect of the size and shape of the micropores in the molecular packing and it is uncorrected to affirm that the adsorbate has always the same properties of the liquid bulk.

Microporous procedures, such as the density functional theory (DFT) and Monte Carlo simulation (MC), are considered superior and more reliable for pore size analysis and microporous treatments. These procedures describe the distribution of the adsorbed molecules in the pores at the molecular level and thus it is possible to trace detailed information on the structure of the fluid near the adsorbing surface. The fluid-solid interaction potential depends on the pore model. Various models have been developed for the different types of materials according to the possible shapes of the pores. In particular, the Non-local-density functional theory (NLDFT) assumes a smooth and homogeneous carbon surface while the Quenched solid density functional theory (QSDFT) model is another approach that takes into account the surface heterogeneity by significantly improving the reliability of the pore size analysis of heterogeneous nanoporous carbons (Thommes et al., 2015). Another great advantage of DFT methods and molecular simulation is that it is possible to obtain an accurate

analysis of the pore size in the entire range of micro/mesopore sizes (Thommes, 2010).

#### 1.2.4. Adsorbent materials

In order to achieve an efficient adsorption process, it is important to choose an appropriate solid adsorbent, whose properties should be compatible with the specific compound to be removed. The adsorbents can be functionalized through the introduction of active phases with a greater affinity towards the chemical substance to be removed in order to improve the adsorption capacity.

The requirements that the adsorbents must have are high absorption capacity, good performance (also after regeneration cycles) and abatement of polluting compounds at low levels coupled to high thermal stability, good mechanical strength, high selectivity, low cost of synthesis. Materials generally used as adsorbents are listed below:

- *Alumina* ( $\text{Al}_2\text{O}_3$ ): one of the most important ceramic materials. It can assume different crystalline forms but the only thermally stable oxide is  $\alpha$ -alumina which has a “corundum” structure. It is characterized by a low vapor pressure and a high melting point ( $2045^\circ\text{C}$ ). Alumina possesses high electrical resistance and great hardness and abrasion resistance. These excellent strength properties are strongly influenced by the microstructure. Finally, alumina is inert against chemical attack and withstands harsh environments. Alumina maintains these characteristics up to  $1500^\circ\text{C}$  (Dias Filho et al., 2006). The disadvantage of using alumina is that it cannot compete in terms of capacity or selectivity with other sorbents such as molecular sieves.
- *Zeolites*: aluminosilicate materials with a crystalline structure composed of tetrahedral units  $[\text{SiO}_4]$  and  $[\text{AlO}_4]$  which are arranged in porous 3D networks forming non-linear bonds with oxygen (Mohan et al., 2020). Zeolites have a regular and interconnected porosity. Zeolites are

classified according to the size of the pores. The zeolites used to capture the molecules are known as highly porous molecular sieves with reticular structures composed of silica and alumina tetrahedra arranged in various ways. The resulting cage structure allows access only to smaller molecules of a certain size (Sinnott, 2005). Zeolites usually require prior activation and packaging steps which make the preparation process longer and more expensive.

- *Mesoporous silica:* Ordered mesoporous silicas (e.g., SBA-15, TUD-1, MCM-41, FSM-16) are a class of silica materials characterized by various cage structures (hexagonal, cubic and lamellar). Ordered mesoporous silica has a high specific surface area, large pore size, chemical inertness, surface functional groups selective towards specific pollutants, good thermal stability and low production cost (Montes et al., 2013; Elyassi et al., 2014).
- *Activated Carbon:* high surface area with the presence microporosity allows Activated Carbon to be widely used as adsorbents. Furthermore, their peculiarity is due to the presence of various types of functional oxygen groups on the surface. The adsorption on Activated Carbon can be weak physical or chemical and therefore is more suitable for the removal of H<sub>2</sub>S at low temperatures (Watanabe, 2020). Activated Carbon has a typical surface area of 500-2000 m<sup>2</sup>/g. The advantage in using ACs as adsorbents is their easy regeneration which requires low energy, the availability of raw materials and high thermal stability.
- *Metal Oxides:* they are considered as good adsorbents due to their high presence in nature and low costs. They are widely used for desulphurization as they react with hydrogen sulphide forming the corresponding metal sulphides according to the reaction  $\text{H}_2\text{S} + \text{MeO} \rightarrow \text{MeS} + \text{H}_2\text{O}$  which is thermodynamically favored already at low temperatures. The problem is that their use is generally limited to T>

250°, due to kinetic limitations, which can lead to rather low utilization factors (Balsamo et al., 2016). These adsorbents are often found in the form of mixed oxide but it is generally preferred to support them on porous materials expanding their application in a greater operating range (Polychronopoulou et al., 2005; Jiang et al., 2010; de Falco et al., 2018).

On the basis of these information, activated carbons have been selected as sorbents for hydrogen sulphide in this thesis thanks to their high stability and low cost of raw materials and also to the possibility to be suitably funzionalized by metal oxides, thus combining specific properties of two classes of compounds.

The study will focus on activated carbon based structured sorbents which, as better explained in the following, represent a critical issue for this kind of material due to the poor adhesion properties.

Synthesis and main properties of activated carbons are discussed below.

### **1.3. Activated Carbons (ACs)**

Activated Carbons are described by Ruthven (1984) as the product of the thermal decomposition of the carbonaceous material followed by activation with carbon dioxide or steam which gives porosity to the structure. Fitzer et al. (1995) defined ACs as porous materials whose adsorbent properties are enhanced by introducing chemicals compounds during or after the carbonization process.

Activated Carbons, a class of microporous carbons, are widely used for their high adsorption capacity linked to high internal surface with pores of sizes and shapes that make them selective. In addition to microporosity, the chemical surface composition of ACs plays an important role in the adsorption process (Rodríguez-Reinoso and Molina-Sabio, 1998). The main characteristics of Activated Carbons are described in detail below.

### 1.3.1. Synthesis and main properties

Carbonaceous materials derive from the carbonization of organic compounds and they are commonly used to remove organic and inorganic pollutants from water and wastewater and for air purification processes. Heat treatment in an inert atmosphere leads to an increase in the carbon content corresponding to the disappearance of heteroatoms (hydrogen, oxygen, nitrogen) and small molecules (the volatiles) as water, methanol and carbon dioxide. Generally, a solid-phase carbonization process starts from an organic macro-system (coals, woods, nutshells, etc.), present in nature or synthetic, which progressively decomposes as the temperature increases up to 800°C (Iwanow et al., 2020; Ogungbenro et al., 2020; Guclu et al., 2021). In the first phase of carbonization, the so-called pyrolysis up to 600°C, the starting material loses the volatile molecules such as water and carbon dioxide and aliphatic acids, carbonyls, alcohols, etc. During the second carbonization phase above 600°C a great change in the polymer network occurs (Rodríguez-Reinoso and Molina-Sabio, 1998).

The carbonaceous structure derives from the movement of the carbon atoms that, resisting high temperature, move slightly in the network to reach positions of greater stability (six-membered ring systems) and minimum energy. Free spaces left by carbon atoms during their motion create the porosity of carbonaceous materials characterized by a large pore size distribution.

Consequently, closed porosity can be defined as porosity which is not accessible to a given adsorbate. If the carbonization process is carried out at temperatures above 800°C, the porosity can disappear due to the crosslinking of the carbon atoms that occupy the vacancies of the structure. The properties as adsorbents are influenced by the heterogeneous structure of ACs not containing only carbon atoms. The presence of oxygen surface groups most influences the characteristics of ACs surface and the consequent adsorption performance since

the surface oxygen groups allow a greater interaction with the adsorbate. Hydrogen is bonded to the edge atoms, but oxygen, nitrogen and sulphur can be bonded both to the edges and inside the graphene layers. However, the greatest influence on the structure, that allows a wide range of industrial application, is given by the presence of oxygen on the surface of ACs. Due to the electronegativity of the oxygenated groups, the adsorbing properties of ACs change. Oxygen is always present on the surface as exposure to air produces these surface oxygen complexes.

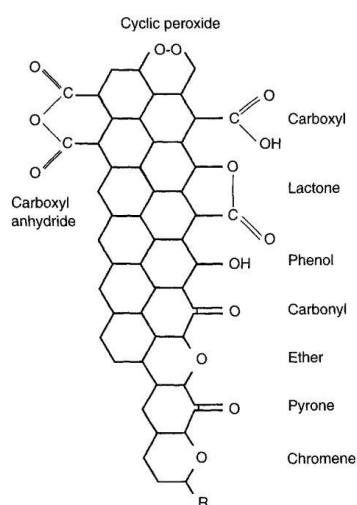


**Figure 1. 4** Oxygen functional groups on carbon surfaces (Rodríguez-Reinoso & Molina-Sabio, 1998)

The carbonization process does not allow the ACs to obtain a very high volume of micropores or surface area which affect the adsorption capacity since the microporosity obtained with carbonization can be blocked, even only partially, by the decomposition products. A coal gasification process is therefore necessary, generally by reaction with steam, carbon dioxide or oxygen, at a temperature above 800°C, which penetrate inside the pores to partially remove carbon atoms. Therefore, industrial processes known as thermal or physical activation and chemical activation are required in order to modify the carbonaceous structure (Iwanow et al., 2020). Physical activation

involves the single or combined use of carbon dioxide and water vapor that extract carbon atoms from the porous structure and cause the formation of chemisorbed oxygen which results in oxygen complexes whose chemistry is a function of temperature.

The chemisorption of oxygen and hydrogen on the surfaces influences the selectivity of the carbon atoms determining the development of porosity during the gasification. Three mechanisms, the opening of pores previously inaccessible, the creation of new pores and enlargement of those already existing, fundamentally take place during gasification. As industrial applications have become more specific, a greater control of the micro- and meso- porosity of the adsorbent is required. Thermal activation does not have much influence on the pore size distribution (Gonzalez et al., 1997), therefore the alternative use of chemical compounds is required in order to have greater control over the development of porosity. Chemical activation involves the addition of compounds such as zinc chloride, magnesium chloride, phosphoric acid, potassium hydroxide, aluminium chloride, sodium hydroxide (Bedia et al., 2020). The degradation of lignocellulose materials essentially occurs between 200-350°C; in this temperature range H<sub>2</sub>O, CO, CO<sub>2</sub>, CH<sub>4</sub> leave the structure. The heavier hydrocarbons evaporate between 350 and 500°C. Above 500°C, only a small weight loss of the structure occurs, indicating that the basic char structure has already been formed. Generally, chemical activation occurs at T = 400-800 °C so that in a single step carbonization and activation take place simultaneously. Chemical Activated Carbon has a surface area of up to 3000 m<sup>2</sup>/g (Abd et al., 2020).

### **1.3.2. Structured ACs**

Most of carbon materials are obtained as powders but in practical applications, Activated Carbons does not have high mechanical properties such as resistance to abrasion or to rapid changes in temperature or pressure (Chen et al., 2020). As the adsorption capacity increases with the microporosity, an

important requirement of the ACs is the packing density in order to minimize the free space which cannot be used for the removal of the pollutants but has still an impact on the micropore volume (Lozano-Castelló et al., 2002). In an adsorption system the total volume is given by the contribution of the free space between the pieces of carbon, by the volume of the macropores and finally by the micropores in which the adsorption takes place. The production of carbon monoliths represents the solution to problems above reported (Quinn and MacDonald, 1992).

Activated Carbons in a structured form is difficult to obtain for the poor cohesion of carbon powder particles. Monoliths can be produced by introducing a binder into the structure to hold the carbon particles together. Generally, the preparation of the monoliths involves mixing the Activated Carbons with a binder using a lower binder/Activated Carbon ratio in order to obtain the maximum amount of Activated Carbon, compression, molding and finally pyrolysis to reduce the weight of the binder in the structure by not blocking the pores of adsorbent. The aim is to increase packing density maintaining a high volume of micropores. The problem is that the introduction of the binders reduces the adsorption performance of the Activated Carbons since they block the microporosity. Generally, the products of the thermochemical processing of coal, lignite and petroleum (tar, pitch, asphalt) and the by-products of the wood and food industry are used as binders (Skoczko and Guminski, 2020; Saeidi and Lotfollahi, 2015). Among the chemicals, however, there are a mixture of hydroxypropyl methylcellulose and ammonium nitrate (Briens and Bowden-Green, 2020), copolymers of ethyl acrylate and xanthan gum (Pandey and Mishra, 2012), adhesive based on cellulose (Lozano-Castelló et al., 2002), lignocelluloses (Yan et al., 1996) polymerized vinyl benzyl trimethylammonium alanate (Pal et al., 2017). The best choice would be to use waste materials as during the regeneration of Activated Carbon chemical compounds are released into the environment and can persist for a long time in the air, soil or ice. ACs monoliths available on the market consist of a layer of

carbon supported on a ceramic substrate with a loading of about 50%. For this reason, the template synthesis of porous carbon using a replica technique on siliceous porous materials has been proposed as a possible solution (Lu et al., 2005; Zhang et al., 2017). This technique allows to obtain a modulation of the textural properties, suitable for the particular required use. A carbonaceous precursor is used to impregnate the silica with interconnected porosity. Activated Carbon is obtained from the pyrolysis of the system. Once the silica skeleton is dissolved, the porous ordered carbon foam obtained represents the negative replica of the starting model (Lu et al., 2005; Zhang et al., 2017). Different and complex steps are involved in this method as the preparation of the nanostructured silica mold, the impregnation with the carbon precursor, the pyrolysis of the precursor and the dissolution of the molds with an acid solution (Lu et al., 2005). Zhang et al., (2017) proposed NaOH etching, filtration and drying of the carbon–silica templates in order to obtain an alkaline mesoporous carbon with high H<sub>2</sub>S adsorption capacity at room temperature, due to the introduction of basic properties greatly enhancing the sorption capacity of the acid. The research aims to obtain structured carbons with simple and not expensive methods avoiding binder or, at least, limiting its use in order to not lower the adsorption capacity too much.

### **1.3.3. ACs Applications**

Activated Carbons are mainly used for adsorptions. The choice between Activated Carbons for adsorption is based on certain criteria such as the size of the particles because if it decreases, the pressure drop in the gas flow strongly increases; the speed of the gas flow because adsorption becomes slow at low rates and therefore greater systems are necessary to achieve the required treatment capacities; pore size distribution as the adsorption capacity improves with the microporosity and the lack of the latter leads to a slower internal diffusion; adsorption capacity and kinetics using equilibrium isotherm.

ACs find applications in various fields including the purification of effluent gases and exhaust gases (containing  $\text{SO}_2$ ,  $\text{H}_2\text{S}$ ,  $\text{CS}_2$ , etc.), the separation of gas mixtures by carbon molecular sieves (CMS), purification of natural gas, storage of  $\text{H}_2$ ,  $\text{CH}_4$  and  $\text{CO}_2$ , etc (Morris and Wheatley, 2008; Marsh and Reinoso, 2006; Yang et al., 2020; García-Díez et al., 2021). Activated Carbons are very effective for the removal of hydrogen sulphide as they represent catalysts for the direct oxidation of  $\text{H}_2\text{S}$  with air and are powerful adsorbents for sulphur oxides. These performances are then improved by functionalizing the Activated Carbon with specific materials such as metal oxides. Carbon Molecular Sieves are used to separate gases in mixtures by sieving controlled by pore size distribution. They are widely used in the separation of air into nitrogen and oxygen, of methane-carbon dioxide mixtures involving landfill gas treatment, natural gas purification and oil recovery. Methane storage has become interesting as natural gas is a promising fuel since it is very abundant in nature and therefore advantageous from an economic point of view with a lower impact on the environment (Lozano-Castelló et al., 2002). Natural gas can be stored as a compressed supercritical fluid at room temperature but since it requires the use of pressurized tanks, porous materials can be an alternative way that can allow to increase the energy density at relatively low pressures (Attia et al., 2020; Zhang et al., 2021). Similarly, these porous materials could be combined in the capture and storage of greenhouse pollutants such as  $\text{CO}_2$  (D'Alessandro et al., 2010; García-Díez et al., 2021). Hydrogen storage is also currently of great interest as a renewable and clean alternative energy carrier, abundant on the Earth and with a higher chemical energy per mass than hydrocarbons (Doğan et al., 2020; Morris and Wheatley, 2008). Hydrogen storage is difficult and dangerous as the tanks are under high pressure and mechanical degradation of steel due to the hydrogen can occur (Zubizarreta et al., 2009). The advantage of carbon materials as storage systems is that they are lighter than inorganic compounds (Wasim and Djukic, 2019). A tailored porosity is required for hydrogen storage as a high value of micropore volume

to achieve large hydrogen storage capacity at room temperature is necessary (Gadiou et al., 2005; Jordá-Beneyto et al., 2007).

## 1.4.H<sub>2</sub>S Adsorption

### 1.4.1. H<sub>2</sub>S properties

Hydrogen sulphide is a sulphur compound present in various industrial exhaust gases. H<sub>2</sub>S occurs naturally in various hydrocarbons such as crude oil, natural gas, liquefied petroleum gas (LPG), industrial catalytic hydrodesulphurization (HDS) exhaust gas which promotes heavy oil (bitumen) and biogas but, in addition, it can be produced from various sources. For example, the sulphate-reducing activity of bacteria that use SO<sub>4</sub><sup>2-</sup> to oxidize organic matter can produce H<sub>2</sub>S. The hydrolysis reaction of metal sulphides in volcanic rocks, landfills and composting sites can also lead to the formation of H<sub>2</sub>S (Shah et al., 2017).

natural gas	petrochemical factories
crude petroleum	oil and gas wells
coke over plants	manure pits
waste management	sewers
paper manufacturing	volcanic gases
hot springs	tanneries
stagnant water	food processing
viscous rayon factories	iron smelters

**Table 1. 1** Sources of Hydrogen Sulfide (Policastro and Otten, 2007)

It is a colorless gas, but its presence can be recognized by the smell of "rotten eggs". H<sub>2</sub>S has a molecular weight of 34.08 g/mol and a vapor density of 1.19.

The boiling, melting and freezing points are -60.3 °C, - 82.3 °C and -86 °C respectively. H<sub>2</sub>S can be oxidized to sulphur dioxide (SO<sub>2</sub>), sulphates such as sulphuric acid and elemental sulphur.

Odor:	rotten eggs
Taste:	sweetish
Boiling point:	-60°C
Melting point:	-85°C
Relative vapor density to air:	1.19
Vapor pressure at 25°C:	19.6 atm
Auto-ignition temperature*:	250°C
Conversion factor for hydrogen sulfide in air:	1 mg/m <sup>3</sup> = 0.717 ppm, or 1 ppm = 1.4 mg/m <sup>3</sup>

**Table 1. 2** Hydrogen Sulphide properties (Policastro & Otten, 2007)

The average stay of H<sub>2</sub>S in the air varies from 12 to 37 h and according to the presence of pollutants and temperature. Temperature also affects the solubility of H<sub>2</sub>S: as the temperature increase, the solubility of H<sub>2</sub>S is higher. H<sub>2</sub>S also evaporates relatively easily from aqueous solutions (vapor pressure =  $18.75 \times 10^5$  Pa). H<sub>2</sub>S is a weak acid in aqueous solution with an acid dissociation constant (pKa) of 6.76 at 37 ° C. It can dissociate into H<sup>+</sup> and HS<sup>-</sup>, which can dissociate into H<sup>+</sup> and S<sup>2-</sup>.

H<sub>2</sub>S is classified as a highly flammable, toxic substance and harmful to the environment. However, the main problem is that the higher H<sub>2</sub>S concentrations in the exhaust gases can reach 500 ppmv and even up to 20,000 ppmv (Woodcock and Gottlieb, 2004). Due to the danger of H<sub>2</sub>S, in recent years, the laws regarding exhaust emissions have become increasingly stringent as air quality standards have become increasingly stringent. Permitted H<sub>2</sub>S concentration limits differ from country to country (Nhut and Le, 2020).

Figure 1.5 reports the possible effects that H<sub>2</sub>S at different concentrations has on human health.

Concentration (ppm)	Symptoms/Effects
0.00011–0.00033	Typical background concentrations
0.01–1.5	Odor threshold (when rotten egg smell is first noticeable to some). Odor becomes more offensive at 3–5 ppm. Above 30 ppm, odor is described as sweet or sickeningly sweet.
2–5	Prolonged exposure may cause nausea, tearing of the eyes, headaches or loss of sleep. Airway problems (bronchial constriction) in some asthma patients.
20	Possible fatigue, loss of appetite, headache, irritability, poor memory, dizziness.
50–100	Slight conjunctivitis and respiratory tract irritation after 1 h. May cause digestive upset and loss of appetite.
100	Coughing, eye irritation, loss of smell after 2–15 minutes (olfactory fatigue). Altered breathing, drowsiness after 15–30 minutes. Throat irritation after 1 h. Gradual increase in severity of symptoms over several hours. Death may occur after 48 h.
100–150	Loss of smell (olfactory fatigue or paralysis).
200–300	Marked conjunctivitis and respiratory tract irritation after 1 h. Pulmonary edema may occur from prolonged exposure.
500–700	Staggering, collapse in 5 min. Serious damage to the eyes in 30 min. Death after 30–60 minutes.
700–1000	Rapid unconsciousness, 'knockdown' or immediate collapse within 1–2 breaths, breathing stops, death within minutes.
1000–2000	Nearly instant death.

**Figure 1. 5** The effect of H<sub>2</sub>S on human health (Nhut and Le, 2020)

The removal of H<sub>2</sub>S is also necessary to avoid corrosion of the engines and the generation and emission of SO<sub>x</sub>. Therefore, the removal of H<sub>2</sub>S is a necessary operation for technical/industrial reasons as well as for environmental health and safety (Fortuny et al., 2008). The reason why H<sub>2</sub>S is very reactive is related to its oxidation-reducing nature and to the high mobility of hydrogen due to the easy break of the S-H bond; furthermore, its low ionization potential acts as an electron donor (Watanabe, 2020).

Since H<sub>2</sub>S is an acid gas, an important parameter influencing the adsorption process is the pH of the adsorbent. In an acid environment the dissociation of H<sub>2</sub>S and the consequent oxidation to elemental sulphur will be limited. In the alkaline pH region, H<sub>2</sub>S adsorption is more effective. However, highly alkaline adsorbents can be considered a problem due to their disposal, that consists of a pH neutralization, which can be an expensive process and can represent a serious environmental hazard. In addition to the pH and porosity, the moisture

content in the adsorption system also favors the capture of  $\text{H}_2\text{S}$  which is easily soluble in water. In the presence of water,  $\text{H}_2\text{S}$  is present as  $\text{H}^+$  and  $\text{HS}^-$ , which in turn facilitates its adsorption onto the adsorbent in the subsequent process (Ahmad et al., 2019).

#### **1.4.2. Adsorbents for $\text{H}_2\text{S}$ removal**

The first adsorbents used for the removal of  $\text{H}_2\text{S}$  from fuels were bulk metal oxides due to the chemical affinity of  $\text{H}_2\text{S}$  for metal cations. The reduction of the  $\text{H}_2\text{S}$  concentration in the exhaust gases to a few ppm is mainly carried out using these solid adsorbents at high temperatures (200-800°C) (Montes et al., 2013). Westmoreland and Harrison (Woodcock and Gottlieb, 2004) studied the high temperature desulphurization capacity of 28 solids, mainly metal oxides. From this research the eleven suitable candidates identified were Fe, Zn, Mo, Mn, V, Ca, Sr, Ba, Co, Cu, and W. Metal oxides are generally used as active phases component to improve the  $\text{H}_2\text{S}$  capture (Montes et al., 2013; Haimour et al., 2005; Yang et al., 2020; Qi et al., 2020; Boutillara et al., 2019; Fang et al., 2013; Oliviero et al., 2009).

Zinc oxide-based sorbents react with  $\text{H}_2\text{S}$  to form a stable compound that is zinc sulphide. Since ZnO is a non-pyrophoric material, it can provide a high level of sulphur removal. Zinc oxide-modified sorbents are widely used due to their high equilibrium constant for the sulphation, thermal stability of the adsorbents and their sulphides and its high sulphur capacity equal to 20-30% by weight of the adsorbent (Watanabe, 2020; Garces et al., 2010). Since bulk ZnO based adsorbents do not have a high absorption capacity of  $\text{H}_2\text{S}$  at room temperature due to kinetic limitations, the disadvantage is to replace the adsorbents, leading to an increase of process costs. Indeed, by increasing the adsorption temperature, sulphidation rates on the  $\text{H}_2\text{S}$  removal by ZnO enhance (Garces et al., 2010; Rosso et al., 2003). ZnO plays a role both as a catalyst to accelerate the dissociation of  $\text{H}_2\text{S}$  and as a reactant that participates in the reaction of  $\text{H}_2\text{S}$  with ZnO which leads to the formation of  $\text{H}_2\text{O}$ . Elemental

sulphur S can be deposited on a surface oxygen vacancy created during the formation of H<sub>2</sub>O leading to the loss of the sulphurization activity of ZnO (Ling et al., 2013).

Davison and Sohail (1995), studying the adsorption of H<sub>2</sub>S over ZnO by FT-IR, found that process is autocatalytic and promoted by water both produced and already present in the feed stream. The main feature of the mechanism is the chemisorption of water in the form of hydroxyls and the subsequent transfer of protons from the hydrogen sulphide to hydroxyl. Neveux et al. (2012) studied the desulphurization process of ZnO through SEM and TEM characterizations and reported that the ZnO sulphidation reaction involves an outward growth of ZnS nanoparticles, as a result of diffusion of zinc and oxygen from the internal interface to the outer surface passing through the formed ZnS layer. They also observed a kinetic blockade for some ZnO particles possibly due to the formation of voids at ZnO/ZnS internal interface making the diffusion of zinc and oxygen atoms from the ZnO phase to the ZnS phase very difficult to obtain. In order to improve the removal of H<sub>2</sub>S, the dispersion of ZnO and the properties of the adsorbent can be increased by adding other transition metal oxides (Cimino et al., 2020).

CuO-based adsorbents reduce H<sub>2</sub>S to very low concentration values due to the highly favored sulphurization thermodynamics of Cu<sup>+2</sup> and Cu<sup>+1</sup> (Watanabe, 2020; Montes et al., 2013). According to Jiang et al. (2010) Cu-based adsorbents are more suitable than Zn-based adsorbents for H<sub>2</sub>S removal at low temperatures probably due to a faster rate of the reticular diffusion of HS<sup>-</sup>, S<sup>2-</sup> and O<sup>2-</sup> or the exchange of HS<sup>-</sup>/S<sup>2-</sup> and O<sup>2-</sup> during the CuO sulphation reaction due to a minor rearrangement of the anionic lattice compared to ZnO. Baird et al. (1992) reports that the H<sub>2</sub>S adsorption capacity of ZnO can be greatly improved by doping with CuO which is not seen as a separate phase but modifies the morphology of the particles. Copper in adsorbents can be present either in metallic (Cu<sup>0</sup>) or oxide form (Cu<sub>2</sub>O, CuO) and Galtayries and Bonnelle (1995) report that dissociative adsorption of H<sub>2</sub>S on copper is strongly

dependent on the chemical nature of the exposed surface that is the oxidation state. If copper is in a lower oxidation states,  $\text{Cu}^\circ$  and  $\text{Cu}^+$  (from  $\text{Cu}_2\text{O}$ ), the adsorption of  $\text{H}_2\text{S}$  leads to the formation of  $\text{Cu}_2\text{S}$  and moreover on  $\text{Cu}^\circ$ , the sulphation reaction involves only the outermost layer of surface; when  $\text{CuO}$  is present ( $\text{Cu}^{2+}$  oxidation state)  $\text{CuS}$  and  $\text{CuSO}_4$  appear (Galtayries and Bonnelle, 1995). The sulphation of copper oxides is attributed to the replacement of the reticular oxygen of the copper oxide with the sulphur of the  $\text{H}_2\text{S}$  (Watanabe, 2020). As in oxygen is more readily available in  $\text{CuO}$ , the purchase of sulphur is therefore favored; if the oxidation state decreases from  $\text{Cu}^{2+}$  to  $\text{Cu}^\circ$ , the sulphation rate decreases (Patrick and Gavalas, 1990; Kyotani et al., 1989).

In turn, the sulphur ion diffuses in the mass to form further bulk sulphide oxide (Hennemann et al., 2015). The mobility ability of ions in copper oxide contributes to more efficient removal of sulphur (Watanabe, 2020). Liu et al. (2015) investigated how the  $\text{H}_2\text{S}$  breakthrough capacities of  $\text{CuO}$ -based sorbents changes after a regeneration process in a temperature range 100-500°C. Recovery of up to 75% of the initial value occurred at regeneration temperatures  $\leq 200^\circ\text{C}$  but by increasing temperature the value decreases. The phenomenon can be explained as copper sulphide ( $\text{CuS}$ ) can be oxidized easily at low temperatures but tends to decompose into more stable sulphides ( $\text{Cu}_2\text{S}$ ) when the temperature is above 220°C.

The utilization of metal oxides as absorbents has the disadvantage of evaporation, loss of surface and porosity, sintering and mechanical disintegration which negatively affect their performance and durability. In order to overcome this problem, they are dispersed on support materials with a high surface area (Montes et al., 2013). In order to develop high performance adsorbents that can work at low temperatures, active metal oxides of nanometric dimensions are dispersed on highly porous substrates, such as zeolites, mesoporous silicas and activated carbons, or in composites with graphite oxides (Balsamo et al., 2016).

As already mentioned, Activated Carbons (ACs) are widely used as an adsorbent for the removal of H<sub>2</sub>S due to their surface chemistry with various types of functional oxygen groups and to the high internal surface area and porosity (Bandosz, 2002; Adib et al., 2000b; Dalai et al., 1999). Both physical and chemical adsorption play an important role in the mechanisms of H<sub>2</sub>S capture on activated carbons; in particular, chemisorption is fast and takes place mainly on the carbon surface, while physical adsorption is a slow process and occurs inside the porous carbonaceous structure (Yan et al., 2002). The presence of other species on the surface of activated carbon, such as water, oxygen, CO<sub>2</sub>, can positively or negatively influence the H<sub>2</sub>S adsorption mechanisms depending on the type of adsorbent used (Sigot et al., 2016; Bagreev et al., 2005). As the surface of the activated carbons is very heterogeneous, an oxidation reaction may also take place, mainly leading to the formation of elemental sulphur or polymeric sulphur chains (S<sub>x</sub>), which in turn can react giving further sulphur compounds (Huang et al., 2006; Feng et al., 2017). However, it is important that the adsorption mechanism and the formed species are well defined in order to improve the process and evaluate the possibility of regeneration operations. In absence of humidity, the so-called “dry condition”, H<sub>2</sub>S is captured by physical adsorption and micropore filling occurs (Adib et al., 2000b). On the other hand, when other species besides H<sub>2</sub>S are involved in adsorption, both chemical and physical mechanisms can occur. It has been reported that the use of ZnO and CuO as an active phase for H<sub>2</sub>S capture leads to the formation of the corresponding metal sulphides (Hernández et al., 2005; Huang et al., 2006). The presence of O<sub>2</sub> promotes the reactive adsorption process of H<sub>2</sub>S on ACs with the formation of sulphates, sulphides and elemental sulphur whereas water favors the desulphurization process thanks to the presence of oxygenated functional groups which accelerate the interaction with H<sub>2</sub>S due to the electrophilic nature of sulphur and also promotes the oxidation of hydrogen sulphide to elemental sulphur (Watanabe, 2020).

On the other hand, the effect of water depends on the specific adsorption system. Generally, the presence of an adsorbed water film on the surface of the activated carbon leads to an increase in the reactive adsorption of H<sub>2</sub>S, as it favors a more rapid dissociation of hydrogen sulphide and subsequent oxidation to SO<sub>2</sub>, elemental sulphur and sulphuric acid. The presence of basic surface functional groups or metal oxides gives a more alkaline character to adsorption system promoting the dissociation of H<sub>2</sub>S (Adib et al., 2000a; Adib et al., 2000b; Bagreev and Bandosz, 2005). Wang et al. (2017) found that metal oxides react with water by hydroxylation reaction leading to an increase in the adsorption of H<sub>2</sub>S by dissociation of H<sub>2</sub>S in HS<sup>-</sup> and S<sup>2-</sup> and subsequent reaction with the metal cation whose product is the corresponding sulphide. In contrast, Huang et al. (2006) found that in the presence of water, competition reactions negatively affected the adsorption of H<sub>2</sub>S on activated carbon supported copper. Finally, according to Yang and Tatarchuk (2010), the effect of water on H<sub>2</sub>S adsorption is negligible.

The effect of gaseous O<sub>2</sub> on H<sub>2</sub>S capture efficiency is enhanced by the co-presence of moisture (Fang et al., 2013; de Falco et al., 2018). In the co-presence of humidity and oxygen H<sub>2</sub>S dissolves in a water film adsorbed on the surface of AC to form HS<sup>-</sup>, which further reacts with oxygen radicals resulting from the dissociation of O<sub>2</sub> adsorbed to produce elemental sulphur (Huang et al., 2006; Liu and Ke, 2020). The sulphur formed is deposited directly in the micropores, causing the deactivation of the carbons (Pan et al., 2021; Zhang et al., 2016).

The functionalization of activated carbons leads to a strong increase in the adsorption capacity of hydrogen sulphide. Balsamo et al. (2017) investigated ZnO/CuO supported on activated carbon in granular form under dry and wet feed conditions. The results showed the existence of two phenomena occurring during H<sub>2</sub>S adsorption: a fast one that involves the formation of sulphates during the initial phases of the reactive adsorption process, due to the presence of copper as an oxygen donor, and a slow one in which Cu and Zn sulphides

begin to form after the corresponding sulphates, probably due to the lack of available oxygen on the sorbent (Balsamo et al., 2017). For the Cu modified sorbents, the co-presence of O<sub>2</sub> and H<sub>2</sub>O in the feed enhances both H<sub>2</sub>S capture rate and adsorption capacity, promoting the formation of sulphur compounds, such as elemental and organic sulphur, in addition to metal sulphates also formed under inert dry feed conditions. By carrying out tests for several days, it has found that the H<sub>2</sub>S capture reached a pseudo-stable rate and the total H<sub>2</sub>S adsorption capacity corresponded to the filling of micro porosity with elemental and organic S species.

Zhang et al. (2016) has reported for the first time that the use of MgO as a basic oxide has much better desulphurization performance respect to salts generally used such as NaOH, Na<sub>2</sub>CO<sub>3</sub>, KOH and K<sub>2</sub>CO<sub>3</sub>. The good catalytic performance of mesoporous carbon impregnated with MgO for the catalytic oxidation of H<sub>2</sub>S at room temperature in the presence of humidity depends on the partial solubility of MgO in water. Magnesium oxide, hydroxylated in the presence of water forming Mg(OH)<sub>2</sub>, provides the continuous formation of OH<sup>-</sup> for the dissociation of H<sub>2</sub>S into HS<sup>-</sup> (Zhang et al., 2016) promoted by the alkaline character of MgO (Bandosz, 2002; Adib et al. 2000a) as showed in Figure 1.6. Since it is not totally soluble in water, not all MgO dissolves at the same time but slowly and in small quantities so once OH<sup>-</sup> is no longer available it continues to dissolve in water and generates other OH<sup>-</sup> until exhaustion. MgO also promotes the regeneration of the sorbent which has an excellent impact on both the environmental economy and the sustainability of resources (Feng et al., 2020).

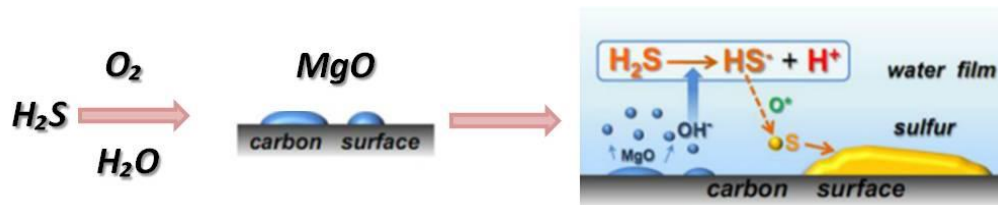


**Figure 1. 6** Rearrangement of the schematic illustration of the H<sub>2</sub>S oxidation process in the presence of MgO proposed by Zhang (2016)

Rodriguez et al. (1999) reported that in the presence of MgO, the removal of H<sub>2</sub>S occurs through the chemical adsorption of HS<sup>-</sup> and S<sup>2-</sup> on flat surfaces of MgO (100) plane, where the direct interaction of H<sub>2</sub>S with MgO is weak. They asserted that the dissociation of H<sub>2</sub>S in the presence of MgO is lower than in zinc and copper oxides. In particular, since MgO is an oxide with greater ionicity, it has a lower reactivity towards H<sub>2</sub>S, indicating that in the adsorption process the role of electrostatic interactions between the dipole of the molecule and the ionic field generated by the charges of the oxides is secondary; moreover, in presence of copper, the adsorption capacity of the system is enhanced by the Cu atoms that facilitate the H<sub>2</sub>S dissociation (Marsh and Reinoso, 2006).

*List of figures*

<b>Figure 1. 1</b> Adsorption isotherms (McCabe, 1993) .....	13
<b>Figure 1. 2</b> IUPAC classification of physisorption isotherms (Thommes et al., 2015) .....	14
<b>Figure 1. 3</b> Breakthrough curve in a fixed bed reactor .....	16
<b>Figure 1. 4</b> Oxygen functional groups on carbon surfaces (Rodríguez-Reinoso & Molina-Sabio, 1998) .....	25
<b>Figure 1. 5</b> The effect of H <sub>2</sub> S on human health (Nhut and Le, 2020).....	32
<b>Figure 1. 6</b> Rearrangement of the schematic illustration of the H <sub>2</sub> S oxidation process in the presence of MgO proposed by Zhang (2016) .....	38

*List of tables*

**Table 1. 1** Sources of Hydrogen Sulfide (Policastro and Otten, 2007) .....30

**Table 1. 2** Hydrogen Sulphide properties (Policastro & Otten, 2007).....31

## *References*

- Abd, A. A., Naji, S. Z., Hashim, A. S., Othman, M. R. (2020). Carbon dioxide removal through Physical Adsorption using Carbonaceous and non-Carbonaceous Adsorbents: A review. *Journal of Environmental Chemical Engineering*, 104-142.
- Abu-Zahra, M. R. M., Sodiq, A., Feron, P. H. M. (2016). Commercial liquid absorbent-based PCC processes. In *Absorption-Based Post-combustion Capture of Carbon Dioxide* (pp. 757-778). Woodhead Publishing.
- Adib, F., Bagreev, A., & Bandosz, T. J. (2000a). Adsorption/oxidation of hydrogen sulfide on nitrogen-containing activated carbons. *Langmuir*, 16(4), 1980-1986.
- Adib, F., A. Bagreev, and T. J. Bandosz. (2000b). Analysis of the Relationship between H<sub>2</sub>S Removal Capacity and Surface Properties of Unimpregnated Activated Carbons. *Environmental Science and Technology* 34(4): 686–92.
- Ahmad, W., Sethupathi, S., Kanadasan, G., Lau, L. C., Kanthasamy, R. (2019). A review on the removal of hydrogen sulfide from biogas by adsorption using sorbents derived from waste. *Reviews in Chemical Engineering*, 1(ahead-of-print).
- Artioli, Y. (2008). Adsorption. *Encyclopedia of Ecology Fath, SEJD*.
- Attia, N. F., Jung, M., Park, J., Jang, H., Lee, K., Oh, H. (2020). Flexible nanoporous activated carbon cloth for achieving high H<sub>2</sub>, CH<sub>4</sub>, and CO<sub>2</sub> storage capacities and selective CO<sub>2</sub>/CH<sub>4</sub> separation. *Chemical Engineering Journal*, 379, 122367.
- Bagreev, A., Bandosz, T. J. (2005). On the mechanism of hydrogen sulfide removal from moist air on catalytic carbonaceous adsorbents. *Industrial*

Engineering Chemistry Research, 44(3), 530-538.

- Bagreev, A., Katikaneni, S., Parab, S., Bandosz, T. J. (2005). Desulfurization of digester gas: prediction of activated carbon bed performance at low concentrations of hydrogen sulfide. *Catalysis Today*, 99(3-4), 329-337.
- Baird, T., Denny, P. J., Hoyle, R., McMonagle, F., Stirling, D., Tweedy, J. (1992). Modified zinc oxide absorbents for low-temperature gas desulfurisation. *Journal of the Chemical Society, Faraday Transactions*, 88(22), 3375-3382.
- Balsamo, M., Cimino, S., De Falco, G., Erto, A., Lisi, L. (2016). ZnO-CuO supported on activated carbon for H<sub>2</sub>S removal at room temperature. *Chemical Engineering Journal*, 304, 399-407.
- Balsamo, M., Cimino, S., Falco, G. D., Erto, A., Lisi, L. (2017). Synergic Effect of Mixed ZnO and CuO Nanoparticles Supported on Activated Carbon for H<sub>2</sub>S Adsorption at Room Temperature. *Advanced Science Letters*, 23(6), 5879-5882.
- Bandosz, T. J. (2002). On the adsorption/oxidation of hydrogen sulfide on activated carbons at ambient temperatures. *Journal of Colloid and Interface Science*, 246(1), 1-20.
- Bedia, J., Peñas-Garzón, M., Gómez-Avilés, A., Rodríguez, J. J., Belver, C. (2020). Review on activated carbons by chemical activation with FeCl<sub>3</sub>. *C-Journal of Carbon Research*, 6(2), 21.
- Bertarione, S., Bonino, F., Cesano, F., Damin, A., Scarano, D., Zecchina, A. (2008). Furfuryl alcohol polymerization in H<sup>+</sup>-Y confined spaces: reaction mechanism and structure of carbocationic intermediates. *The Journal of Physical Chemistry B*, 112(9), 2580-2589.
- Bertarione, S., Bonino, F., Cesano, F., Jain, S., Zanetti, M., Scarano, D.,

- Zecchina, A. (2009). Micro-FTIR and micro-raman studies of a carbon film prepared from furfuryl alcohol polymerization. *The Journal of Physical Chemistry B*, 113(31), 10571-10574.
- Boutillara, Y., Tombeur, J. L., De Weireld, G., Lodewyckx, P. (2019). In-situ copper impregnation by chemical activation with CuCl<sub>2</sub> and its application to SO<sub>2</sub> and H<sub>2</sub>S capture by activated carbons. *Chemical Engineering Journal*, 372, 631-637.
- Briens, L., Bowden-Green, B. (2020). A comparison of liquid binders for drum granulation of biochar powder. *Powder Technology*.
- Cesano, F., Rahman, M. M., Bertarione, S., Vitillo, J. G., Scarano, D., Zecchina, A. (2012). Preparation and adsorption properties of activated porous carbons obtained using volatile zinc templating phases. *Carbon*, 50(5), 2047-2051.
- Cesano, F., Scarano, D., Bertarione, S., Bonino, F., Damin, A., Bordiga, S., Prestipito, C., Lamberti, C., Zecchina, A. (2008). Synthesis of ZnO-carbon composites and imprinted carbon by the pyrolysis of ZnCl<sub>2</sub>-catalyzed furfuryl alcohol polymers. *Journal of Photochemistry and Photobiology A: Chemistry*, 196(2-3), 143-153.
- Chen, H., Zhang, Y. J., He, P. Y., Li, C. J., Liu, L. C. (2020). Facile synthesis of cost-effective iron enhanced hetero-structure activated carbon/geopolymer composite catalyst for NH<sub>3</sub>-SCR: Insight into the role of iron species. *Applied Catalysis A: General*, 605, 117804.
- Choura, M., Belgacem, N. M., Gandini, A. (1996). Acid-catalyzed polycondensation of furfuryl alcohol: mechanisms of chromophore formation and cross-linking. *Macromolecules*, 29(11), 3839-3850.
- Cimino, S., Lisi, L., De Falco, G., Montagnaro, F., Balsamo, M., Erto, A.

- (2018). Highlighting the effect of the support during H<sub>2</sub>S adsorption at low temperature over composite Zn-Cu sorbents. *Fuel*, 221, 374-379.
- Cimino, S., Lisi, L., Erto, A., Deorsola, F. A., de Falco, G., Montagnaro, F., Balsamo, M. (2020). Role of H<sub>2</sub>O and O<sub>2</sub> during the reactive adsorption of H<sub>2</sub>S on CuO-ZnO/activated carbon at low temperature. *Microporous and Mesoporous Materials*, 295, 109949.
- D'Alessandro, D. M., Smit, B., Long, J. R. (2010). Carbon dioxide capture: prospects for new materials. *Angewandte Chemie International Edition*, 49(35), 6058-6082.
- Dalai, A. K., Majumdar, A., Tollefson, E. L. (1999). Low temperature catalytic oxidation of hydrogen sulfide in sour produced wastewater using activated carbon catalysts. *Environmental Science Technology*, 33(13), 2241-2246.
- Davidson, J. M., Sohail, K. (1995). A DRIFTS study of the surface and bulk reactions of hydrogen sulfide with high surface area zinc oxide. *Industrial Engineering Chemistry Research*, 34(11), 3675-3677.
- Dias Filho, N. L., Do Carmo, D. R. (2006). Adsorption at silica, alumina, and related surfaces. Somasundaran P. *Encyclopedia of Surface and Colloid Science*. 2nd ed. New York: Ed. Taylor Francis, 209-228.
- Doğan, M., Sabaz, P., Bicil, Z., Kizilduman, B. K., Turhan, Y. (2020). Activated carbon synthesis from tangerine peel and its use in hydrogen storage. *Journal of the Energy Institute*, 93(6), 2176-2185.
- Dunlop, A. P., Peters, F. N. (1953). *The furans*, Reinhold Pub. Corp., New York, 398-399.
- Eddaoudi, M. (2005). *Characterization of Porous Solids and Powders: Surface Area, Pore Size and Density by S. Lowell* (Quantachrome Instruments,

Boynton Beach), JE Shields (CW Post Campus of Long Island University), MA Thomas, and M. Thommes (Quantachrome Instruments).

Elyassi, B., Al Wahedi, Y., Rajabbeigi, N., Kumar, P., Jeong, J. S., Zhang, X., Kumar, P., Balasubramanian, V.V., Mkhoyan, K.A., Boukos, N., Al Hashimi, S., Tsapatsis, M. (2014). A high-performance adsorbent for hydrogen sulfide removal. *Microporous and Mesoporous Materials*, 190, 152-155.

de Falco, G., Montagnaro, F., Balsamo, M., Erto, A., Deorsola, F. A., Lisi, L., Cimino, S. (2018). Synergic effect of Zn and Cu oxides dispersed on activated carbon during reactive adsorption of H<sub>2</sub>S at room temperature. *Microporous and Mesoporous Materials*, 257, 135-146.

Fang, H. B., Zhao, J. T., Fang, Y. T., Huang, J. J., Wang, Y. (2013). Selective oxidation of hydrogen sulfide to sulfur over activated carbon-supported metal oxides. *Fuel*, 108, 143-148.

Feng, Y., Wen, J., Hu, Y., Wu, B., Wu, M., Mi, J. (2017). Evaluation of the cycling performance of a sorbent for H<sub>2</sub>S removal and simulation of desulfurization-regeneration processes. *Chemical Engineering Journal*, 326, 1255-1265.

Feng, Y., Lu, J., Wang, J., Mi, J., Zhang, M., Ge, M., Li, Y., Zhang, Z., Wang, W. (2020). Desulfurization sorbents for green and clean coal utilization and downstream toxics reduction: A review and perspectives. *Journal of Cleaner Production*, 273, 123080.

Fitzer, E., Kochling, K. H., Boehm, H. P., Marsh, H. (1995). Recommended terminology for the description of carbon as a solid (IUPAC Recommendations 1995). *Pure and Applied Chemistry*, 67(3), 473-506.

- Fortuny, M., Baeza, J. A., Gamisans, X., Casas, C., Lafuente, J., Deshusses, M. A., Gabriel, D. (2008). Biological sweetening of energy gases mimics in biotrickling filters. *Chemosphere*, 71(1), 10-17.
- Medek, J. (1977). Possibility of micropore analysis of coal and coke from the carbon dioxide isotherm. *Fuel*, 56(2), 131-133.
- Gadiou, R., Saadallah, S. E., Piquero, T., David, P., Parmentier, J., Vix-Guterl, C. (2005). The influence of textural properties on the adsorption of hydrogen on ordered nanostructured carbons. *Microporous and Mesoporous Materials*, 79(1-3), 121-128.
- Galtayries, A., Bonnelle, J. P. (1995). XPS and ISS studies on the interaction of H<sub>2</sub>S with polycrystalline Cu, Cu<sub>2</sub>O and CuO surfaces. *Surface and Interface Analysis*, 23(3), 171-179.
- Garces, H. F., Galindo, H. M., Garces, L. J., Hunt, J., Morey, A., Suib, S. L. (2010). Low temperature H<sub>2</sub>S dry-desulfurization with zinc oxide. *Microporous and Mesoporous Materials*, 127(3), 190-197.
- García-Díez, E., Castro-Muñiz, A., Paredes, J. I., Maroto-Valer, M. M., Suárez-García, F., García, S. (2021). CO<sub>2</sub> capture by novel hierarchical activated ordered micro-mesoporous carbons derived from low value coal tar products. *Microporous and Mesoporous Materials*, 110986.
- Guclu, C., Alper, K., Erdem, M., Tekin, K., Karagoz, S. (2021). Activated carbons from co-carbonization of waste truck tires and spent tea leaves. *Sustainable Chemistry and Pharmacy*, 21, 100410.
- Gonzalez-Serrano, E., Cordero, T., Rodriguez-Mirasol, J., Rodríguez, J. J. (1997). Development of porosity upon chemical activation of kraft lignin with ZnCl<sub>2</sub>. *Industrial Engineering Chemistry Research*, 36(11), 4832-4838.

- Haimour, N. M., El-Bishtawi, R., Ail-Wahbi, A. (2005). Equilibrium adsorption of hydrogen sulfide onto CuO and ZnO. *Desalination*, 181(1-3), 145-152.
- Hennemann, J., Kohl, C. D., Smarsly, B. M., Metelmann, H., Rohnke, M., Janek, J., Reppin, D., Meyer, B.K., Russ, S., Wagner, T. (2015). Copper oxide based H<sub>2</sub>S dosimeters - Modeling of percolation and diffusion processes. *Sensors and Actuators B: Chemical*, 217, 41-50.
- Hernández, S. P., Chiappero, M., Russo, N., Fino, D. (2011). A novel ZnO-based adsorbent for biogas purification in H<sub>2</sub> production systems. *Chemical Engineering Journal*, 176, 272-279.
- Huang, C. C., Chen, C. H., Chu, S. M. (2006). Effect of moisture on H<sub>2</sub>S adsorption by copper impregnated activated carbon. *Journal of Hazardous Materials*, 136(3), 866-873.
- Nhut, H. H., Le, L. T. (2020). Removal of H<sub>2</sub>S in biogas using biotrickling filter: Recent development. *Process Safety and Environmental Protection*.
- Inglezakis, V., Pouloupoulos, S. (2006). Adsorption, ion exchange and catalysis (Vol. 3, pp. 498-520). Amsterdam: Elsevier.
- Iwanow, M., Gärtner, T., Sieber, V., König, B. (2020). Activated carbon as catalyst support: precursors, preparation, modification and characterization. *Beilstein Journal of Organic Chemistry*, 16(1), 1188-1202.
- Jiang, D., Su, L., Ma, L., Yao, N., Xu, X., Tang, H., Li, X. (2010). Cu-Zn-Al mixed metal oxides derived from hydroxycarbonate precursors for H<sub>2</sub>S removal at low temperature. *Applied Surface Science*, 256(10), 3216-3223.
- Jordá-Beneyto, M., Suárez-García, F., Lozano-Castelló, D., Cazorla-Amorós,

- D., Linares-Solano, A. (2007). Hydrogen storage on chemically activated carbons and carbon nanomaterials at high pressures. *Carbon*, 45(2), 293-303.
- Kyotani, T., Kawashima, H., Tomita, A. (1989). High-temperature desulfurization with copper-containing sorbents. *Environmental Science Technology*, 23(2), 218-223.
- Landers, J., Gor, G. Y., Neimark, A. V. (2013). Density functional theory methods for characterization of porous materials. *Colloids and Surfaces A: Physicochemical and Engineering Aspects*, 437, 3-32.
- Ling, L., Zhang, R., Han, P., Wang, B. (2013). DFT study on the sulfurization mechanism during the desulfurization of H<sub>2</sub>S on the ZnO desulfurizer. *Fuel Processing Technology*, 106, 222-230.
- Liu, B., Gu, J., Zhou, J. (2016). High surface area rice husk-based activated carbon prepared by chemical activation with ZnCl<sub>2</sub>-CuCl<sub>2</sub> composite activator. *Environmental Progress & Sustainable Energy*, 35(1), 133-140.
- Liu, B. T., Ke, Y. X. (2020). Enhanced selective catalytic oxidation of H<sub>2</sub>S over Ce-Fe/AC catalysts at ambient temperature. *Journal of the Taiwan Institute of Chemical Engineers*.
- Liu, D., Chen, S., Fei, X., Huang, C., Zhang, Y. (2015). Regenerable CuO-based adsorbents for low temperature desulfurization application. *Industrial & Engineering Chemistry Research*, 54(14), 3556-3562.
- Liu, L., Liu, Z., Huang, Z., Liu, Z., Liu, P. (2006). Preparation of activated carbon honeycomb monolith directly from coal. *Carbon (New York, NY)*, 44(8), 1598-1601.
- Lozano-Castello, D., Alcaniz-Monge, J., De la Casa-Lillo, M. A., Cazorla-Amoros, D., Linares-Solano, A. (2002). Advances in the study of

methane storage in porous carbonaceous materials. *Fuel*, 81(14), 1777-1803.

Lozano-Castelló, D., Cazorla-Amorós, D., Linares-Solano, A., Quinn, D. F. (2002). Activated carbon monoliths for methane storage: influence of binder. *Carbon*, 40(15), 2817-2825. 7

Lu, A. H., Smått, J. H., Lindén, M. (2005). Combined surface and volume templating of highly porous nanocast carbon monoliths. *Advanced Functional Materials*, 15(5), 865-871.

Marsh, H., Reinoso, F. R. (2006). *Activated carbon*. Elsevier.

McCabe, W. L. (1993). *JC Smith, P. Harriott, Unit Operations of Chemical Engineering*.

Mohan, S., Dinesha, P., Kumar, S. (2020). NO<sub>x</sub> reduction behaviour in copper zeolite catalysts for ammonia SCR systems: A review. *Chemical Engineering Journal*, 384, 123253.

Montes, D., Tocuyo, E., González, E., Rodríguez, D., Solano, R., Atencio, R., Ramos, M.A., Moronta, A. (2013). Reactive H<sub>2</sub>S chemisorption on mesoporous silica molecular sieve-supported CuO or ZnO. *Microporous and Mesoporous Materials*, 168, 111-120.

Morris, R. E., Wheatley, P. S. (2008). Gas storage in nanoporous materials. *Angewandte Chemie International Edition*, 47(27), 4966-4981.

Neveux, L., Chiche, D., Bazer-Bachi, D., Favergeon, L., Pijolat, M. (2012). New insight on the ZnO sulfidation reaction: Evidences for an outward growth process of the ZnS phase. *Chemical Engineering Journal*, 181, 508-515.

Ogungbenro, A. E., Quang, D. V., Al-Ali, K. A., Vega, L. F., Abu-Zahra, M. R.

- (2020). Synthesis and characterization of activated carbon from biomass date seeds for carbon dioxide adsorption. *Journal of Environmental Chemical Engineering*, 8(5), 104257.
- Oliviero, L., Leclerc, H., Manoilova, O. V., Blasin-Aube, V., Mauge, F., Kondratieva, E. V., Poretsky, M. S., Tsyganenko, A. A. (2009). Brønsted acidity of MgO induced by H<sub>2</sub>S adsorption. *Industrial & Engineering Chemistry Research*, 48(3), 1237-1241.
- Pal, A., Shahrom, M. S. R., Moniruzzaman, M., Wilfred, C. D., Mitra, S., Thu, K., Saha, B. B. (2017). Ionic liquid as a new binder for activated carbon based consolidated composite adsorbents. *Chemical Engineering Journal*, 326, 980-986.
- Pan, Y., Chen, M., Su, Z., Wu, K., Zhang, Y., & Long, D. (2020). Two-dimensional CaO/carbon heterostructures with unprecedented catalytic performance in room-temperature H<sub>2</sub>S oxidization. *Applied Catalysis B: Environmental*, 280, 119444.
- Pandey, S., Mishra, S. B. (2012). Microwave synthesized xanthan gum-g-poly (ethylacrylate): An efficient Pb<sup>2+</sup> ion binder. *Carbohydrate Polymers*, 90(1), 370-379.
- Patrick, V., Gavalas, G. (1990). Structure and Reduction and Mixed Copper-Aluminum Oxide. *Journal of the American Ceramic Society*, 73(2), 358-369.
- Policastro, M. A., Otten, E. J. (2007). Case files of the University of Cincinnati fellowship in medical toxicology: two patients with acute lethal occupational exposure to hydrogen sulfide. *Journal of Medical Toxicology*, 3(2), 73-81.
- Polychronopoulou, K., Galisteo, F. C., Granados, M. L., Fierro, J. L. G., Bakas,

- T., Efstathiou, A. M. (2005). Novel Fe–Mn–Zn–Ti–O mixed-metal oxides for the low-temperature removal of H<sub>2</sub>S from gas streams in the presence of H<sub>2</sub>, CO<sub>2</sub>, and H<sub>2</sub>O. *Journal of Catalysis*, 236(2), 205-220.
- Qi, J., Wei, G., Sun, X., Wang, L., Li, J. (2020). Enhanced removal for H<sub>2</sub>S by Cu-ordered mesoporous carbon foam. *Journal of Hazardous Materials*, 396, 122710.
- Quinn, D. F., MacDonald, J. A. (1992). Natural gas storage. *Carbon*, 30(7), 1097-1103.
- Rodriguez, J. A., Jirsak, T., Chaturvedi, S. (1999). Reaction of H<sub>2</sub>S with MgO (100) and Cu/MgO (100) surfaces: Band-gap size and chemical reactivity. *The Journal of Chemical Physics*, 111(17), 8077-8087.
- Rodriguez-Reinoso, F., Molina-Sabio, M. (1998). Textural and chemical characterization of microporous carbons. *Advances in Colloid and Interface Science*, 76, 271-294.
- Rosso, I., Galletti, C., Bizzi, M., Saracco, G., Specchia, V. (2003). Zinc oxide sorbents for the removal of hydrogen sulfide from syngas. *Industrial & Engineering Chemistry Research*, 42(8), 1688-1697.
- Rouquerol, J., Rouquerol, F., Llewellyn, P., Maurin, G., Sing, K. S. (2013). *Adsorption by powders and porous solids: principles, methodology and applications*. Academic press.
- Ruthven, D. M. (1984). *Principles of adsorption and adsorption processes*. John Wiley & Sons.
- Saeidi, N., Lotfollahi, M. N. (2015). A procedure to form powder activated carbon into activated carbon monolith. *The International Journal of Advanced Manufacturing Technology*, 81(5-8), 1281-1288.

- Shah, M. S., Tsapatsis, M., Siepmann, J. I. (2017). Hydrogen sulfide capture: From absorption in polar liquids to oxide, zeolite, and metal–organic framework adsorbents and membranes. *Chemical Reviews*, 117(14), 9755-9803.
- Shimekit, B., Mukhtar, H. (2012). Natural gas purification technologies-major advances for CO<sub>2</sub> separation and future directions. *Advances in Natural Gas Technology*, 2012, 235-270.
- Sigot, L., Obis, M. F., Benbelkacem, H., Germain, P., Ducom, G. (2016). Comparing the performance of a 13X zeolite and an impregnated activated carbon for H<sub>2</sub>S removal from biogas to fuel an SOFC: Influence of water. *International Journal of Hydrogen Energy*, 41(41), 18533-18541.
- Sinnott, R. (2005). *Chemical Engineering Design: Chemical Engineering Volume 6*. Elsevier.
- Skoczko, I., Guminski, R. (2020). Research on the Development of Technologies for the Production of Granulated Activated Carbons Using Various Binders. *Materials*, 13(22), 5180.
- Skoulikides, T. (1989). Physical Chemistry I. Continuous ion exchange plant design methods and problems. *Hydrometallurgy. Symetria Editions*, 4, 299-316.
- Taguchi, A., Smått, J. H., Lindén, M. (2003). Carbon monoliths possessing a hierarchical, fully interconnected porosity. *Advanced Materials*, 15(14), 1209-1211.
- Thommes, M. (2010). Physical adsorption characterization of nanoporous materials. *Chemie Ingenieur Technik*, 82(7), 1059-1073.
- Thommes, M., Kaneko, K., Neimark, A. V., Olivier, J. P., Rodriguez-Reinoso,

- F., Rouquerol, J., Sing, K. S. (2015). Physisorption of gases, with special reference to the evaluation of surface area and pore size distribution (IUPAC Technical Report). *Pure and Applied Chemistry*, 87(9-10), 1051-1069.
- Wang, H., Yao, J. (2006). Use of poly (furfuryl alcohol) in the fabrication of nanostructured carbons and nanocomposites. *Industrial & engineering chemistry research*, 45(19), 6393-6404.
- Wang, J., Wang, L., Fan, H., Wang, H., Hu, Y., Wang, Z. (2017). Highly porous copper oxide sorbent for H<sub>2</sub>S capture at ambient temperature. *Fuel*, 209, 329-338.
- Wasim, M., Djukic, M. B. (2020). Hydrogen embrittlement of low carbon structural steel at macro-, micro-and nano-levels. *International Journal of Hydrogen Energy*, 45(3), 2145-2156.
- Watanabe, S. (2020). Chemistry of H<sub>2</sub>S over the Surface of Common Solid Sorbents in Industrial Natural Gas Desulfurization. *Catalysis Today*.
- Wei, X., Li, H., Li, Q., Chen, S. (2009). Preparation of nano-ZnO supported on porous carbon and the growth mechanism. *Microporous and Mesoporous Materials*, 118(1-3), 307-313.
- Woodcock, K. E., Gottlieb, M. (2004). Natural gas. *Kirk-Othmer Encyclopedia of Chemical Technology*, 12, 377-386.
- Yan, R., Liang, D. T., Tsen, L., Tay, J. H. (2002). Kinetics and mechanisms of H<sub>2</sub>S adsorption by alkaline activated carbon. *Environmental Science & Technology*, 36(20), 4460-4466.
- Yan, Z. Q., McCue, J. C., Tolles, E. D. (1996). Preparation of high activity, high density activated carbon with activatable binder. U.S. Patent No. 5,538,932.

- Yang, C., de Falco, G., Florent, M., Fan, H., Bandosz, T. J. (2020). Support features govern the properties of the active phase and the performance of bifunctional ZnFe<sub>2</sub>O<sub>4</sub>-based H<sub>2</sub>S adsorbents. *Carbon*, 169, 327-337.
- Yang, H., Tatarchuk, B. (2010). Novel-doped zinc oxide sorbents for low temperature regenerable desulfurization applications. *AIChE journal*, 56(11), 2898-2904.
- Yang, Y. B., Hao, Q., Müller-Plathe, F., Böhm, M. C. (2020). Monte Carlo Simulations of SO<sub>2</sub>, H<sub>2</sub>S, and CO<sub>2</sub> Adsorption in Charged Single-Walled Carbon Nanotube Arrays. *The Journal of Physical Chemistry C*, 124(10), 5838-5852.
- Zhang, Z., Wang, J., Li, W., Wang, M., Qiao, W., Long, D., Ling, L. (2016). Millimeter-sized mesoporous carbon spheres for highly efficient catalytic oxidation of hydrogen sulfide at room temperature. *Carbon*, 96, 608-615.
- Zhang, Z., Jiang, W., Long, D., Wang, J., Qiao, W., Ling, L. (2017). A general silica-templating synthesis of alkaline mesoporous carbon catalysts for highly efficient H<sub>2</sub>S oxidation at room temperature. *ACS Applied Materials & Interfaces*, 9(3), 2477-2484.
- Zhang, S., Chen, H. Q., Kan, X. T., Tai, Y. L., Liu, W. L., Dong, B. X., & Teng, Y. L. (2021). Storage and in-situ preparation of H<sub>2</sub>-mixed CH<sub>4</sub> fuel by thermochemical reduction of inorganic carbonates with activated metal hydrides. *Fuel*, 292, 120395.
- Zubizarreta, L., Arenillas, A., Pis, J. J. (2009). Carbon materials for H<sub>2</sub> storage. *International Journal of Hydrogen Energy*, 34(10), 4575-4581.

## **Chapter 2. Mechanism of H<sub>2</sub>S adsorption on metal modified commercial activated carbon monoliths**

In this second part of the PhD thesis commercial activated carbon honeycombs have been modified with suitable metal oxides in order to improve the H<sub>2</sub>S capture capacity by analogy with granular AC system, and also to study the different adsorption mechanism activated by two metals with different behavior as copper and magnesium investigating on the nature of sulphur species formed during the adsorption and on their subsequent thermal regeneration. The study has been carried out in the presence of H<sub>2</sub>O and O<sub>2</sub> in order to explore conditions closer to real ones.

## 2.1. Materials and Methods

### 2.1.1. Sorbent preparation

Activated carbon monoliths were provided by Helsa Functional Coating. By cutting the original samples, monoliths with 4x4 cells and 26 mm length were obtained (Figure 2.1). Some monoliths were impregnated by incipient wetness technique with an aqueous solution of  $\text{Cu}(\text{NO}_3)_2 \cdot 5/2 \text{H}_2\text{O}$  and  $\text{Mg}(\text{NO}_3)_2 \cdot 6 \text{H}_2\text{O}$  (Sigma Aldrich) followed by drying at 120°C and thermal treatment in  $\text{N}_2$  flow for 1 h at 350°C.



**Figure 2. 1.** Monolith obtained by cutting the original sample provided by Helsa Functional Coating

The same procedure was followed in order to prepare reference monolith containing copper or magnesium only. The nominal total metal loading was set to 5wt% metal (2.5wt% Cu+2.5wt% Mg for the mixed monolith) and 2.5wt% for copper only. The sorbents are labelled as  $\text{Cu}_x\text{Mg}_y$  where x and y represent the nominal metal content of copper and magnesium, respectively.

In Table 2.1 a list of metal modified sorbents is reported with the corresponding metal load.

**Table 2. 1** List of metal modified sorbents

Sorbent	Nominal copper load (wt%)	Nominal magnesium load (wt%)
2.5Cu	2.5	-
5.0Cu	5.0	-
2.5Cu2.5Mg	2.5	2.5

5.0Mg	-	5.0
-------	---	-----

### 2.1.2. Sorbent characterization

A TG experiment under air up to 850°C was carried out with a Setaram Labsys Evo thermobalance in order to determine the carbon content in the sample as the carbon fraction in the commercial monolith was not provided by the supplier.

The structure of the monoliths, the size of the cells and the channels were investigated by Scanning electron microscopy (SEM) analysis using a FEI Inspect instrument.

The textural properties of sorbents were determined by N<sub>2</sub> adsorption at -196°C with a Quantachrome Autosorb 1-C, after degassing for 2h at 120°C. The Brunauer-Emmett-Teller (BET) method was adopted for the evaluation of the specific surface area, while pore size distribution was calculated by DFT method using slit/cylindrical pore QSDFT fitting.

XPS analysis of used sorbents after some months after adsorption tests was carried out on a XPS PHI 5000 Versa probe apparatus, using band-pass energy of 187.85 eV, a 45° take-off angle and a 100.0 µm diameter X-ray spot size for survey spectra. High-resolution XP-spectra were recorded in the following conditions: pass energy of 20 eV, resolution of 1.1 eV, and step of 0.2 eV. Sample charging effects were eliminated by referring to the spectral line shift to the C 1s Binding Energy (BE) value of 284.8 eV. XP-spectra were analysed by means of a commercial software (CasaXPS, version 2.3.16), by applying mixed Gaussian–Lorentzian (70–30%) profiles. The assignation of XPS signals was based on the NIST compilation of spectral data (Naumkin et al., 2012).

### 2.1.3. H<sub>2</sub>S adsorption/desorption tests

H<sub>2</sub>S adsorption tests have been carried out at T=30°C and total P = 1 atm in the lab-scale experimental apparatus showed in Figure 2.2.

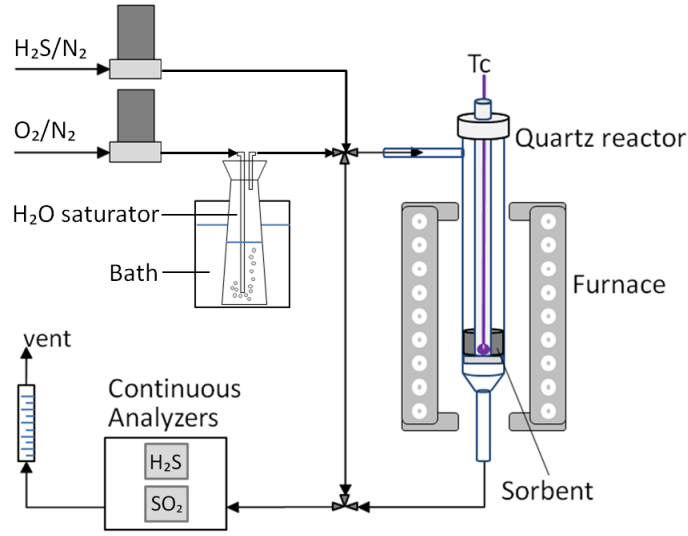


**Figure 2. 2** Schematic representation of the experimental equipment used for H<sub>2</sub>S adsorption tests

The feed concentration of H<sub>2</sub>S and O<sub>2</sub> was set to 100 ppm and 2500 ppm respectively using two independent mass flow controllers by suitably regulating the flow rate of H<sub>2</sub>S/N<sub>2</sub> and O<sub>2</sub>/N<sub>2</sub> gas mixtures. The total inlet flow rate was 20 SL h<sup>-1</sup>. H<sub>2</sub>O was introduced through the line of O<sub>2</sub>/N<sub>2</sub> mixture using a water vapor saturator consisting of a gurgler immersed in a thermostatic bath at room temperature ensuring 50% of humidity. This avoided the possible dissolution of H<sub>2</sub>S into water that could significantly reduce its feed concentration.

Gas analysis was performed with a continuous analyser (ABB Optima Advance Limas 11 UV) for the simultaneous measurement of H<sub>2</sub>S and SO<sub>2</sub>, with cross-sensitivity correction and accuracy better than 1% of span (200 ppmv). As already reported in Section 1.2.2, H<sub>2</sub>S adsorption capacity at saturation,  $\omega_s$  [mmol g<sup>-1</sup>], was determined through a material balance on H<sub>2</sub>S over the adsorption column, leading to the following expression:

$$\omega_{\text{ads}} = \frac{Q^t C_{\text{H}_2\text{S}}^{\text{in}} \rho_{\text{H}_2\text{S}}}{m_{\text{MH}_2\text{S}}} \int_0^{t^*} \left(1 - \frac{C_{\text{H}_2\text{S}}^{\text{out}}(t)}{C_{\text{H}_2\text{S}}^{\text{in}}}\right) dt \quad (2.1)$$

where  $Q^t$  [L s<sup>-1</sup>] is the total gas flow rate,  $C_{\text{H}_2\text{S}}^{\text{in}}$  [-] is the H<sub>2</sub>S volumetric fraction in the gas feed,  $C_{\text{H}_2\text{S}}^{\text{out}}$  [-] is the H<sub>2</sub>S volumetric fraction at the bed

outlet;  $\rho_{\text{H}_2\text{S}}$  is  $\text{H}_2\text{S}$  density ( $1370 \text{ mg L}^{-1}$  at  $30 \text{ }^\circ\text{C}$  and  $1 \text{ bar}$ ) and  $M_{\text{H}_2\text{S}}$  [ $\text{mg mmol}^{-1}$ ] is its molecular weight;  $m$  [ $\text{g}$ ] is the sorbent dose and  $t^*$  [ $\text{s}$ ] represents the whole time test.

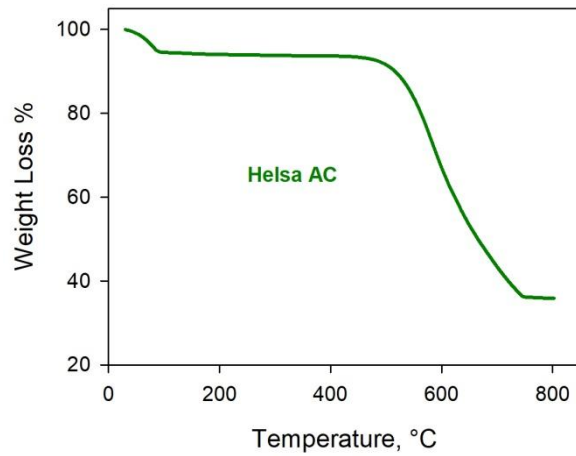
The resolution of Eq. (1) allows to determinate the adsorption isotherm, under the verified assumption of constant total flow during the test.

Temperature Programmed Desorption (TPD) tests were carried out in the Setaram Labsys Evo thermobalance coupled to a Pfeiffer ThermoStar MS under argon in order to evaluate the amount of species desorbed from the saturated AC monoliths. The following mass/charge ratios ( $m/z$ ) were monitored: 16, 34, 44, 48, 64, 76 corresponding to the following species: O,  $\text{H}_2\text{S}$ ,  $\text{CO}_2$ , SO,  $\text{SO}_2$ ,  $\text{CS}_2$ . The carrier gas (Ar) flow rate was set at  $30 \text{ ml min}^{-1}$  and the temperature raised up to  $620^\circ\text{C}$  with a ramp of  $10^\circ\text{C/min}$ .

## **2.2. Results and Discussion**

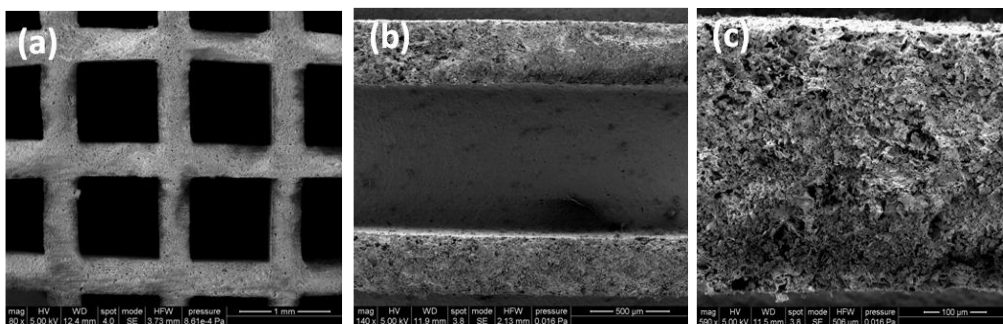
### **2.2.1. Sorbent characterization**

TG experiment on Helsa AC monolith under air up to  $850^\circ\text{C}$  were carried out to estimate the fraction of carbon or carbon+organic binder which burns under this condition leaving the ceramic scaffold as solid residue. Figure 2.3 shows the TG curve that, after a small weight loss at low temperature, associated with the release of adsorbed water and  $\text{CO}_2$ , reports a stable weight up to about  $450^\circ\text{C}$ . Carbon oxidation then starts and it is complete at  $T=750^\circ\text{C}$ , as the weight of the ceramic scaffold remains constant at higher temperatures. The evidence that all the organic matter was burnt was also clear by the color change of starting black monolith completely turning into white scaffold at the end of the analysis. According to the TG experiments the carbon content of Helsa AC monolith is about 65wt.%.



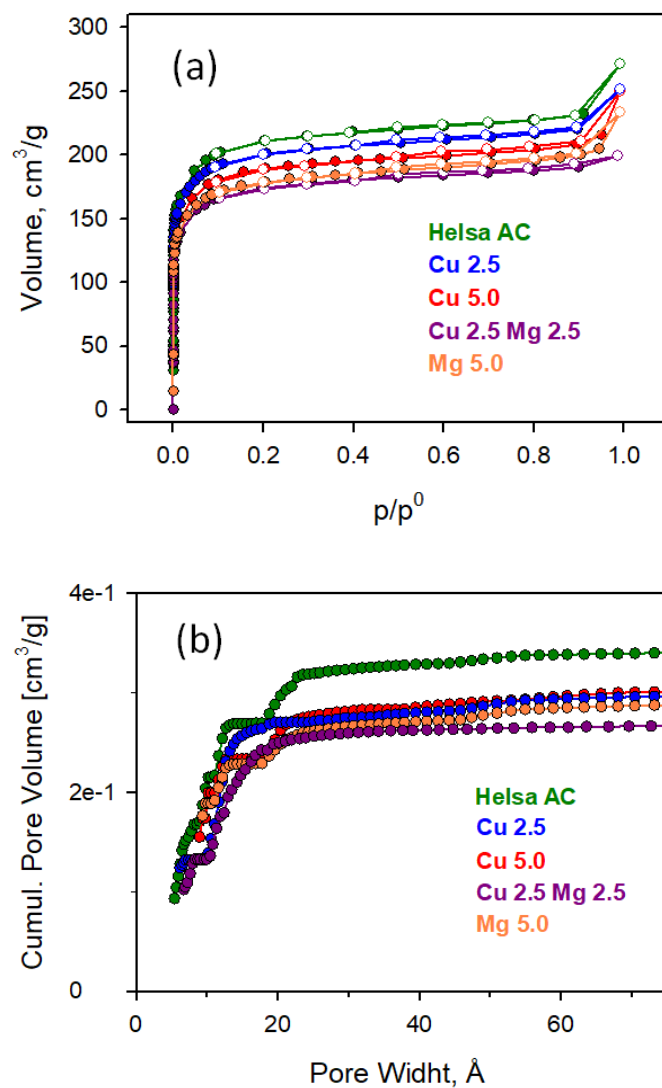
**Figure 2. 3** Weight loss as a function of temperature of Helsa AC monolith under air flow

Figure 2.4(a) shows the SEM images of the monolithic structure characterized by square section channels and walls of rather constant thickness. The characteristic size of the square channel is about  $0.92\pm 0.3$  mm while the thickness of the walls between the channels is  $0.37\pm 0.3$  mm. It was supposed that the honeycombs could have been obtained by extruding a mixture of activated carbon and minerals since a clear carbon layer is not evident, also from the magnifications of channel walls reported in Figure 2.4(b) and (c). This evidence suggests that the monoliths consist of activated carbon particles integrated into the ceramic matrix. The ceramic skeleton is characterized by large pores, well visible in Figure 2.4(c).



**Figure 2. 4** SEM images of monolith cross section (a) at increasing magnifications (channel with two adjacent walls (b); wall (c))

In Figure 2.5 the N<sub>2</sub> adsorption and desorption isotherms of AC and metal modified monoliths (a), cumulative pore volume (b) and pore size distribution evaluated according to the DFT method (c) are reported.



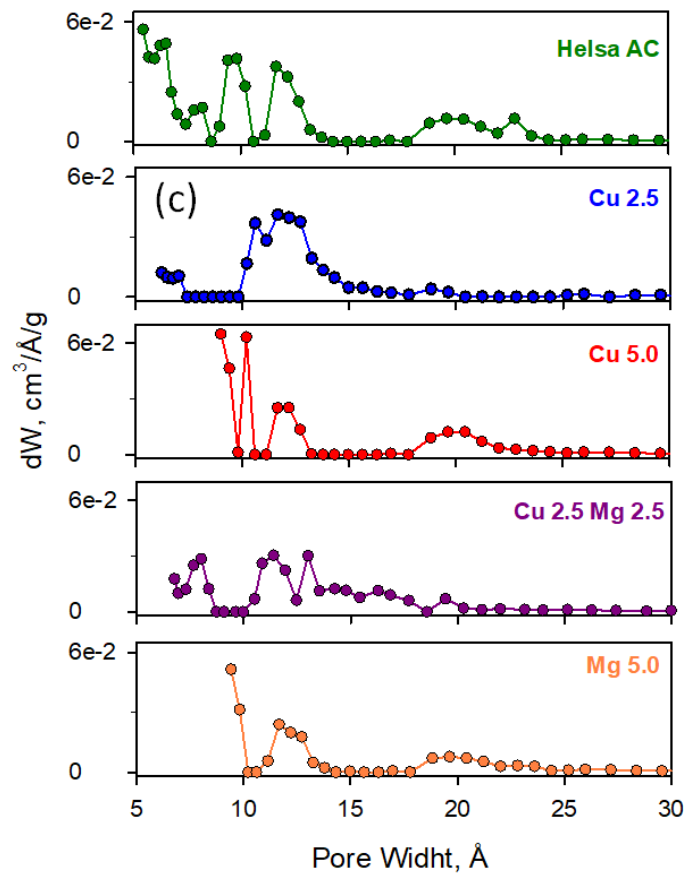


**Figure 2. 5** N<sub>2</sub> physisorption isotherms at 77K (a), cumulative pore volume (b) and pore size distribution (c) for monoliths

In Table 2.2 the BET surface area and the pore volume, divided into micro and mesopores contribution, are reported. By supposing that the ceramic substrate is not porous and it has a negligible surface area, we can attribute the BET surface area and pore volume to carbon only, representing 65% total weight. Consequently, the estimated BET area of AC only should be 1234 m<sup>2</sup>/g.

**Table 2. 2** Area and pore volume of pure and metal modified AC monoliths as fresh, spent and regenerated after TPD

Sorbent	$A_{\text{BET,monolith}}$ $\text{m}^2/\text{g}$	Cumulative Micropore Volume <sub>,monolith</sub> * $\text{cm}^3/\text{g}$	Cumulative Mesopore Volume <sub>,monolith</sub> ** $\text{cm}^3/\text{g}$	Cumulative Total Volume <sub>,monolith</sub> $\text{cm}^3/\text{g}$
AC	802	0.2464	0.0794	0.3258
Cu2.5	762	0.2145	0.061	0.2806
Cu5.0	719	0.2177	0.0667	0.2844
Cu2.5Mg2.5	640	0.1917	0.0686	0.2603
Mg5.0	676	0.2159	0.0544	0.2703

\*The cumulative micropore volume is the volume of pores with a diameter up to 20Å

\*\*The cumulative mesopore volume is the volume of pores with a diameter from 20Å up to 70Å

The results confirm that all sorbents are basically microporous as the contribution of mesopores represents about 20% of total pore volume. As expected, depending on the nature and the amount of metal, the addition of metal oxides leads to a decrease of the surface area. A reduction of the original surface area of AC was observed upon addition of copper, more limited for 2.5wt% Cu with respect of 5%wt Cu.

Moreover, the addition of 5wt% Mg results in a higher reduction of BET area compared to the sample with the same amount of copper. Furthermore, Figure 2.4 (c) shows that, for sorbents containing 5wt% Cu or Mg, pores with dimensions lower than 10 Å are occluded as they are not accessible by the N<sub>2</sub> molecule. Moreover, surface area is further reduced when Cu and Mg are both introduced into AC. Location of metals into micropores seems responsible for this reduction for both Cu and Mg containing sorbents.

### 2.2.2. H<sub>2</sub>S adsorption tests

The positive effect of the co-presence of humidity and oxygen in the feed is shown by the breakthrough curves of AC monolith under a feed containing O<sub>2</sub> only and one containing O<sub>2</sub> and H<sub>2</sub>O in addition to H<sub>2</sub>S, reported in Figure 2.6.

In wet condition, when water vapor is present in the feed, the exit  $\text{H}_2\text{S}$  concentration reaches more slowly the initial value and, after 1500s operation, it is still increasing. On the contrary, under dry condition, the  $\text{H}_2\text{S}$  feed concentration was recovered after less than 1000s.

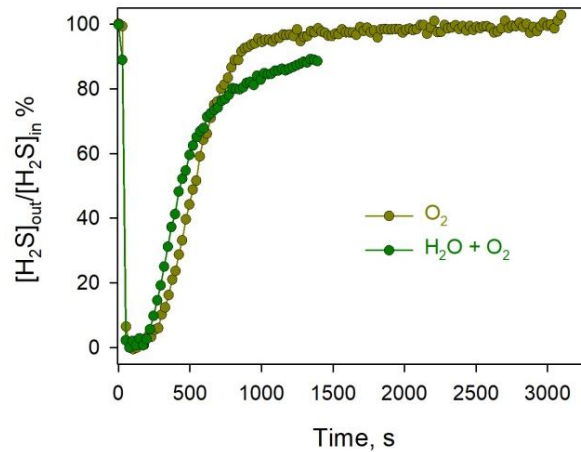


**Figure 2. 6** Breakthrough curves of AC monolith in dry and wet conditions. Inlet conditions:  $[\text{H}_2\text{S}]=100\text{ppm}$ ,  $[\text{O}_2]=2500\text{ppm}$ ,  $T=30^\circ\text{C}$ ,  $P=1\text{ atm}$

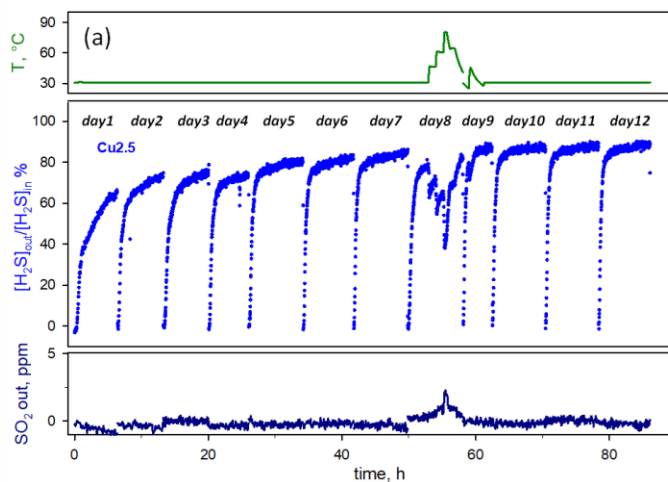
The adsorption capacity at saturation ( $\omega_{\text{ads}}$ ) of AC monolith is  $0.77\text{ mg S/g}$  referred to AC only that, compared to that evaluated for the granular sorbent under the same condition ( $11.6\text{ mg S/g}$ ) is much lower (Cimino et al., 2020), despite the very high surface area of AC monolith. This result suggests that the supposed presence of a binder in the commercial sample negatively affects the sorbent performance, likely preferentially occluding mesopores. Indeed, although the micropores volume of granular AC is comparable with that of the monolith a higher mesopores volume ( $0.58\text{ cm}^3/\text{g}$ ) is associated to granular AC particles.

For Cu-modified AC monoliths (2.5%wt and 5%wt Cu nominal loading) under wet conditions, the curve very slowly approaches the saturation, as also reported for Cu/AC granular sorbent (Cimino et al., 2020). As a consequence, the adsorption experiment was carried out in some days after overnight interruption (Figure 2.7). In some cases, temperature was also increased up to a max of  $90^\circ\text{C}$  to better understand how this parameter influences the adsorption

capacity of  $\text{H}_2\text{S}$ . At the end of each day, after suspension and re-start, the output concentration of  $\text{H}_2\text{S}$  returned to a value close to the initial one recorded for the fresh materials, then, in a quite short time it reaches the last value recorded the day before and then continued slowly to increase. The same behavior was observed for granular Cu-AC (Cimino et al., 2020) and attributed to the restoration of original active CuO sites via re-oxidation of metal sulphides (by dissolved oxygen) or via reduction of metal sulphates by reaction with additional  $\text{HS}^-$ .

Additional  $\text{H}_2\text{S}$  was adsorbed during day 8 (Figure 2.7 (a)), when temperature was increased, confirming the chemical nature of this phenomenon. Furthermore, the  $\text{SO}_2$  concentration can be considered negligible up to  $50^\circ\text{C}$  whilst few (3-4) ppm were detected at higher temperature suggesting some oxidation activity.

As expected, due to the higher copper load, both Cu-AC monoliths show the same qualitative trend although Cu5.0 requires more days to approach saturation (Figure 2.6 (b)).



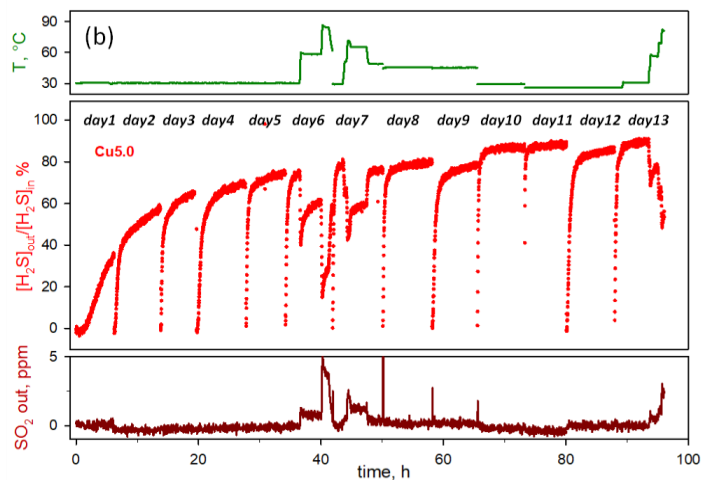


**Figure 2. 7** Breakthrough curves of 2.5% wt (a) and 5% wt (b) Cu-modified monoliths for H<sub>2</sub>S capture and SO<sub>2</sub> formation during adsorption test by varying T at P=1 atm in presence of humidity (HR=50%) and O<sub>2</sub>=2500 ppm

In Figure 2.8 the breakthrough curves of AC monoliths containing Mg are reported. For both Mg-containing sorbents H<sub>2</sub>S concentration is far from the feed concentration even after 6-7 days, suggesting a higher capture capacity with respect to Mg-free sorbents. For Cu2.5Mg2.5 sorbent, recovering of adsorption capacity of the fresh sorbent, although less marked, was observed after the overnight interruption, that very rapidly approaches that recorded at the end of the day before when the process restarts. On the contrary, for Mg5.0 only the quick response to the valve opening including the reactor again was observed.

When the temperature increases the curve moves faster towards saturation following an opposite trend with respect to Cu/AC sorbents (Zhang et al., 2006). Actually, this result is associated to an adsorption process with a prevailing physical nature.

Zhang et al. (2006) proposed that the basic character of MgO promotes the dissociation of H<sub>2</sub>S in HS<sup>-</sup> and H<sup>+</sup> and the formation of available sites for the oxidation of HS<sup>-</sup> to elemental sulphur. Therefore, MgO does not directly react with H<sub>2</sub>S but rather catalyzes H<sub>2</sub>S adsorption process.

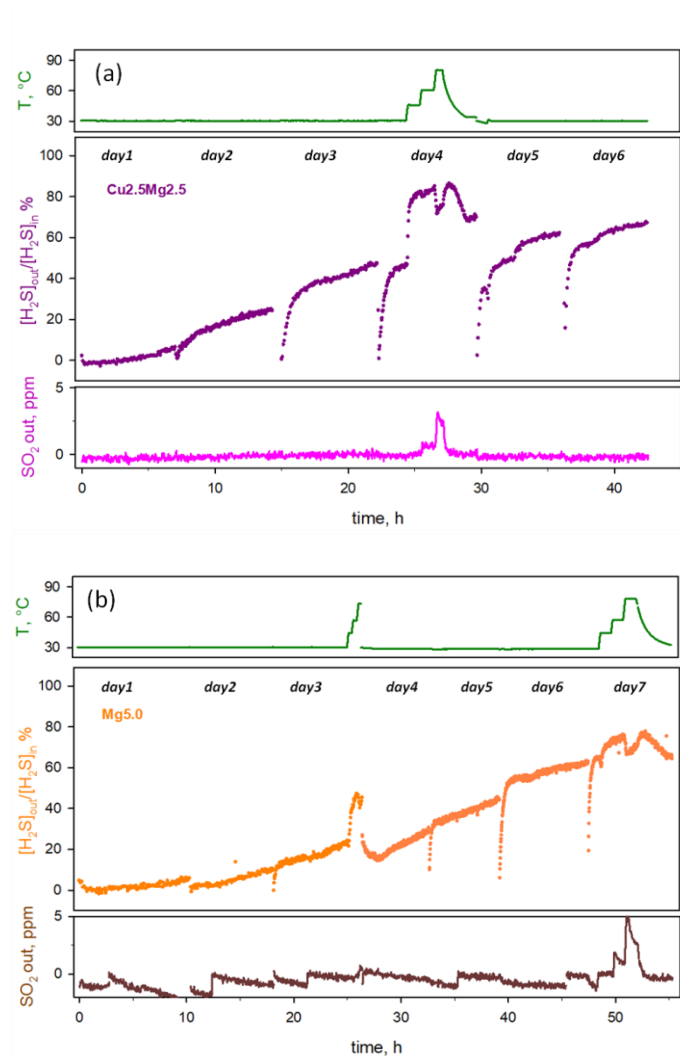


**Figure 2. 8** Breakthrough curves of 2.5% wt (a) and 5% wt (b) Mg-modified monoliths for H<sub>2</sub>S capture and SO<sub>2</sub> formation during adsorption test by varying T at P=1 atm in presence of humidity (HR=50%) and O<sub>2</sub>=2500 ppm

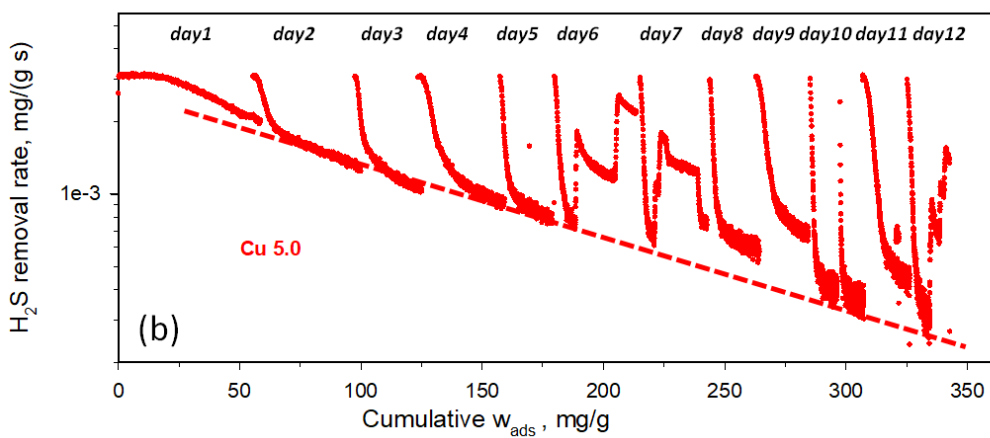
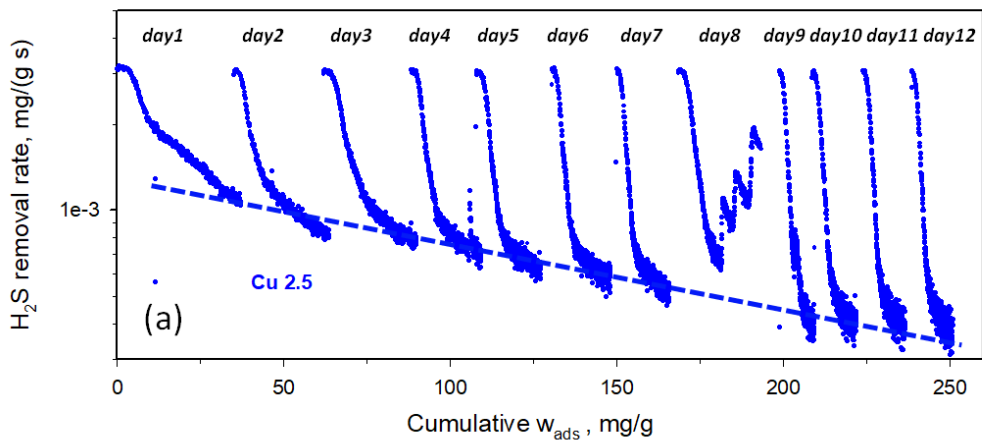
Figure 2.9 shows the trend of the apparent H<sub>2</sub>S removal rate as a function of cumulative amount of H<sub>2</sub>S adsorbed onto metal-modified ACs.

$$\text{H}_2\text{S removal rate} = \frac{Q^t C_{\text{H}_2\text{S}}^{\text{in}} \rho_{\text{H}_2\text{S}}}{m_{\text{MH}_2\text{S}}} \left( 1 - \frac{C_{\text{H}_2\text{S}}^{\text{out}}(t_i)}{C_{\text{H}_2\text{S}}^{\text{in}}} \right) \quad (2.2)$$

where  $Q^t$  [L s<sup>-1</sup>] is the total gas flow rate,  $C_{\text{H}_2\text{S}}^{\text{in}}$  [-] is the H<sub>2</sub>S volumetric fraction in the gas feed,  $C_{\text{H}_2\text{S}}^{\text{out}}$  [-] is the H<sub>2</sub>S volumetric fraction at time  $t_i$ ;  $\rho_{\text{H}_2\text{S}}$  is H<sub>2</sub>S density (1370 mg L<sup>-1</sup> at 30 °C and 1 bar) and  $M_{\text{H}_2\text{S}}$  [mg mmol<sup>-1</sup>] is its

molecular weight;  $m$  [g] is the sorbent dose and  $t_i$  represents the cumulative test time or calculated from the beginning of the test to second  $i$ .

This rate is maximum during the first day, then rapidly declines but starts from its maximum value the day after. The lower values reached at the end of each day seem to merge in a single master line which slowly declines with time. As Cimino et al. (2020) report for Cu/AC granular sorbent, at the very beginning of every daily experiment the rate is very high suggesting that a fast mechanism is activated again that in a short time is substituted by a slower mechanism. Nevertheless, it can be noticed that for Mg-containing sorbents the rate value is quite stable, i.e. it does not show an oscillating trend, and only after the 3<sup>rd</sup> day a very slow decline was observed.



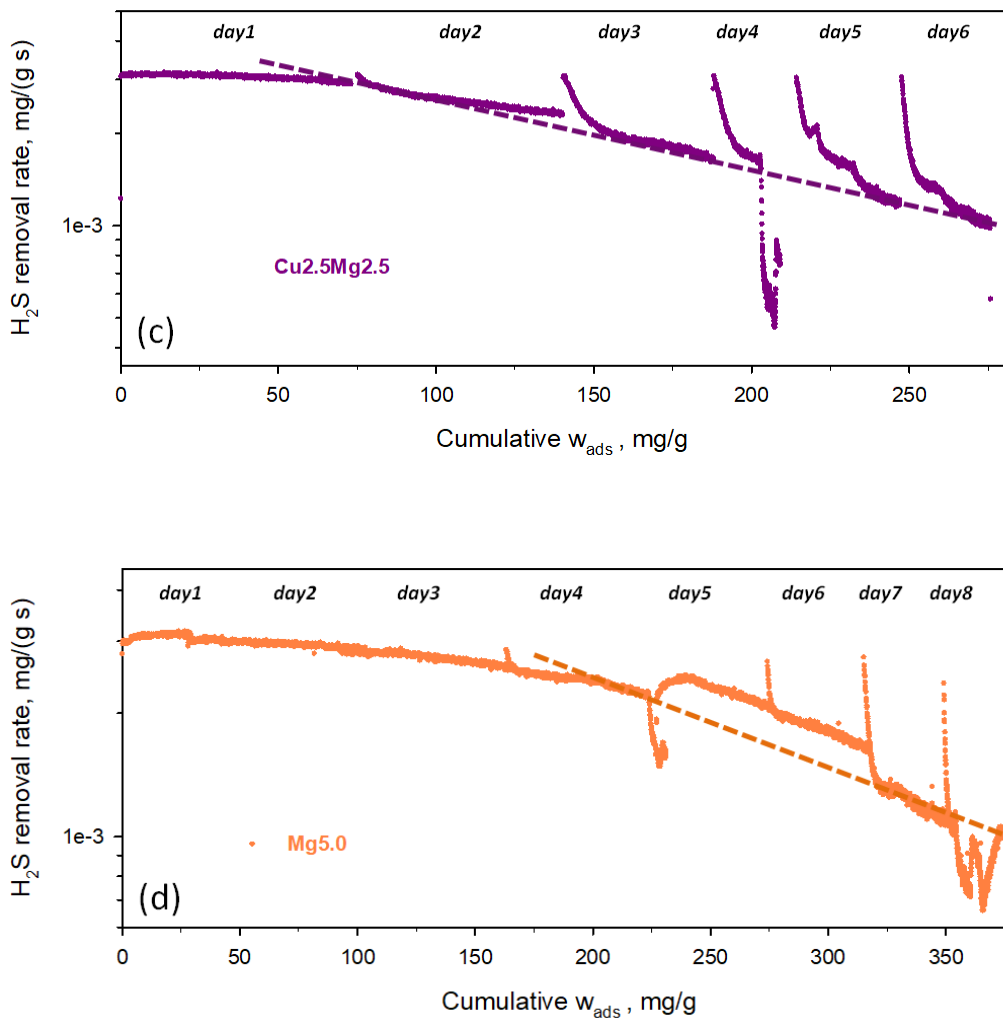


**Figure 2.9** Trend of apparent H<sub>2</sub>S removal rate over time of Cu<sub>2.5</sub> (a), Cu<sub>5.0</sub> (b), Cu<sub>2.5</sub>Mg<sub>2.5</sub> (c) and Mg<sub>5.0</sub> (d) (solid line). A master line (dashed line) connecting the values of H<sub>2</sub>S removal rate at the end of each day is reported.

Figure 2.10 reports a comparison of H<sub>2</sub>S adsorption capacity (a) and removal rate (b) in order to better show how the introduction of MgO positively affects the performance of modified monoliths. This rate is still very high also for large H<sub>2</sub>S capture values when it is strongly reduced for AC monolith and the two sorbents containing copper only.

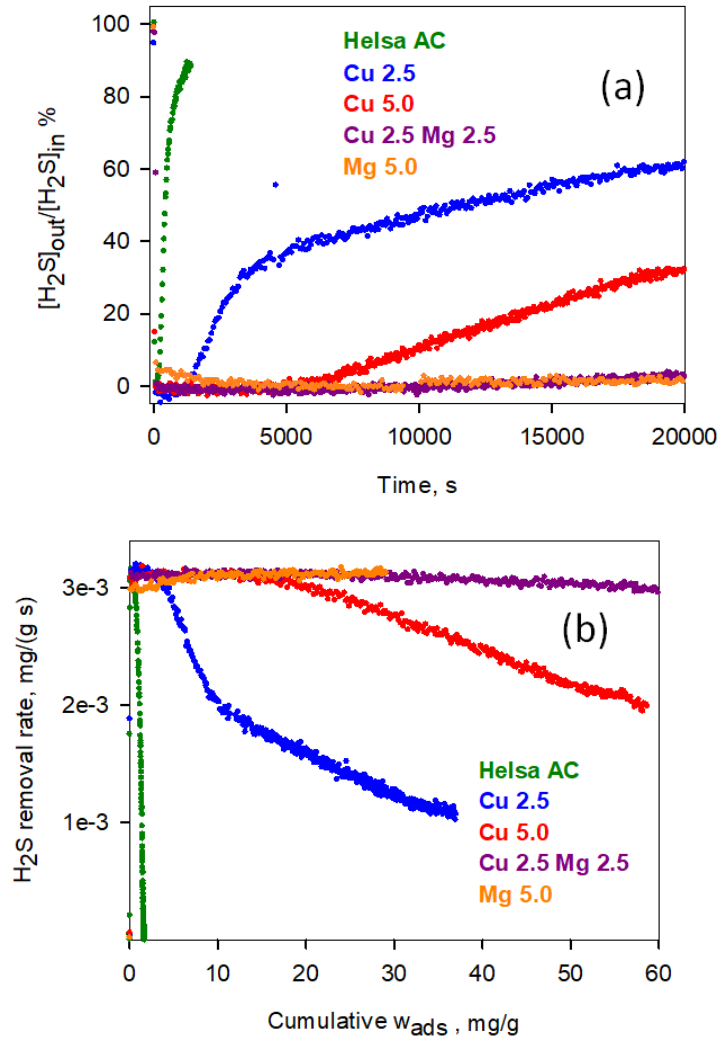


**Figure 2.10** Comparison of breakthrough curves (a) and apparent H<sub>2</sub>S removal rate (b) of monoliths for H<sub>2</sub>S capture at T=30°C, P=1atm in presence of humidity (HR=50%) and O<sub>2</sub>=2500 ppm

In Table 2.3 breakthrough time  $t_{br}$  [h] corresponding to  $C_{H_2S}^{out}(t)/C_{H_2S}^{in}(t) = 0.05$  and  $\omega_{br}$ , defined as the specific amount of sulphur captured from the starting to breakthrough time, are reported. In the last column of the same table  $\omega_{test}$ , corresponding to the amount of H<sub>2</sub>S captured up to the end of the adsorption test, is reported together with the time length of the test.  $\omega_{test}$  coincides with  $\omega_{ads}$ , i. e. the specific amount of sulphur captured up the time corresponding to 99% H<sub>2</sub>S capture, only for the AC monolith. As a

consequence, values of  $\omega_{test}$  are not directly comparable but the time length must be taken into account.

**Table 2. 3** Specific amount of sulphur captured out up to the breakthrough point ( $\omega_{br}$ ) and up to the end of the tests ( $\omega_{tests}$ ) during H<sub>2</sub>S adsorption experiments carried t at 30°C under co-presence of H<sub>2</sub>O + O<sub>2</sub>

	$t_{br}$ [h]	$\omega_{br}$ [mg S g <sup>-1</sup> ]	t [h]	$\omega_{tests}$ [mg S g <sup>-1</sup> ]
<b>Helsa AC</b>	0.06	0.24	0.4	0.77
<b>Cu 2.5</b>	0.43	4.39	86	252.3
<b>Cu 5.0</b>	2.11	21.89	96	341.4
<b>Cu 2.5 Mg 2.5</b>	6.10	63.12	42	274.0
<b>Mg 5.0</b>	9.33	82.90	55	371.9

*All values were calculated referred to the carbon content in the monolith only*

The amount of H<sub>2</sub>S captured at the breakthrough point increases with copper load and for Cu5.0 it approaches that evaluated for a granular AC sorbent (25 mg S g<sup>-1</sup>) containing a double total amount of metals (5%Cu+5%Zn) (Cimino et al., 2020). Moreover, it is much higher for the Mg-based monolith with respect to that of the Cu-based monolith with the same metal load and reached in a longer time due to an evident different adsorption kinetics.

The capture capacity at the breakthrough point, which corresponds to a breakthrough time as high as 560min (about 9h), so assuring an exit H<sub>2</sub>S concentration equal to zero for a very long time, is largely enhanced by the introduction of Mg.

Since duration of tests reported in Table 2.3 is not comparable with that of granular sorbents, in Table 2.4 the H<sub>2</sub>S amount captured up to 5.5 h by structured and granular sorbents is reported. Taking into account that the monolith sorbents have a half metal load with respect to granular sorbents, the H<sub>2</sub>S capture capacity is about the same.

**Table 2. 4** Comparison of specific H<sub>2</sub>S adsorption capacity ( $\omega_{ads}$ ) up to 5.5h of monoliths and granular ACs at 30°C under co-presence of H<sub>2</sub>O + O<sub>2</sub>

<b>Monoliths</b>	<b><math>\omega_{ads}</math> [mg S g<sup>-1</sup>]</b>	<b>Granular ACs</b>	<b><math>\omega_{ads}</math> [mg S g<sup>-1</sup>]</b>
<b>Cu 5.0</b>	50.84	<b>Cu 10%</b>	129.2*
<b>Cu 2.5 Mg 2.5</b>	57.63	<b>Cu 5% Zn 5%</b>	118*
<b>Mg 5.0</b>	52.87		

\* Referred to (Cimino et al., 2020)

In order to underline how considerably temperature influences the efficiency of H<sub>2</sub>S capture process, Figure 2.10 shows how both the trend of H<sub>2</sub>S adsorption capacity and apparent removal rate changes up to 90°C. By increasing the temperature, the H<sub>2</sub>S adsorption capacity of Cu2.5 (Figure 2.11(a)) and Cu5.0 (Figure 2.11(b)) increases linearly and to a greater extent in presence of a higher copper content and, at same time, H<sub>2</sub>S removal rate increases. For both samples, SO<sub>2</sub> begins to form (3-4 ppm) only when the temperature reaches the maximum of 80°C. As soon as the temperature decreases, even the small concentration of sulphur dioxide goes to zero. As previously reported, the opposite effect was observed in the presence of magnesium as a rapid approach to saturation occurs. In particular, for Mg-containing sorbents, a non-linear decrease of the adsorption capacity is recorded when the temperature rises up to about 50°C, while over 80°C the H<sub>2</sub>S concentration at bed outlet returns to decrease again (i.e. the adsorption capacity increases). The variation of temperature leads to a greater change in the adsorption capacity in the case of the mixed sorbent (Figure 2.11(c)) compared to Mg5.0 (Figure 2.11(d)). Also in this case, a few ppm of SO<sub>2</sub> appears at about 80°C.

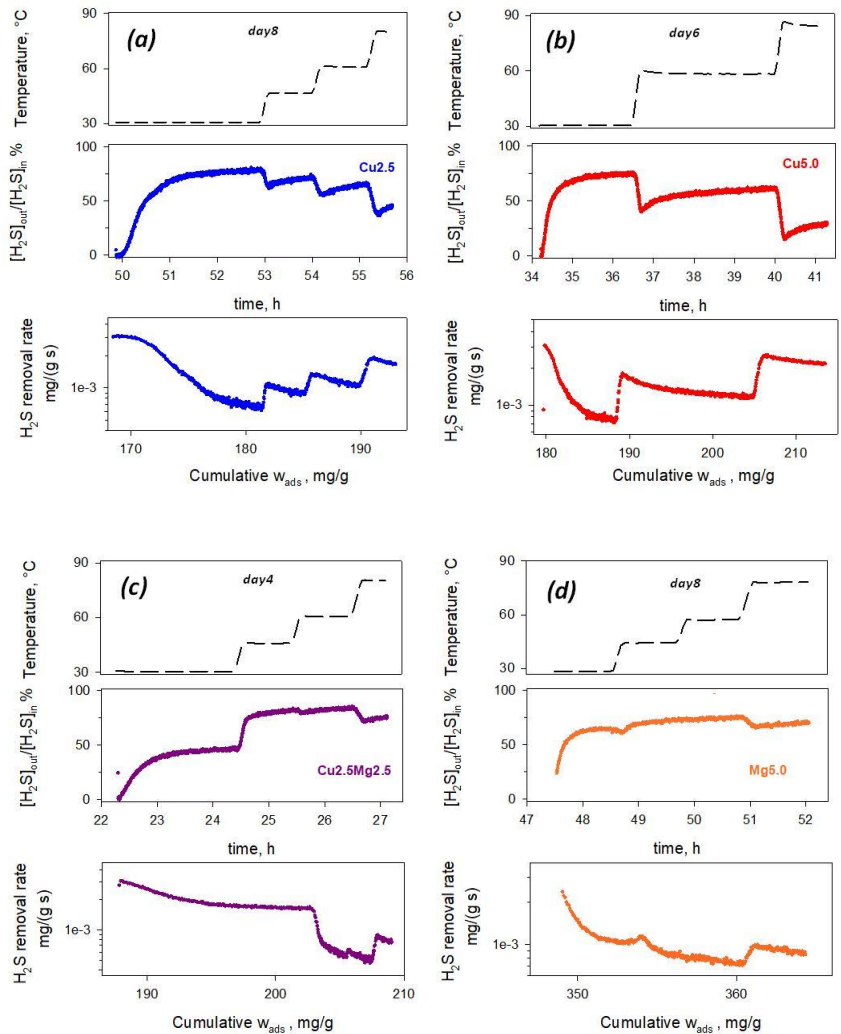


**Figure 2. 11** Effect of temperature on the H<sub>2</sub>S adsorption capacity and the apparent H<sub>2</sub>S removal rate of Cu2.5 (a), Cu5.0 (b), Cu2.5Mg2.5 (c) and Mg5.0 (d)

With the aim of evaluating how both the H<sub>2</sub>S adsorption capacity and its removal rate change with the flow rate, additional adsorption tests were carried out on the mixed Cu and Mg modified sorbent setting an inlet flow rate at 25 sL h<sup>-1</sup> keeping constant the H<sub>2</sub>S concentration. Figure 2.12 shows a comparison of adsorption tests lasted two days for both Q=20 sl h<sup>-1</sup> and Q=25 sl h<sup>-1</sup>.

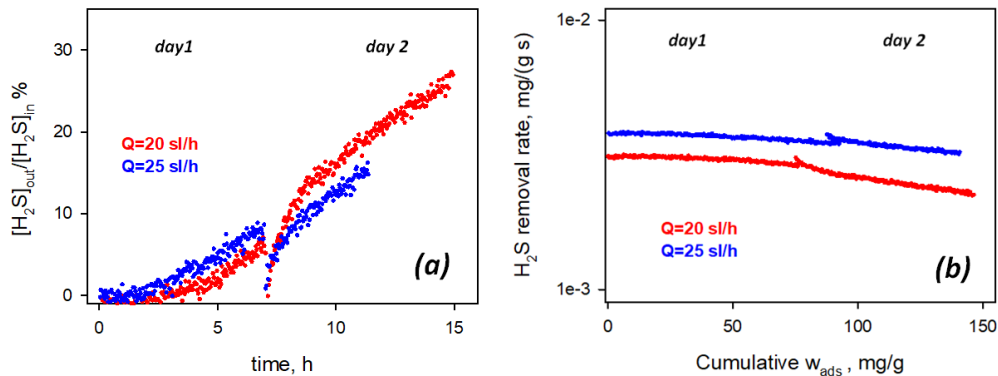


**Figure 2. 12** Effect of inlet flow rate on breakthrough curves and the apparent H<sub>2</sub>S removal rate of Cu<sub>2</sub>.5Mg<sub>2</sub>.5 by varying inlet flow rate at P=1 atm in presence of humidity (HR=50%) and O<sub>2</sub>=2500 ppm

As clearly shown in Figure 2.12(a) a lower flow rate during the first day results in a higher removal efficiency (red curve). Actually, a lower amount of H<sub>2</sub>S per unit time contacts the sorbent since the feed H<sub>2</sub>S concentration is the same in both cases. Nevertheless, the day after an inversion of curves was observed due to a lower slope of the blue curve. This can be better highlighted in Figure 2.12(b). Indeed, during the first day the removal rate are rather parallel even if the rate corresponding to 25sl/h is always higher, whereas during the second day the removal rate decreases with a greater slope at lower flow rate. Despite this difference between the first and second day, the removal rate is always greater operating at higher total flow rate, as shown in Fig. 2.12 (b).

In Table 2.5 breakthrough time  $t_{br}$  [h] corresponding to  $C_{H_2S}^{out}(t)/C_{H_2S}^{in}(t) = 0.05$  and  $\omega_{br}$ , defined as the specific amount of sulphur captured from the starting to breakthrough time, is reported for the two flow rates. In the last column of the same table  $\omega_{10}$ , corresponding to the amount of H<sub>2</sub>S captured up to 10h of the adsorption test, is reported. As expected, a shorter time is required to capture about the same amount of sulphur ( $\omega_{br}$ ) when a larger amount of H<sub>2</sub>S is fed per unit time and for a time length of 10h a greater amount of sulphur is captured for Q=25 sl h<sup>-1</sup>. This result suggests that the slow adsorption process, occurring after the sorbent is not able any more to capture most of H<sub>2</sub>S from the

gas stream, depends on the flow rate. The complex phenomena taking place after the initial fast adsorption are better explained on the basis of the results of TPD experiment reported in the next paragraph.

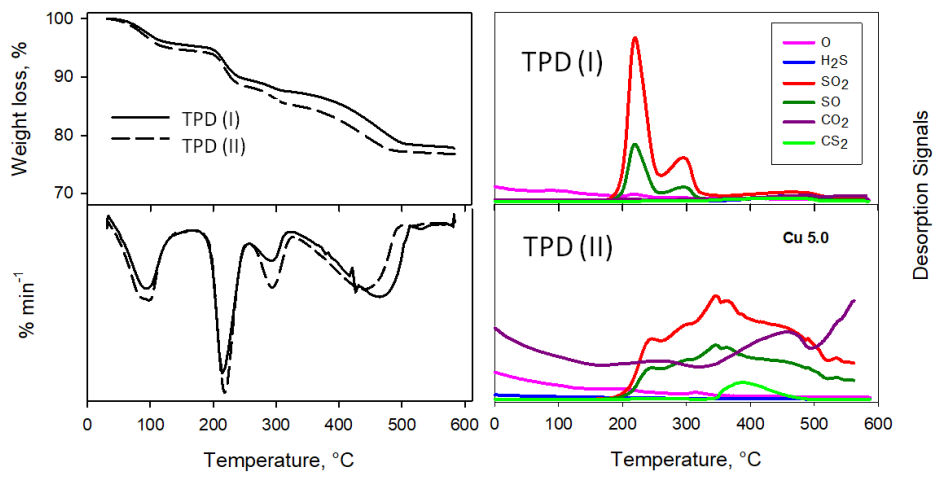
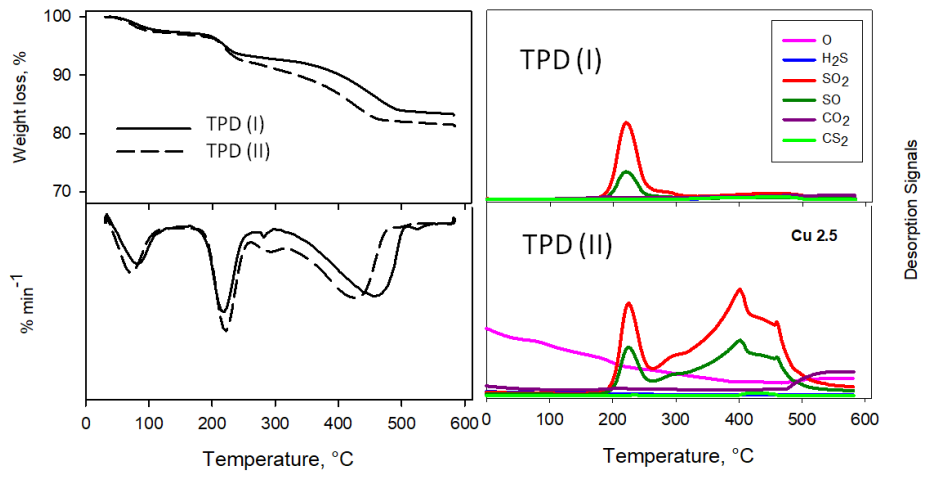
**Table 2. 5** Specific amount of sulphur captured out up to the breakthrough ( $\omega_{br}$ ) and up to 10h of the tests ( $\omega_{10}$ ) during H<sub>2</sub>S adsorption experiments carried t at 30°C under co-presence of H<sub>2</sub>O + O<sub>2</sub> with different flow rates

<b>Inlet Flow Rate</b> [sL h <sup>-1</sup> ]	<b>t<sub>br</sub></b> [h]	<b>ω<sub>br</sub></b> [mg S g <sup>-1</sup> ]	<b>ω<sub>10</sub></b> [mg S g <sup>-1</sup> ]
20	6.09	63.12	99.64
25	4.95	61.89	122.48

### 2.2.3. Temperature Programmed Desorption tests

Results of tests carried out over more days with the overnight interruption suggested that freshly adsorbed sulphur species underwent some modifications under static conditions occurring during the night, when no further H<sub>2</sub>S is fed to the reactor, for Cu-containing sorbents.

To this end Temperature Programmed Desorption (TPD) tests carried out in TG-MS systems after a short time (few hours) (TPD (I)) and 2 months (TPD (II)) after the same H<sub>2</sub>S capture experiments were made in order to highlight, the slow reactions that took place leading to the stabilization of different sulphur species. Results are reported in Figure 2.13 as weight loss recorded during the TGA experiments together with the derivative curves and signals of m/z recorded by the coupled MS.



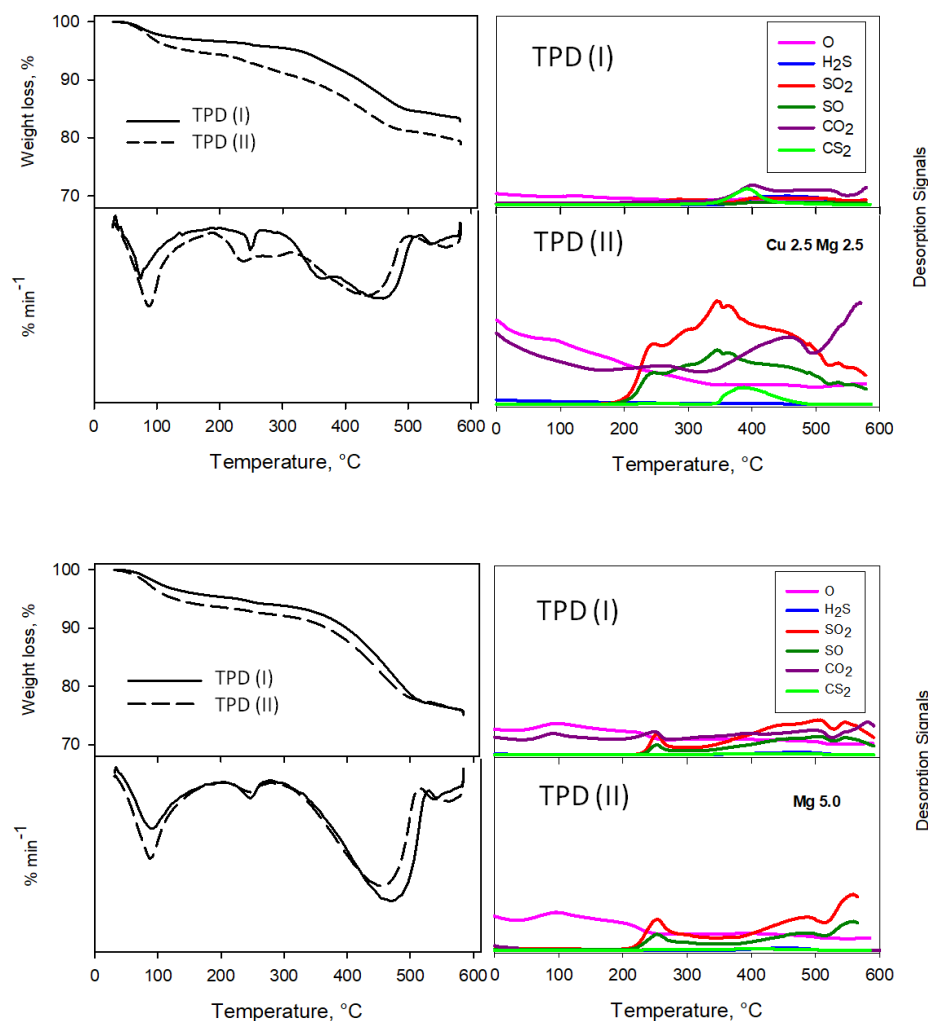


**Figure 2. 13** Comparison of weight loss % and species release during TPD tests under Ar flux from H<sub>2</sub>S saturated modified AC after few minutes (TPD (I)) and two months (TPD(II)) respectively later H<sub>2</sub>S adsorption tests. Derivative curves (down) of weight losses.

Some common qualitative features can be observed for all sorbents and for both types of test: a first weight loss at 100°C, basically related to the release of physisorbed water, a second weight loss at 200-350°C, and a weight loss at higher temperature (400-550°C). Nevertheless, these features quantitatively changes both changing the sorbent formulation and the time elapsed between adsorption and TPD, especially for Cu-containing materials. In particular, a higher weight loss is recorded for all Cu-containing sorbents at the end of the TPD experiment carried out after two months suggesting a transformation of

the freshly adsorbed sulphur species into more easily desorbed species with time.

The first main difference was observed in the range 200-350°C. In the TPD (I) of Cu modified sorbents, the weight loss corresponds to the emission of two SO<sub>2</sub> peaks (coupled to the SO fragment) at 220°C and 300°C, that at higher temperature more evident Cu5.0. For Mg containing sorbents in the same range of temperature a weight loss with a gentler slope does not correspond to none of the species monitored by MS in the TPD (I).

All the samples show a last weight loss, significantly greater for Mg5.0, starting from 430-450° C. This weight loss does not correspond to detection of species at MS for all sorbents during TPD (I) and can be reasonably associated to elemental sulphur which evaporates as S<sub>x</sub> chains. Indeed, the formation of elemental sulphur is reported for both Cu- (Haimour et al., 2005) and Mg-modified (Boutillara et al., 2019) carbons by oxidation of H<sub>2</sub>S catalyzed by the metal. In conclusion, the presence of copper in the sorbent formulation seems associated to the formation of both sulphates and elemental sulphur, the former decomposed at lower temperature, whereas magnesium promotes the formation of elemental sulphur representing the prevailing species when copper is absent.

Different results were obtained by TPD tests carried out on H<sub>2</sub>S-saturated sorbents stored at room temperature for two months (TPD II), confirming what suggested in the adsorption tests carried out after the overnight interruption, i.e. the nature of adsorbed sulphur changes.

For both Cu2.5 and Cu5.0 the emission of SO<sub>2</sub>/SO at high temperature associated to the last weight loss, corresponding to species not detected by MS in TPD (I), was recorded. Probably transformation of elemental sulphur into sulphates occurs in presence of copper which slowly catalyzes its oxidation in the presence of gaseous O<sub>2</sub>. The decomposition of these new sulphates occurs at higher temperature with respect to that of sulphates formed at the beginning of the adsorption step. In order to verify that the new species consist of copper sulphate a AC monolith was impregnated by incipient wetness technique with

an aqueous solution of  $\text{CuSO}_4 \cdot 5 \text{H}_2\text{O}$  to obtain a nominal Cu loading of 5% wt. followed by drying at  $120^\circ\text{C}$  and a TPD was carried out. Results are reported in Figure 2.14.

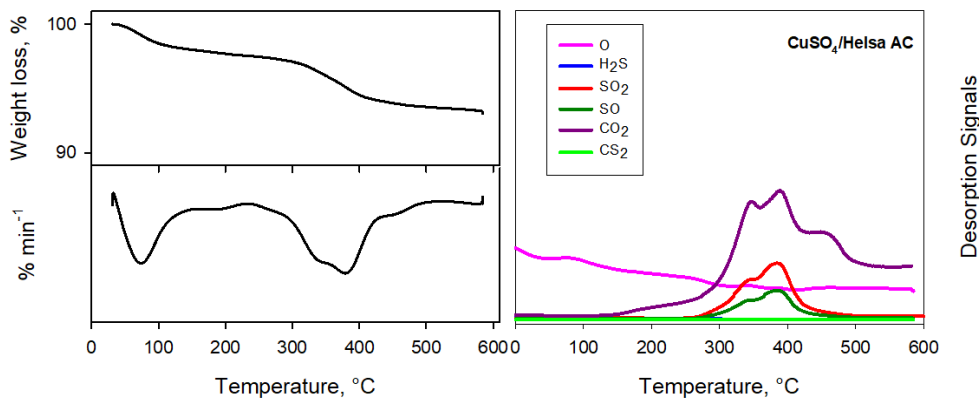


**Figure 2. 14** Weight loss % and species release during sulphates decomposition under  $\text{N}_2$  flux from  $\text{CuSO}_4$  impregnated on AC

The decomposition of the supported copper sulphate resulted in the desorption of  $\text{SO}_2$  (coupled to the corresponding SO signal) in the range  $300\text{--}500^\circ\text{C}$ , suggesting that the additional  $\text{SO}_2$  emission observed in the “aged” sorbents in this temperature range can be associated to the formation  $\text{CuSO}_4$ . On the other hand, this also suggests that the supposed sulphate initially formed, associated to  $\text{SO}_2$  emission at lower temperature, are not copper sulphate but more easily decomposable species due to different nature, location or dimension with respect to  $\text{CuSO}_4$ .

Both TPD tests carried out, both after few hours and two months, on Mg5.0 show a different behavior in contrast with that of the two Cu/AC sorbents. The intermediate weight loss, that occurring after adsorbed water was released, can be considered negligible, whereas a larger weight loss was detected at  $350\text{--}500^\circ\text{C}$ . This last phenomenon is not associated to one of the species followed by MS and can reasonably associated to the formation of Sx chains whilst only a weak emission of  $\text{SO}_2$  was detected at high temperature.

To sum up, the very first difference of behavior between Cu- and Mg-based sorbents is that the evolution/transformation observed for copper containing sample with time is basically negligible when magnesium is the only added element of the monolith formulation. In other words, magnesium does not seem able to catalyze the oxidation of elemental sulphur to sulphates.

These results are in agreement with the absence of initial adsorption rate recovery observed in the long run tests after the overnight interruption for Cu-containing sorbents.

As expected, an intermediate behavior is reported for the mixed sorbent containing both Cu and Mg. H<sub>2</sub>S capture seems to occur with a mechanism mostly associated to the presence of magnesium as shown by the absence of the low temperature peak related to the sulphate-like species. Nevertheless, after two months storage the sulphur accumulated in the material is partially converted into CuSO<sub>4</sub>, and some low temperature sulphate species as well, due to the presence of copper.

The corresponding values of the weight losses for the various sorbents in the two temperature ranges of interest (excluding the first weight loss associated to water desorption) are reported in Table 2.6.

**Table 2. 6** Weight loss % during TPD tests under Ar flux from H<sub>2</sub>S saturated modified AC

Sorbent	Weight loss %			
	TPD I		TPD II	
	150-320°C	350-500°C	150-320°C	350-500°C
<b>Cu2.5</b>	4.85	8.02	6.60	7.48
<b>Cu5.0</b>	8.05	8.39	9.41	7.37
<b>Cu2.5Mg2.5</b>	1.86	9.26	4.46	8.32
<b>Mg5.0</b>	2.59	13.97	2.62	12.89

It is interesting to notice that the weight loss related to the first SO<sub>2</sub> emission recorded in the TPD carried out just after the adsorption is proportional to the copper content for Cu2.5 and Cu5.0 whereas it is lower for the mixed sorbent and Mg5.0. The weight loss in the range 350-500°C is quite similar except for Mg5.0, giving a higher contribution and seems related to the higher capacity of magnesium to promote the formation of elemental sulphur.

An increase of sulphate-like species desorbing SO<sub>2</sub> in the low temperature range was observed for both Cu2.5 and Cu5.0 samples at expense of elemental sulphur initially formed in the TPD (II), the higher total weight loss can indicate that oxygen from oxygenated surface groups in addition to gaseous O<sub>2</sub> was used to form sulphate-like species.

Interestingly, for Mg5.0 sorbent, the two contributions do not significantly change after the storage of the saturated sorbent. The absence of copper in this sample is a clear indication that the modification of sulphur species with time is promoted/catalyzed by copper. In agreement with this hypothesis the sorbent containing both copper and magnesium is able to convert with time a significant fraction of elemental sulphur initially formed, due to the presence of magnesium, into sulphate species.

Although a material balance of sulphur is impossible due to the impossibility to detect the emission of elemental sulphur, the repeatability of results of cyclic experiments (adsorption/TPD) suggests that most of sulphur is desorbed up to 620°C leaving the active metals able to activate the H<sub>2</sub>S adsorption again.

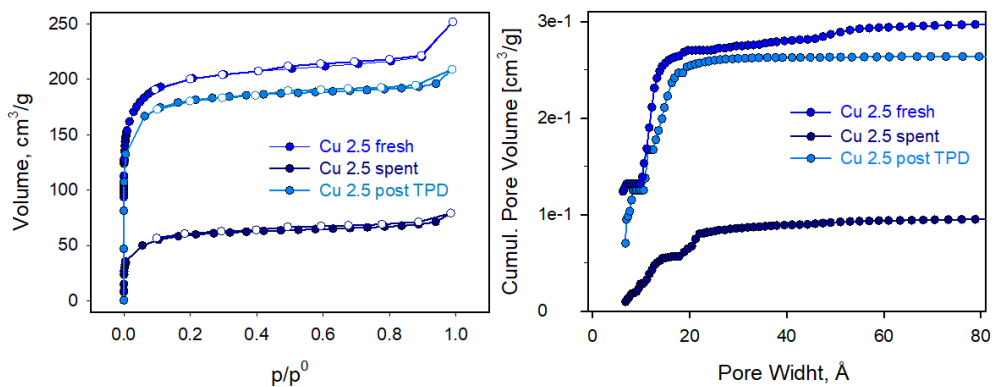
The results of all these experiments clearly highlight the different role of copper and magnesium in H<sub>2</sub>S reactive adsorption. Copper oxide activates a fast chemical adsorption with a rapid formation of sulphate-like species and, only after saturation of centers promoting this phenomenon, adsorption of H<sub>2</sub>S as elemental sulphur occurs. If H<sub>2</sub>S feed is interrupted a slow transformation of elemental sulphur into additional sulphates, identified as CuSO<sub>4</sub>, takes place. On the other hand, magnesium oxide promotes the oxidation of H<sub>2</sub>S to

elemental sulphur and, in the absence of copper, is not able to activate the further oxidation to sulphate. When both metals are present in the sorbent formulation, the mechanism activated by magnesium prevails on that activated by copper and a very limited fast formation of sulphates occurs. Nevertheless, copper is able with time to transform the elemental sulphur into copper sulphate. In other words, magnesium activates only one type of mechanism whilst copper activates two mechanisms: a fast mechanism of oxidation of H<sub>2</sub>S to sulphate-like species and a slow mechanism of oxidation of elemental sulphur to CuSO<sub>4</sub>.

#### 2.2.4. Sorbent characterization after adsorption/desorption tests

Textural properties of metal modified AC honeycomb after adsorption and desorption tests have been investigated using N<sub>2</sub> physisorption at -196°C. Figure 2.15 reports the adsorption and desorption isotherms of metal modified honeycomb and cumulative pore volume after TPD up to 620°C with N<sub>2</sub> gaseous stream.

All adsorption isotherms show a dramatic decrease of N<sub>2</sub> adsorbed volume after H<sub>2</sub>S adsorption which, on the other hand, is almost totally recovered after TPD test.



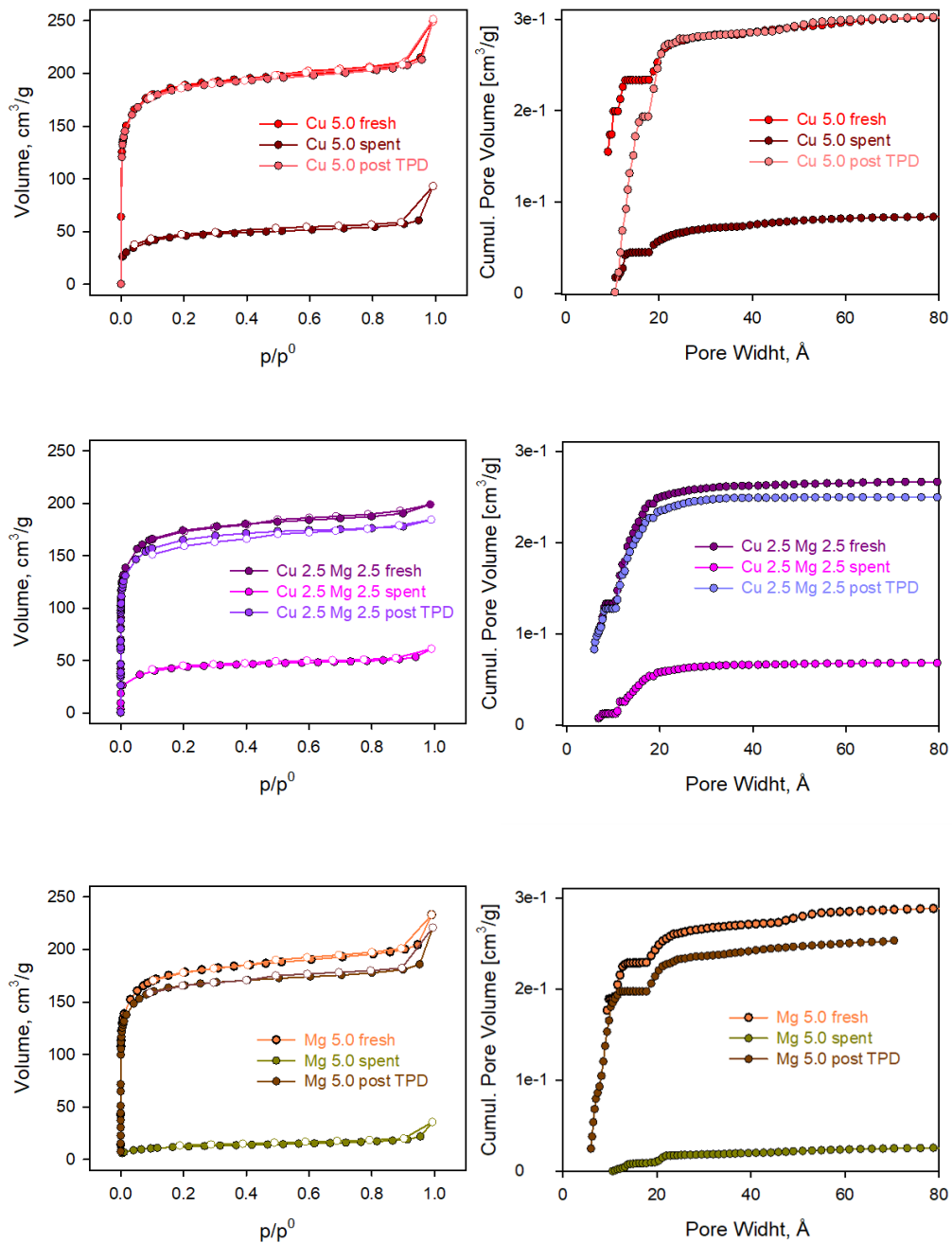


**Figure 2.15**  $N_2$  physisorption isotherms at 77K and PSD for fresh and spent modified monoliths

In Table 2.7 values of BET surface area and micro-, meso- and total pore volume is reported for both spent and regenerated (after TPD) sorbents compared with those of the fresh samples, already reported in Table 2.2. In the

same Table the total amount of sulphur adsorbed at the end of the H<sub>2</sub>S capture test is also reported in order to recall this quantity which is strictly correlated with the reduction of pore volume.

**Table 2. 7** BET area and pore volume of pure of metal modified AC monoliths as fresh, spent and regenerated after TPD

<b>Sorbents</b>		<b>Cu2.5</b>	<b>Cu5.0</b>	<b>Cu2.5Mg2.5</b>	<b>Mg5.0</b>
<b>A<sub>BET,monolith</sub></b> <b>m<sup>2</sup>/g</b>	<i>fresh</i>	762	719	640	676
	<i>spent</i>	209	172	155	44
	<i>regen.</i>	682	707	606	632
<b>ω<sub>tests</sub></b> <b>[mg S g<sup>-1</sup>]</b>	<i>spent</i>	253.3	341.4	274.0	371.9
<b>Cumulative Micropore</b> <b>Volume<sub>monolith</sub>*</b> <b>cm<sup>3</sup>/g</b>	<i>fresh</i>	0.2145	0.2177	0.1917	0.2159
	<i>spent</i>	0.0045	0.0397	0.0323	0.006
	<i>regen.</i>	0.1868	0.2230	0.1799	0.1893
<b>Cumulative Mesopore</b> <b>Volume<sub>monolith</sub>**</b> <b>cm<sup>3</sup>/g</b>	<i>fresh</i>	0.061	0.0667	0.0686	0.0544
	<i>spent</i>	0.0825	0.0337	0.0321	0.0137
	<i>regen.</i>	0.0745	0.0621	0.0662	0.0503
<b>Cumulative Total</b> <b>Volume<sub>monolith</sub>**</b> <b>cm<sup>3</sup>/g</b>	<i>fresh</i>	0.2806	0.2844	0.2603	0.2703
	<i>spent</i>	0.0870	0.0734	0.0644	0.0197
	<i>regen.</i>	0.2613	0.2851	0.2461	0.2396

Indeed, all sorbents undergo a dramatic decrease of surface area upon H<sub>2</sub>S adsorption mostly assignable to the occlusion of micropores. Mesopores, present in a lower extent, are less involved in the sorption mechanism. The highest loss of surface area is associated to Mg5.0, as expected due to the large amount of sulphur captured. This sorbent, as evaluated by TGA-MS experiments adsorbs H<sub>2</sub>S mostly as elemental sulphur. Assuming the density of elementary sulphur 2 cm<sup>3</sup>/g, the volume occupied by the sulphur in the sorbents corresponds to about the half of difference between the total cumulative volume of the fresh and spent sorbents, as shown in Table 2.8. The inconsistency in

volumes can be probably attributed to the high-vacuum degassing treatment to which the samples are subjected before N<sub>2</sub> adsorption measurements at -196°C, likely promoting the release of some sulphur.

Nevertheless, it must be noticed that all these porosimetric measures were made 2-3 months after the capture test and, as a consequence, the estimation of volume of sulphur can be reliably made for Mg5.0 only, being the fraction of different sulphates not easily estimable.

**Table 2. 8** Comparison of volume occupied by elemental sulphur and the difference between the total cumulative volume of the fresh and spent sorbents

<b>Sorbent</b>	<b>V<sub>Sulphur</sub>, cm<sup>3</sup>/g</b>	<b>V<sub>fresh</sub>-V<sub>spent</sub>, cm<sup>3</sup>/g</b>
<b>Cu2.5</b>	0.08	0.19
<b>Cu5.0</b>	0.11	0.21
<b>Cu2.5Mg2.5</b>	0.09	0.20
<b>Mg5.0</b>	0.12	0.25

#### **2.2.5. XPS analysis**

Both fresh and spent Cu5.0 and Cu2.5Mg2.5 sorbents have been analyzed by XPS after few months after the H<sub>2</sub>S capture test. Comparison of XPS spectra in Cu2p spectral region of fresh and spent samples are reported in Figure 2.16.

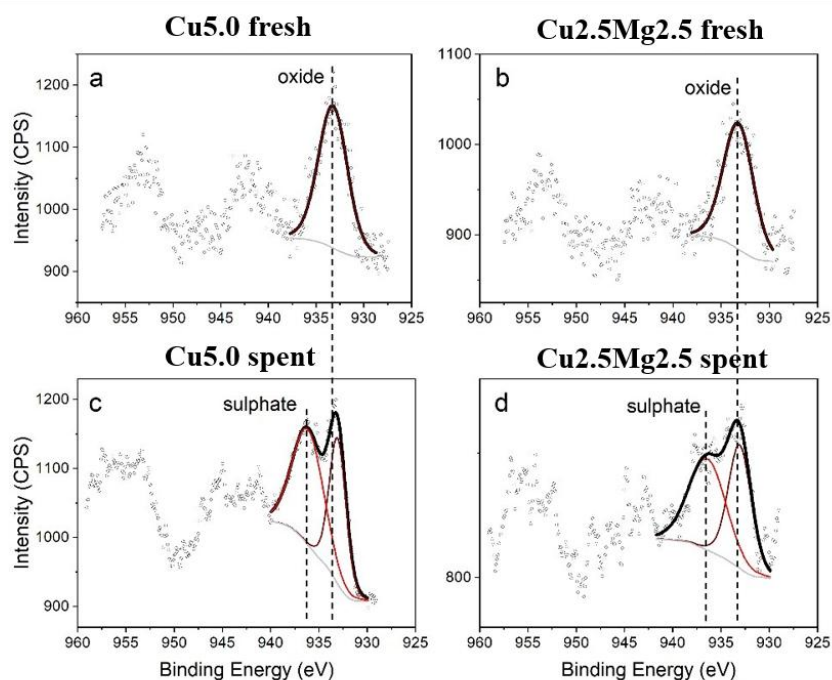


**Figure 2. 16** XPS spectra in Cu2/p spectral region of fresh (a and b) and spent (c and d) Cu5.0 and Cu2.5Mg2.5 sorbents.

Both fresh sorbents show the presence of copper oxide which is partially converted into sulphate after H<sub>2</sub>S adsorption, as highlighted by the 2p<sub>3/2</sub> spectral line at 932.45 eV of CuO in Figure 2.16 (a and b). An additional signal at higher binding energy, appearing for spent sorbents and overlapping that of CuO, account for the formation of sulphates. A higher ratio between sulphate and oxide can be observed for the Cu5.0 sample with respect to Cu2.5Mg2.5 sorbent, confirming that copper favors the formation of sulphates further enhanced after an ageing period.

Formation of sulphates was also confirmed by spectra collected in the O1s region, shown in Figure 2.17 which have a higher intensity thus allowing a better deconvolution of the signals.

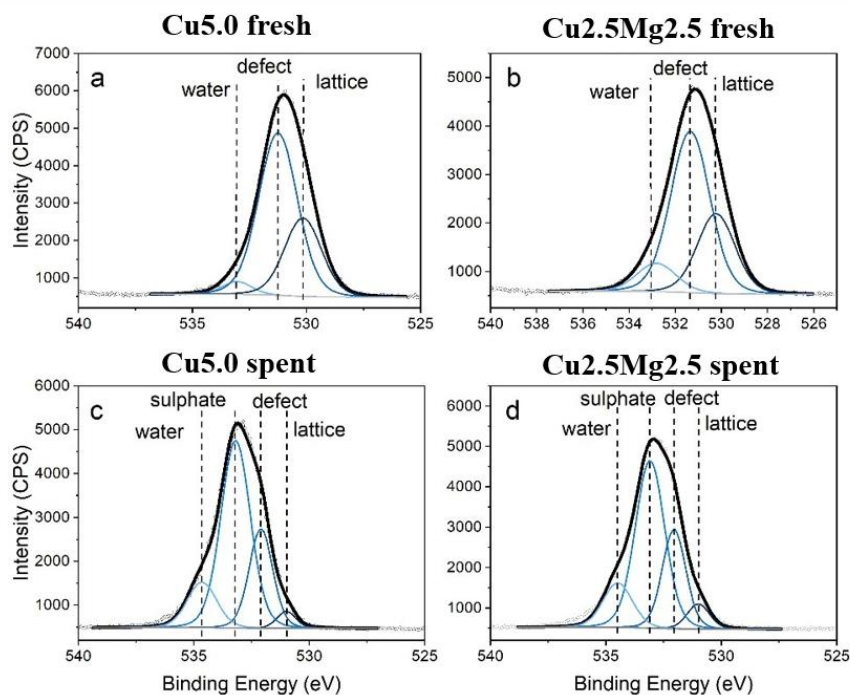


**Figure 2. 17** XPS spectra in O1s spectral region of fresh (a and b) and spent (c and d) Cu5.0 and Cu2.5Mg2.5 sorbents

Finally, spectra in the S2p region (Figure 2.18 (a and c)) confirms the formation of sulphates in addition to elemental and organic sulphur. Both spectra in Figure 2.18 (a) and Figure 2.18 (c) of spent aged sorbents suggest the formation of two types of sulphates, as also highlighted by TPD experiments. The quite low intensity of the signal of elemental sulphur can be related to the possible loss under the high vacuum condition of XPS analysis of this more labile species.

Spectra in Figure 2.18 (b) and Figure 2.18 (d) show Cu2.5Mg2.5 sorbent both as fresh and as spent in the Mg1s spectral region indicating the presence of a magnesium oxide/hydroxide in the fresh sorbent and the formation of magnesium sulphate, in addition to copper sulphate, in this mixed sorbent.

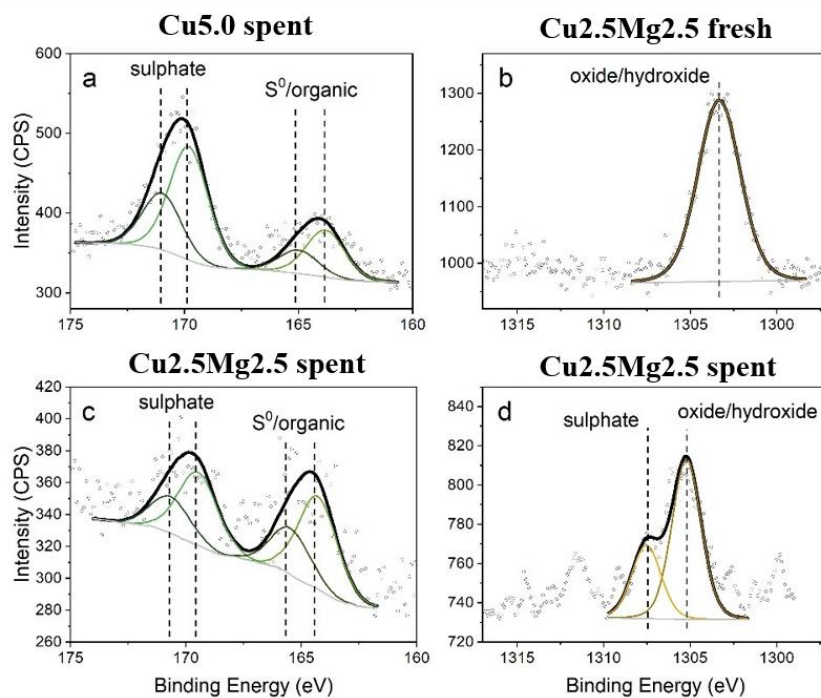


**Figure 2. 18** XPS spectra in S2p spectral region of spent Cu5.0 and Cu2.5Mg2.5 sorbents (a and c) and in the Mg1s region of fresh and spent Cu2.5Mg2.5 (c and d).

The XPS results confirm the complexity of sulphur species formed during the adsorption and their evolution with time in the presence of oxygen and water vapour. Furthermore, the results confirm the main role of copper in catalysing this transformation further promoted by the presence of oxygen and water.

### 2.2.6. Sorbents regeneration

With the aim of verifying the sorbents regenerability, four cycles of adsorption tests setting the total inlet flow rate at  $25 \text{ SL h}^{-1}$ , each lasted two days, in co-presence of humidity and  $\text{O}_2$  at  $T=30^\circ\text{C}$ ,  $P=1\text{atm}$  and subsequent TPD at  $600^\circ\text{C}$  in  $\text{N}_2$  flow were conducted on the sorbent containing both metals, Cu2.5Mg2.5. As shown by the overlapping of the adsorption isotherms reported in Figure 2.18, the sorbent is completely regenerated at the end of each adsorption/TPD cycle. The isotherms relating to both cycles 1 and 2 are

perfectly stackable as the sorbent completely resumes its activity. The last two cycles (3 and 4) were performed in conditions of higher external temperature of the saturator (4-5 °C more) and consequently with a higher percentage of humidity. The increase of H<sub>2</sub>S capture capacity of the last two cycles underlines that adsorption is favoured by a higher amount of humidity in the system. Also under this condition, cycles are repeatable, as shown by the overlapping of curves 3 and 4.

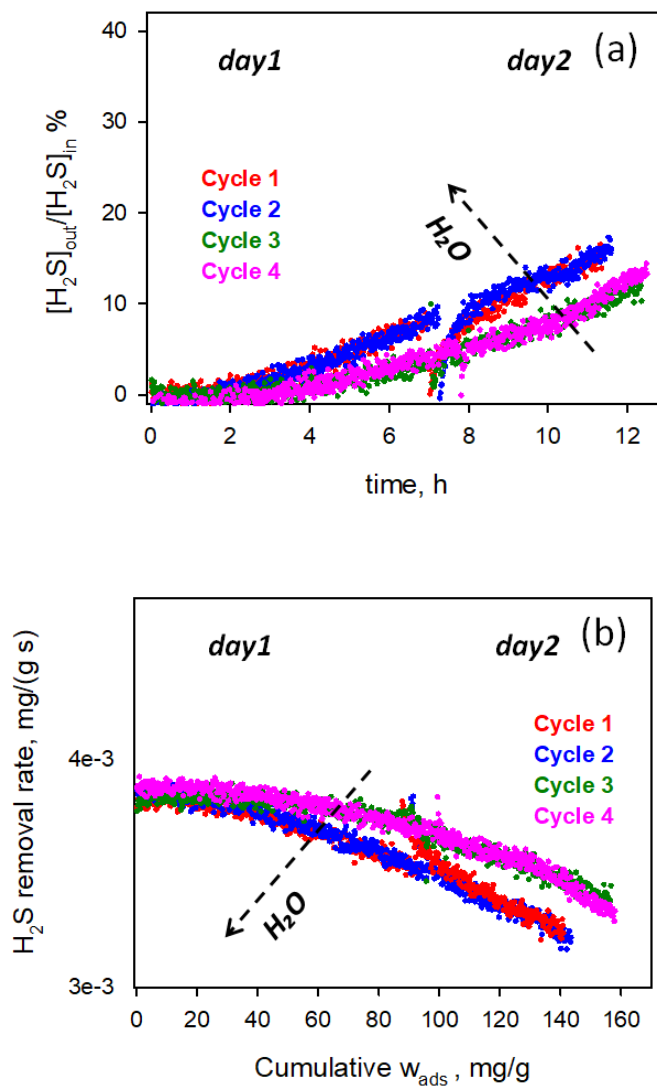


**Figure 2. 19** Breakthrough curves (a) and apparent H<sub>2</sub>S removal rate (b) of Cu<sub>2</sub>.5Mg<sub>2</sub>.5-modified monolith for H<sub>2</sub>S after four cycles of adsorption tests at T=30°C, P=1 atm in presence of humidity (HR=50%) and O<sub>2</sub>=2500 ppm and subsequent TPD at T=600°C in N<sub>2</sub>

*List of figures*

<b>Figure 2. 1.</b> Monolith obtained by cutting the original sample provided by Helsa Functional Coating.....	57
<b>Figure 2. 2</b> Schematic representation of the experimental equipment used for H <sub>2</sub> S adsorption tests .....	59
<b>Figure 2. 3</b> Weight loss as a function of temperature of Helsa AC monolith under air flow .....	61
<b>Figure 2. 4</b> SEM images of monolith cross section (a) at increasing magnifications (channel with two adjacent walls (b); wall (c)).....	61
<b>Figure 2. 5</b> N <sub>2</sub> physisorption isotherms at 77K (a), cumulative pore volume (b) and pore size distribution (c) for monoliths .....	63
<b>Figure 2. 6</b> Breakthrough curves of AC monolith in dry and wet conditions. Inlet conditions: [H <sub>2</sub> S]=100ppm, [O <sub>2</sub> ]=2500ppm, T=30°C, P=1 atm .....	65
<b>Figure 2. 7</b> Breakthrough curves of 2.5%wt (a) and 5% wt (b) Cu-modified monoliths for H <sub>2</sub> S capture and SO <sub>2</sub> formation during adsorption test by varying T at P=1 atm in presence of humidity (HR=50%) and O <sub>2</sub> =2500 ppm.....	67
<b>Figure 2. 8</b> Breakthrough curves of 2.5% wt (a) and 5% wt (b) Mg-modified monoliths for H <sub>2</sub> S capture and SO <sub>2</sub> formation during adsorption test by varying T at P=1 atm in presence of humidity (HR=50%) and O <sub>2</sub> =2500 ppm.....	68
<b>Figure 2. 9</b> Trend of apparent H <sub>2</sub> S removal rate over time of Cu2.5 (a), Cu5.0 (b), Cu2.5Mg2.5 (c) and Mg5.0 (d) (solid line). A master line (dashed line) connecting the values of H <sub>2</sub> S removal rate at the end of each day is reported. .	70
<b>Figure 2. 10</b> Comparison of breakthrough curves (a) and apparent H <sub>2</sub> S removal rate (b) of monoliths for H <sub>2</sub> S capture at T=30°C, P=1atm in presence of humidity (HR=50%) and O <sub>2</sub> =2500 ppm .....	71

<b>Figure 2. 11</b> Effect of temperature on the H <sub>2</sub> S adsorption capacity and the apparent H <sub>2</sub> S removal rate of Cu <sub>2.5</sub> (a), Cu <sub>5.0</sub> (b), Cu <sub>2.5</sub> Mg <sub>2.5</sub> (c) and Mg <sub>5.0</sub> (d).....	74
<b>Figure 2. 12</b> Effect of inlet flow rate on breakthrough curves and the apparent H <sub>2</sub> S removal rate of Cu <sub>2.5</sub> Mg <sub>2.5</sub> by varying inlet flow rate at P=1 atm in presence of humidity (HR=50%) and O <sub>2</sub> =2500 ppm.....	75
<b>Figure 2. 13</b> Comparison of weight loss % and species release during TPD tests under Ar flux from H <sub>2</sub> S saturated modified AC after few minutes (TPD (I)) and two months (TPD(II)) respectively later H <sub>2</sub> S adsorption tests. Derivative curves (down) of weight losses. ....	78
<b>Figure 2. 14</b> Weight loss % and species release during sulphates decomposition under N <sub>2</sub> flux from CuSO <sub>4</sub> impregnated on AC .....	80
<b>Figure 2. 15</b> N <sub>2</sub> physisorption isotherms at 77K and PSD for fresh and spent modified monoliths .....	84
<b>Figure 2. 16</b> XPS spectra in Cu2/p spectral region of fresh (a and b) and spent (c and d) Cu <sub>5.0</sub> and Cu <sub>2.5</sub> Mg <sub>2.5</sub> sorbents. ....	87
<b>Figure 2. 17</b> XPS spectra in O1s spectral region of fresh (a and b) and spent (c and d) Cu <sub>5.0</sub> and Cu <sub>2.5</sub> Mg <sub>2.5</sub> sorbents .....	88
<b>Figure 2. 18</b> XPS spectra in S2p spectral region of spent Cu <sub>5.0</sub> and Cu <sub>2.5</sub> Mg <sub>2.5</sub> sorbents (a and c) and in the Mg1s region of fresh and spent Cu <sub>2.5</sub> Mg <sub>2.5</sub> (c and d). ....	89
<b>Figure 2. 19</b> Breakthrough curves (a) and apparent H <sub>2</sub> S removal rate (b) of Cu <sub>2.5</sub> Mg <sub>2.5</sub> -modified monolith for H <sub>2</sub> S after four cycles of adsorption tests at T=30°C, P=1 atm in presence of humidity (HR=50%) and O <sub>2</sub> =2500 ppm and subsequent TPD at T=600°C in N <sub>2</sub> .....	91

*List of tables*

<b>Table 2. 1</b> List of metal modified sorbents.....	57
<b>Table 2. 2</b> Area and pore volume of pure and metal modified AC monoliths as fresh, spent and regenerated after TPD.....	64
<b>Table 2. 3</b> Specific amount of sulphur captured out up to the breakthrough point ( $\omega_{br}$ ) and up to the end of the tests ( $\omega_{test}$ ) during H <sub>2</sub> S adsorption experiments carried t at 30°C under co-presence of H <sub>2</sub> O + O <sub>2</sub> .....	72
<b>Table 2. 4</b> Comparison of specific H <sub>2</sub> S adsorption capacity ( $\omega_{ads}$ ) up to 5.5h of monoliths and granular ACs at 30°C under co-presence of H <sub>2</sub> O + O <sub>2</sub> .....	73
<b>Table 2. 5</b> Specific amount of sulphur captured out up to the breakthrough ( $\omega_{br}$ ) and up to 10h of the tests ( $\omega_{10}$ ) during H <sub>2</sub> S adsorption experiments carried t at 30°C under co-presence of H <sub>2</sub> O + O <sub>2</sub> with different flow rates .....	76
<b>Table 2. 6</b> Weight loss % during TPD tests under Ar flux from H <sub>2</sub> S saturated modified AC.....	81
<b>Table 2. 7</b> BET area and pore volume of pure of metal modified AC monoliths as fresh, spent and regenerated after TPD .....	85
<b>Table 2. 8</b> Comparison of volume occupied by elemental sulphur and the difference between the total cumulative volume of the fresh and spent sorbents .....	86

## *References*

- Boutillara, Y., Tombeur, J. L., De Weireld, G., Lodewyckx, P. (2019). In-situ copper impregnation by chemical activation with CuCl<sub>2</sub> and its application to SO<sub>2</sub> and H<sub>2</sub>S capture by activated carbons. *Chemical Engineering Journal*, 372, 631-637.
- Cimino, S., Lisi, L., Erto, A., Deorsola, F. A., de Falco, G., Montagnaro, F., Balsamo, M. (2020). Role of H<sub>2</sub>O and O<sub>2</sub> during the reactive adsorption of H<sub>2</sub>S on CuO-ZnO/activated carbon at low temperature. *Microporous and Mesoporous Materials*, 295, 109949.
- Haimour, N. M., El-Bishtawi, R., Ail-Wahbi, A. (2005). Equilibrium adsorption of hydrogen sulfide onto CuO and ZnO. *Desalination*, 181(1-3), 145-152.
- Naumkin, A. V., Kraut-Vass, A., Gaarenstroom, S. W., & Powell, C. J. (2012). NIST X-ray photoelectron spectroscopy database, NIST standard reference database 20, version 4.1. US Department of Commerce, Washington.
- Zhang, Z., Wang, J., Li, W., Wang, M., Qiao, W., Long, D., Ling, L. (2016). Millimeter-sized mesoporous carbon spheres for highly efficient catalytic oxidation of hydrogen sulfide at room temperature. *Carbon*, 96, 608-615.

## **Chapter 3. Synthesis and Characterization of Activated Carbon Foam**

### 3.1. Activated Carbon Foam

As reported in §1.3.2, methods to obtain a carbon foam are based on the impregnation with a carbonaceous precursor of a silica foam with interconnected porosity, followed by polymerization, pyrolysis and, finally, by selective dissolution of silica scaffold. The complexity of this procedure which can become even more complex by the deposition of active metals on AC, in order to increase the H<sub>2</sub>S capture capacity, suggested to search for easier techniques.

Attempts to combined at least this final step were recently made by Boutillara et al. (2019). The authors proposed to introduce active copper directly impregnating the active carbon precursor (olive stone) with CuCl<sub>2</sub> and then carrying out carbonization at 800°C. Although they obtained a powder material they avoided the impregnation step.

The carbonaceous precursor generally used to obtain a high carbon yield using the above mentioned template technique is polyfurfuryl alcohol (PFA). PFA is produced by an acid-catalyzed polymerization of furfuryl alcohol (FA) and it represents the most common thermosetting polymer used for porous carbon production by pyrolysis (Wang and Yao, 2006). Polymerization of FA is activated by mineral acids (H<sub>2</sub>SO<sub>4</sub>, etc.), organic acid (p-toluenesulphonic, etc.), acid zeolites (HY, HZSM-5) and Lewis acid (I<sub>2</sub>, SnCl<sub>4</sub>, TiCl<sub>4</sub>).

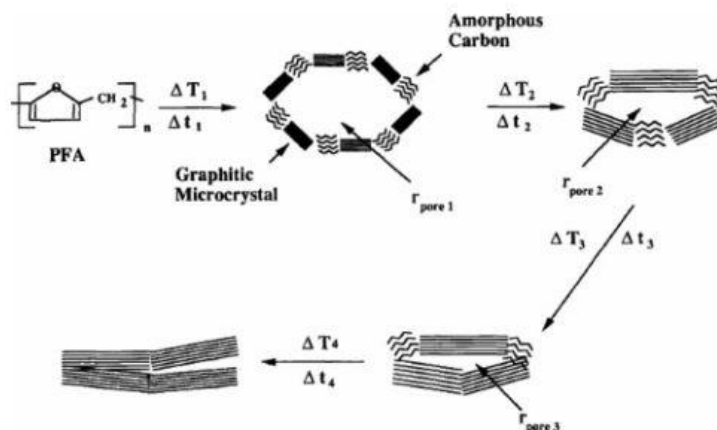


**Figure 3. 1** Evolution of the carbon structure deriving from the polymerization of FA (Wang and Yao, 2006)

ZnCl<sub>2</sub> was proposed by Cesano et al. (2008) for the first time as acid promoter for FA polymerization at 60-70°C to obtain porous ZnO-carbon composites characterized by a uniform layer of highly dispersed ZnO crystallites on the surface of the carbon matrix or, at high pyrolysis temperatures, of a pure carbon phase containing holes whose distribution and size is driven by the Zn content.

Wei et al. (2009) also studied ZnO-porous carbon composites starting from FA/ZnCl<sub>2</sub>/water solution used to dip-coat glass mats focusing on the effect of the pyrolysis time at 450°C on the morphology of ZnO crystals more than on that of the carbon matrix.

The work of Cesano et al. (2008; 2012) suggested the possibility to disperse directly during the synthesis of Activated Carbon the metal promoters producing a material which could be potentially used in H<sub>2</sub>S adsorption.

In this thesis the possibility of introducing another metal has been explored. Copper has been used as it can potentially act as a Lewis acid activating the polymerization of furfuryl alcohol in order to produce activated carbons with particular adsorption characteristics determined not only by the textural properties, but also by the presence of a given metal, properly regulating the polymerization conditions. Similarly, ZnCl<sub>2</sub> has also been studied as a promoter

of FA polymerization, in order to have a direct comparison with the material activated by Cu.

These two metals were chosen because previous studies reported a highly enhanced H<sub>2</sub>S adsorption capacity of the original activated carbon in the presence of Zn and Cu oxides when supported on activated carbons in granular form (Balsamo et al. 2016; Cimino et al. 2018; de Falco et al. 2018; Cimino et al. 2020). As a consequence, the attempts to obtain Activated Carbon in a foamy structure in a single step, avoiding the complex and long multi-step procedure, have been analyzed. This method allowed to simultaneously carry out the polymerization of FA to PFA and the dispersion of metals avoiding, not only the steps of impregnation of silica matrix and final dissolution, but also the subsequent impregnation with aqueous solutions of metal nitrates. The different polymerization and pyrolysis conditions, determining the main features of carbon but also the amount of metals present in the structure are also discussed. Synthesis conditions for Zn-activated polymerization was based on the work of Cesano et al. (2008; 2012). On the other hand, the use of CuCl<sub>2</sub> as activator of FA polymerization is not reported and, as a consequence, the conditions were determined on the basis of the following consideration: cupric ion is a Lewis acid stronger than the zinc ion since the ionic radius of the Cu<sup>2+</sup> (72pm) is smaller than that of the Zn<sup>2+</sup> (74 pm) and the electronegativity (Pauling) is higher (Cu<sup>2+</sup> 1.9eV versus 1.6eV of Zn<sup>2+</sup>) (Boutillara et al., 2019; Liu et al., 2016).

As it will be shown in the following section, the activation of FA solutions by Lewis acids can lead to a slower or a faster polymerization depending on the system temperature and strength of the acid that produce materials with different structure and porosity. The first explanation of the phenomenon of rapid polymerization of the FA was given by Dunlop and Peters (1953). They proposed a scheme of two simultaneous reactions occurring during the polymerization of FA in acid aqueous solutions, both involving the condensation of the OH groups. Figure 3.2 shows a rearrangement of these mechanisms proposed by Bertarione et al. (2008).

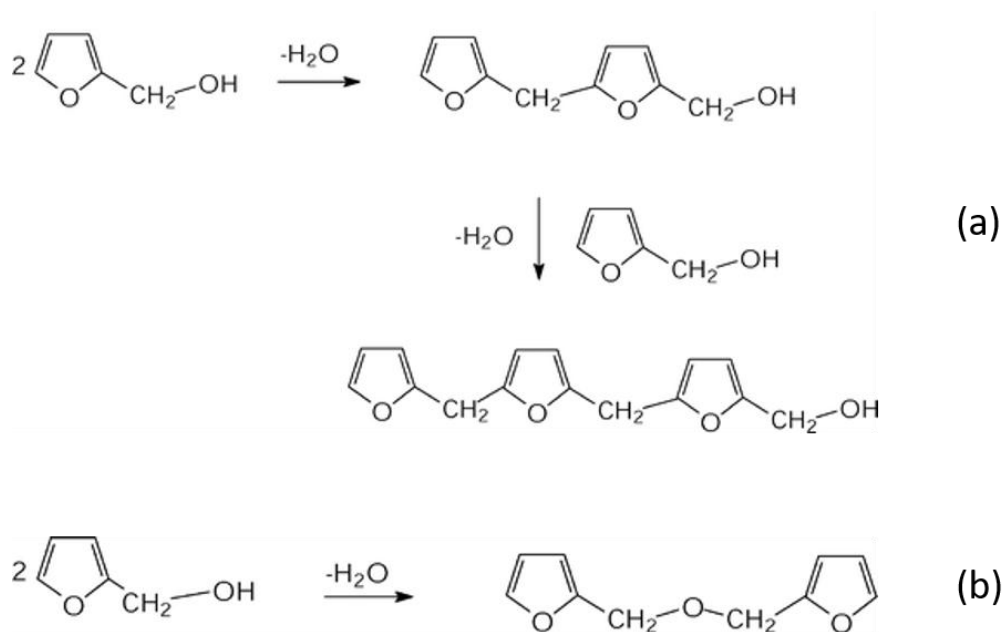


**Figure 3. 2** Condensation Reaction Schemes between the OH of the Methylol Group of One Furan Ring and (a) the 5-Position of Another Furan Ring and (b) the Methylol Group of Another Furan Ring (Bertarione et al., 2008)

Then, branching and cross-linking can take place, and the rate at which these reactions occur increases with the formation of oligomers. These mechanisms only explain the formation of linear macromolecules but not the increasing phenomenon of branching and cross-linking associated to a more viscous and darker liquid solution. The formation of sequences of conjugate double bonds seems responsible for the dark colouring of the solution (Bertarione et al., 2008). Choura et al. (1996) as well proposed a mechanism that explains the progressive darker colour of the solutions in which acid-catalyzed polycondensation of the FA occurs. The scheme of the reactions has been reported in Figure 3.3 (Bertarione et al., 2008).

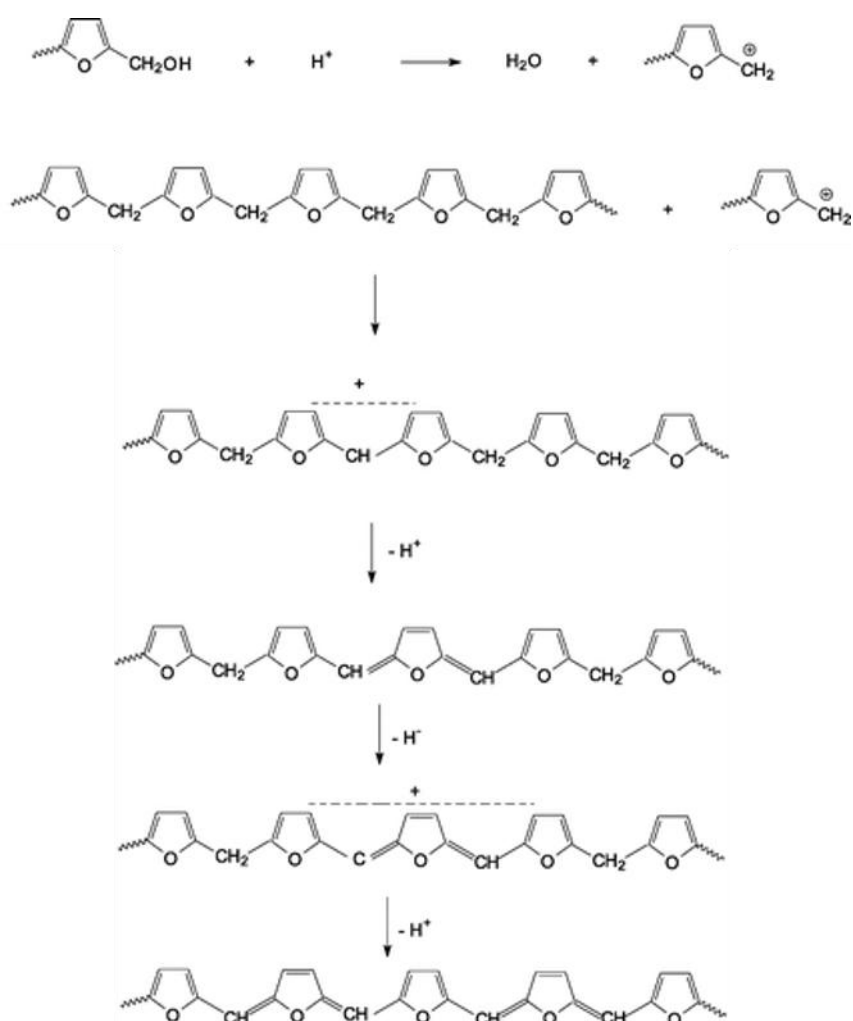


**Figure 3. 3** Scheme of reactions responsible of progressive darker colour of the solutions in which acid-catalyzed polycondensation of the FA occurs (Bertarione et al. 2008)

Oligomers produced by linear condensations can undergo hydride ion exchanges with the protonated chain ends of growing species leading to the formation of methyl-terminated oligomers and carbon ions with the positive charge shared by a methine carbon atom and two adjacent furans rings (Choura et al., 1996). The corresponding conjugate structure that has lost a proton may further lose a hydride ion. This pattern of reactions can occur numerous times by increasing the degree of conjugation. The main responsible for the dark colour are the hydrogen atoms of the methylene group that separate the furan rings in the oligomers while positions H3 and H4 are not involved.

The formation of foamy polymers goes through a gelly phase. Vaporization of water produced from branching and cross-linking due to the exothermal character of these reaction likely creates the cavities of the PFA foam.

It must be noted that, under above described conditions, the presence of water different from that produced by the polymerization reactions, introduced from the very beginning into FA for the dissolution of the metal chlorides, can contribute to the formation of a foamy material, rapidly evaporating when the exothermal reactions take place.

The polymeric foam obtained is then carbonized during a heat treatment in a flow of inert gas raising the temperature up to 800 °C.

Bertarione et al. (2008) have proposed a possible scheme (Figure 3.4) of carbon formation when, thermally treated in an inert gas flow, the viscous and dark brown material becomes stiff and black leading to the formation of amorphous carbon with release of H<sub>2</sub>O and other gases.

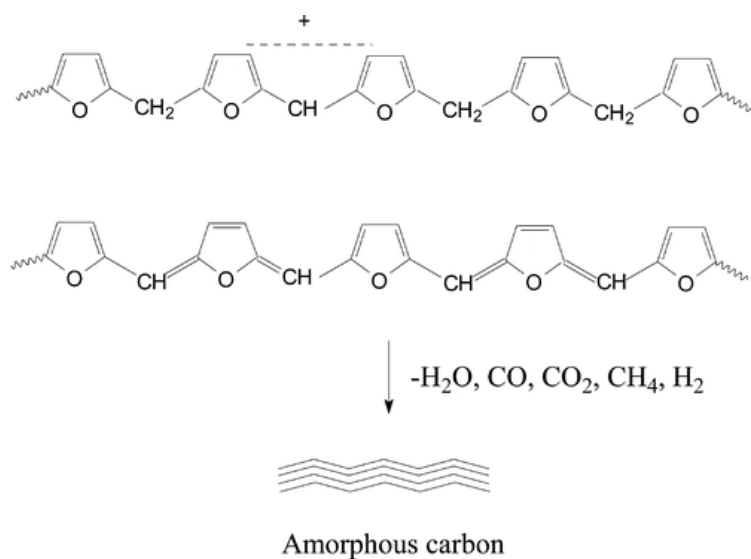


**Figure 3. 4** Scheme of amorphous carbon formation (Bertarione et al. 2008)

### 3.2. ACs synthesis

The preparation of porous carbon involves two phases: polymerization of FA and pyrolysis.

In this work two samples with different metals and different metal chloride/FA ratio were prepared:

- Sample 1: 17% wt ZnCl<sub>2</sub>
- Sample 2: 7% wt CuCl<sub>2</sub>

High purity (98%) polyfurfuryl alcohol (FA) supplied by Sigma Aldrich was used as starting material for polymerization. ZnCl<sub>2</sub> (RPE-Carlo Erba, 98% purity) and CuCl<sub>2</sub> (Aldrich, >99% purity) were used as Lewis acids to activate the FA polymerization. The amount corresponding to the desired load in the FA precursor was preliminarily dissolved in the minimum volume of water. The aqueous solution in which the salt is dissolved has been then added to FA.

This preparation procedure was adopted due to the poor solubility of both metal chlorides into liquid FA which leads to a rapid FA polymerization on the outer surface of metal salt granules and creates a compact layer of PFA which inhibits the further occurrence of the reaction due to the hard penetration of FA towards the core of the salt particles

#### *Zn/AC sample*

This sample was prepared by dissolving a suitable (to obtain 17% ratio) amount of ZnCl<sub>2</sub> (5.667 g) in 1.5 ml of water then added to 24.45 mL of FA. The solution was stirred at two different temperatures (25 and 80°C).

The initially light solution slowly becomes brownish and more viscous up to the formation of a porous solid with the appearance of a foam at a different time depending on the temperature. The mixture required several days to reach a highly viscous texture at room temperature. Cesano et al. (2011) reported that, at room temperature, a time >12 h was necessary to obtain PFA, whereas in our experiment at room temperature a highly viscous material was obtained after times as long as 10 days.

For this reason, another synthesis keeping the same composition of the mixture was performed, increasing the temperature to 80 °C. Under this condition, after about 40 min, an instantaneous formation of a foamy polymer

occurred, as shown in Figure 3.5. This was considered a positive event. Actually, this could represent an easy and rapid method for producing a structured activated carbon since the large foam could be suitably cut and shaped for adsorption tests.



**Figure 3. 5** Foamy PFA obtained from Zn-activated polymerization of FA at 80 °C

#### *Cu/AC sample*

As previously mentioned,  $\text{Cu}^{2+}$  is a stronger Lewis acid than  $\text{Zn}^{2+}$  due to its smaller ion radius and higher Pauling electronegativity and, as a result, stronger activation of branching and cross-linking can be expected. For this reason, a lower concentration of  $\text{CuCl}_2$  was chosen to balance the stronger Lewis acid strength of copper chloride with respect to zinc chloride. This sample was prepared by dissolving an amount  $\text{CuCl}_2$  (1.165 g) to obtain 7% ratio in 1.5 mL of water then added to 14 mL of FA. The solution was stirred at two different temperatures: 0 and 25°C. Nevertheless, despite the reduction of copper chloride concentration with respect to that of the zinc salt, at room temperature FA polymerization took place with the formation of the polymer in only two hours, compared to the several days required for Zn-activated polymerization at the same temperature, coupled to a violent and uncontrolled formation of

carbon foam. The same occurred at 80 °C in only a few minutes. For this reason, FA was polymerized at 0 °C, a condition that allowed a mild and controlled polymerization that occurred in 3 days.

The effect of temperature of polymerization strongly influences the reaction time and, otherwise, the temperature necessary to obtain the polymerization in a given time shifts to lower values if the cation is a stronger Lewis acid. Of course, experimental conditions must be carefully chosen to carry out a controlled formation of foamy PFA. In Table 3.1, the conditions of polymerization are summarized.

**Table 3. 1** Effect of temperature of polymerization condition on polymer formation

Activators of polymerization	$T_{\text{polymerization}}$		
	0°C	25°C	80°C
ZnCl <sub>2</sub>	/	The polymerization lasts up to 10 days and the polymer is not porous.	The polymerization takes place in 30 min < t < 2h and the formation of a foamy polymer occurs.
CuCl <sub>2</sub>	The polymerization lasts 2-3 days and the formation of a foamy polymer occurs (controlled polymerization).	The polymerization takes place explosively in 2 hours.	/

Due to the too long time required to polymerize at room temperature for the Zn-activated system and to the uncontrolled polymerization of the Cu-activated system at 25 and 80 °C, characterization was done on PFA obtained at 80 and 0 °C for ZnCl<sub>2</sub> and CuCl<sub>2</sub> activation, respectively.

The solid-like PFA was then pyrolyzed under pure He or 1000 ppm O<sub>2</sub>/He mixture, heating to 600 or 850°C at 5°C/min for 3h. O<sub>2</sub> traces in the gas mixture were added in some pyrolysis steps in order to verify the possible formation of metal oxides (more thermally stable in the case of zinc), as suggested by

Cesano et al. (2008) but also to investigate whether O<sub>2</sub> traces could affect the porosity causing a limited carbon burning that could potentially open or widen some pores.

### 3.3. Sample Characterization

Pyrolysis of PFA was investigated by simulating the process in a Setaram Labsys Evo thermobalance by increasing the temperature up to 850 °C at 5 °C/min under pure N<sub>2</sub>.

The morphology of the AC samples and the metal distribution were investigated by SEM/EDX FEI Inspect instrument equipped with an energy dispersive X-ray probe.

The actual zinc and copper content in the AC samples was verified with ICP-MS analysis using an Agilent 7500 instrument after MW-assisted dissolution of the samples in HCl/HF/H<sub>2</sub>O<sub>2</sub> (4/1/1 volume) solution.

X-ray diffraction (XRD) of powdered samples was performed by means of a Philips X'Pert PRO apparatus working radiation CuK $\alpha$ , anti-scatter slit width: 7.5 mm); the 2 $\theta$  range of collected patterns was 5-100°, which was scanned using a step size of 0.013° and a scan speed of 0.156° s<sup>-1</sup>.

Raman spectra were recorded using a Horiba XploRA Raman microscope system with an excitation wavelength of  $\lambda = 532$  nm (frequency doubled Nd:YAG-solid state laser, 25 mW) in the range 500-4000 cm<sup>-1</sup> (Stokes Raman shift).

The surface area and the pore volume of all AC samples after pyrolysis were evaluated by N<sub>2</sub> physisorption at 77 K using a Quantachrome Autosorb 1C gas porosimeter after degassing the samples at 150°C for 4 h. Surface area was estimated according to BET, DFT and DR models. Pore volume was evaluated according to both DFT and DR models. Even though the BET model was originally formulated for calculating the specific surface area of materials that give IUPAC Type II or Type IV isotherms, it is usually also employed to provide an appraisal of the specific surface area of materials, like activated

carbons, which generally give Type I isotherms (Landers et al., 2013). DFT was applied using a typical kernel for carbon materials having slit pore geometry. The DR model was chosen for providing an estimation of the micropore volume and the corresponding surface area (Medek, 1977). Due to the presence of an open hysteresis loop, suggesting the presence of narrow micropores and/or bottle neck pores (Marsh and Reinoso, 2006; Rouquerol et al., 2013), additional textural characterization was carried out through CO<sub>2</sub> adsorption at 273 K by means of a Micromeritics ASAP 2020 (Norcross, Georgia, US).

### 3.4. Results and Discussion

The results of TG analysis carried out on both Zn- and Cu-PFA under N<sub>2</sub> are reported in Figure 3.6:

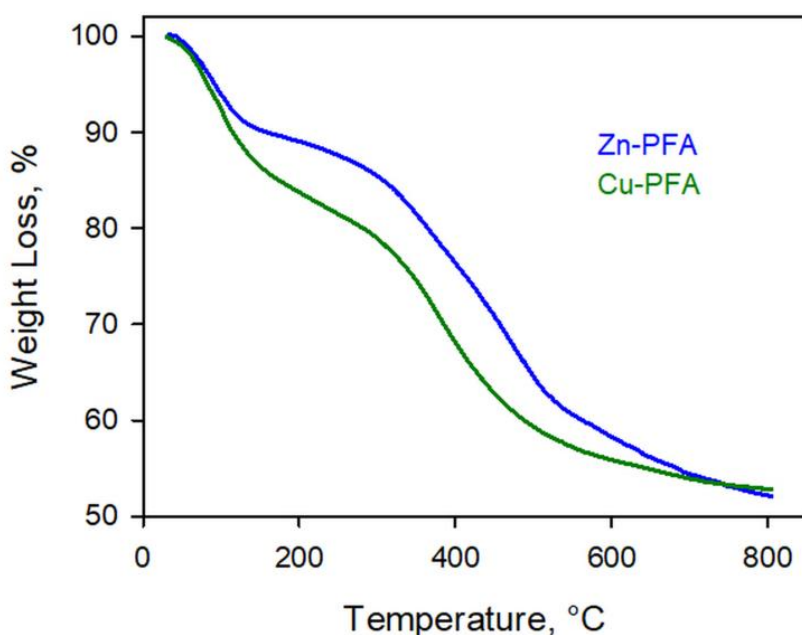


**Figure 3. 6** Weight loss as a function of temperature of Zn- and Cu-activated PFA under N<sub>2</sub> flow

Two main weight losses providing a total loss of about 50% of the initial weight are recorded for both samples. The first, at T < 150 °C, was attributed to the sample evaporation of H<sub>2</sub>O, whereas the second, in the range 350–550 °C,

was attributed to the carbonization process in which PFA degradation leads to the formation of carbon (Bertarione et al. 2009; Wang and Yao, 2006).

From these results, the temperature sufficient to pyrolyze PFA was set as 600°C. In order to investigate how the temperature affects the final properties of the activated carbon, some samples were also pyrolyzed up to 850 °C. The pyrolysis step was carried out both under pure helium flow or under 1000 ppm O<sub>2</sub>/He mixture, as proposed by Cesano et al. (2008).

All samples prepared with different temperature of pyrolysis and composition of pyrolysis gas are listed in Table 3.2 and labelled as Me/AC-T, where Me represents the metal, AC the activated carbon and T the temperature of pyrolysis. The presence of an asterisk in some samples indicates the presence of O<sub>2</sub> in the pyrolysis gas.

**Table 3. 2** List of ACs with the preparation conditions

<b>Samples</b>	<b>T(Pyrolysis)</b>	<b>Gas Composition (Pyrolysis)</b>
<b>Zn/AC-600</b>	600°C	He
<b>Zn/AC-850</b>	850°C	He
<b>Cu/AC-850</b>	850°C	He
<b>Zn/AC-600*</b>	600°C	1000ppm O <sub>2</sub> / He
<b>Zn/AC-850*</b>	850°C	1000ppm O <sub>2</sub> / He
<b>Cu/AC-850*</b>	850°C	1000ppm O <sub>2</sub> / He

The foamy structure of AC is easily visible in Figure 3.7 (a) that shows the SEM image of Zn/AC-850. A similar structure, even if less “open”, was also observed for Cu/AC-850 (Figure 3.7 (b)).

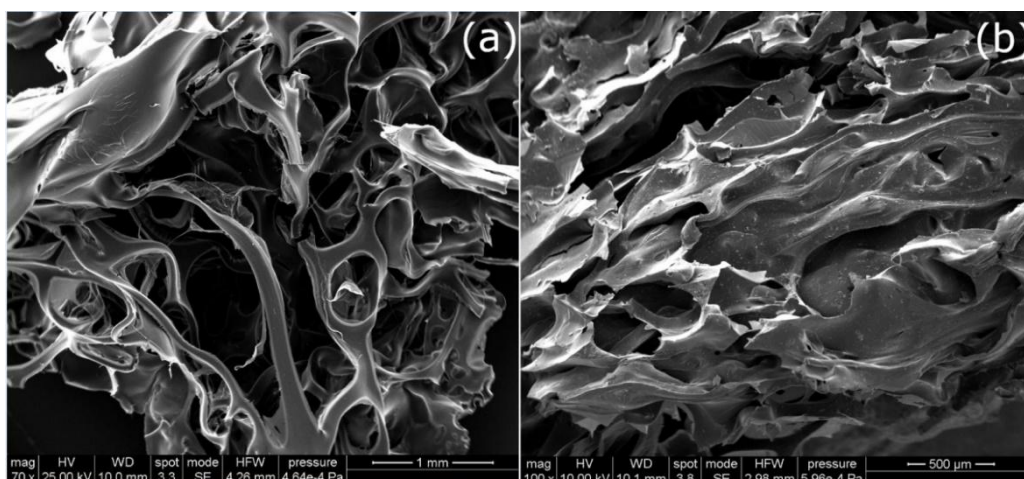


**Figure 3. 7** SEM images of Zn/AC-850 (a) and Cu/AC-850 (b)

The same foamy structure was observed for the sample treated at 600°C. A detail of the surface of the rods constituting the carbon matrix after treatment at 600°C is reported in Figure 3.8 (a).

Comparison with a SEM image with the same magnification of Zn/AC-850 highlights the presence of particles on the surface of AC, almost absent in the sample treated at 850°C (Figure 3.8 (a)).

A greater magnification of Cu and Zn-based AC treated at 600°C highlights the presence of needle-like particles on the carbon surface for Zn/AC-600 sample and of spherical particles for Cu/AC-600 (Figure 3.9 (b)) (Figure 3.9 (a)).

These correspond to the shape of the typical ZnO and CuO crystals respectively.

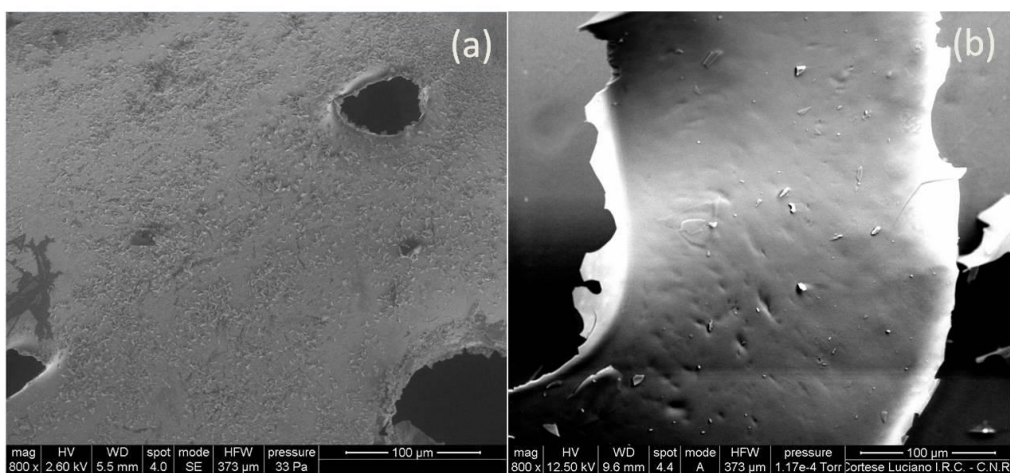


**Figure 3. 8.** SEM images of Zn/AC-600 (a) and Zn/AC-850 (b)

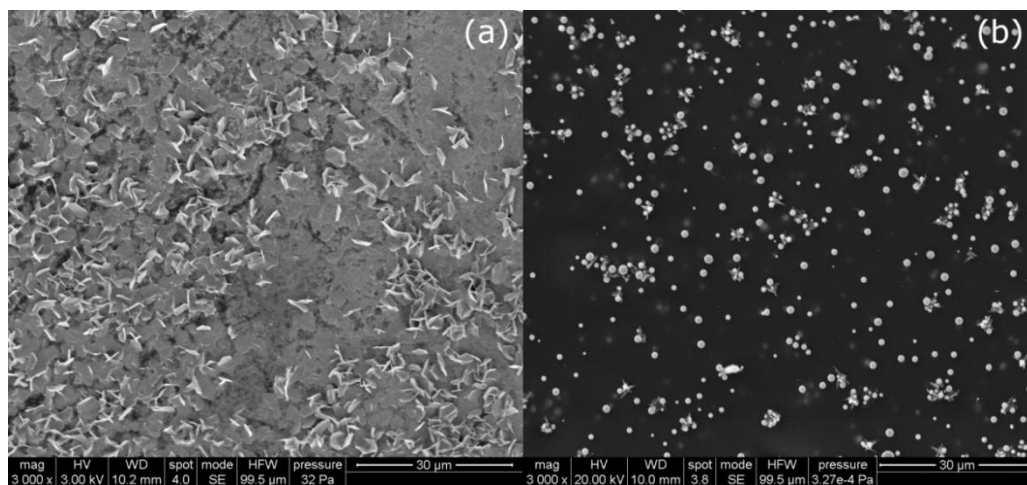


**Figure 3. 9** SEM images of Zn/AC-600 (a) and Cu/AC-600 (b) with a greater magnification

As reported above, zinc is completely lost if the pyrolysis temperature raises up to 850°C, whereas, copper is preserved also after pyrolysis temperature reaches 850°C, both under pure helium or 1000ppmO<sub>2</sub>/He mixture, as showed in Figure 3.10 showing the presence of the spherical particles in both cases.

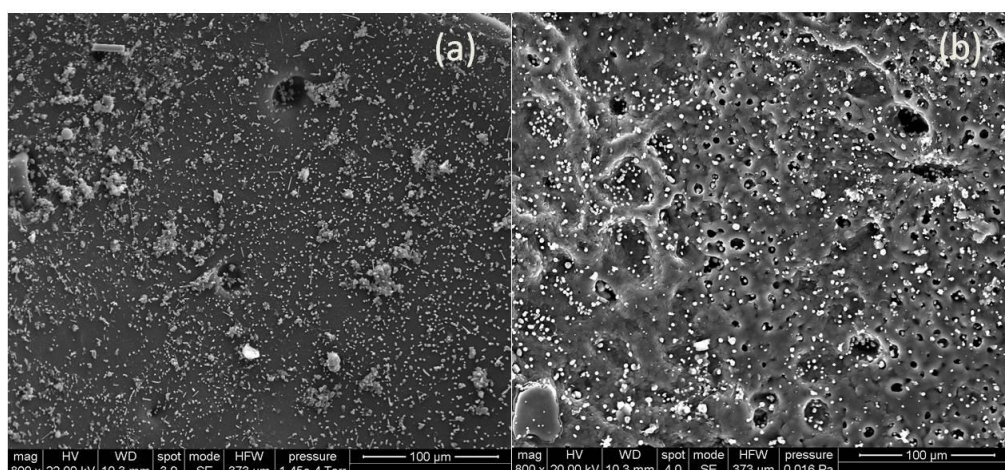


**Figure 3. 8** SEM images of Cu/AC-850 (a) and Cu/AC-850\* (b)

Furthermore, when the pyrolysis gas stream contains traces of O<sub>2</sub>, the surface of AC is more porous, as expected due to local combustion of some carbon.

The coupled EDX analysis confirmed that the particles detected were made of copper and zinc, respectively.

Results of ICP-MS analysis, carried out for all samples by dissolving different portion of the foams to determine the actual metal content, are reported in Table 3.3 where they are compared with the nominal content.

**Table 3. 3** Cu and Zn content in AC samples determined by ICP-MS analysis and nominal content of metals evaluated on the basis of metal chlorides introduced in FA for polymerization

	<b>Nominal Content</b>	<b>Zn/AC-600</b>	<b>Zn/AC-850</b>	<b>Cu/AC-850</b>	<b>Zn/AC-600*</b>	<b>Zn/AC-850*</b>	<b>Cu/AC-850*</b>
<b>% Cu</b>	3.31	-	-	4.68	-	-	3.37
<b>% Zn</b>	8.15	0.45	0.01	-	1.05	0.01	-

The values reported in the Table 3.3 represent average contents, which changed by 13 and 15% for copper and zinc, respectively, when moving from one sample portion to another. In the first column of the same table, the nominal metal content is also reported in order to evaluate the fraction of metal

preserved upon the thermal treatment. For Zn-modified materials, all values were much lower than the nominal one. On the contrary, also when treated at 850 °C, copper load was quite close to the nominal one. This result, as also confirmed by the SEM images reported above, was expected for the Zn-activated PFA pyrolyzed at 850 °C due to the lower temperature of evaporation of metallic Zn with respect to metallic Cu leading to the complete disappearance of the metal in both Zn samples. This is in agreement with results reported by Cesano et al. (2008) who found by XANES experiments that Zn concentration decreased of about 50% in the samples treated at 600 °C and about 90% in the samples treated at 800 °C with respect to the supposed initial concentration in the PFA. They assumed that reduction of Zn(II) to metallic Zn occurred in the temperature range 400–800 °C that easily evaporates due to the high volatility of the metal. The evaporation of metallic zinc at  $T > 800$  °C, also if starting from its oxide, was also found by other authors (Grabda et al., 2011; Zhang et al., 2020). Nevertheless, the very low Zn concentration, also for the sample treated at 600 °C, can probably be explained with some confinement on the outer surface of the metal during the fast PFA foam formation. This external portion of PFA foam was, however, removed in all cases before subsequent pyrolysis of PFA.

Figure 3.12 compares XRD patterns of Zn/AC-850\*, Zn/AC-600\* and Cu/AC-850\* sorbents in a  $2\theta$  range of 20–100°. All patterns show the broad signals of the amorphous carbon formed upon pyrolysis treatment of PFA. No peaks associable to Zn were observed for Zn/AC-850\* sorbents, which is in agreement with the results of ICP-MS analysis and with Cesano et al. (2008) who reported that at higher temperature (800°C) ZnO is reduced to metallic Zn and then evaporates. Negligible signals corresponding to zinc oxide and metallic zinc were detectable in the pattern of Zn/AC-600\*, indicating that for lower pyrolysis temperatures some zinc is preserved in the carbon matrix. On the contrary copper is present in different forms and oxidation states (Cu, CuO,

Cu<sub>2</sub>O) as different peaks with a high intensity, in addition to the carbon background, overlap in the pattern of Cu/Ac-850\*.

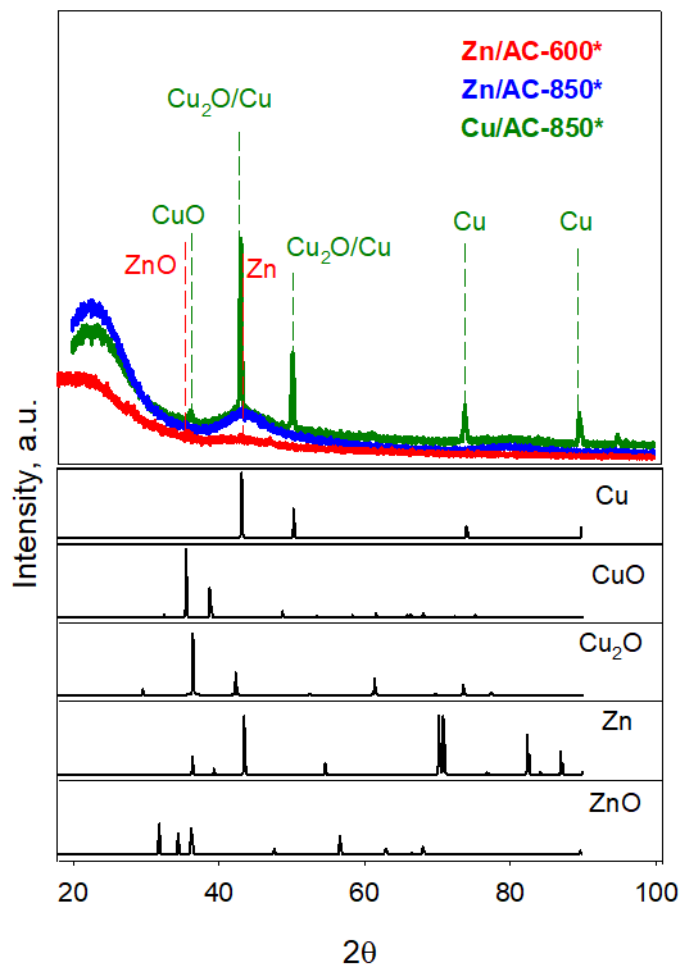


**Figure 3. 9** XRD patterns of Zn/AC-850\*, Zn/AC-600\* and Cu/AC-850\*. In the lower graph patterns of reference Zn (PDF 1-1244), ZnO (PDF 36-1451), Cu (PDF 4-836), Cu<sub>2</sub>O (PDF 5-667) and CuO (PDF 45-937) are reported

In Figure 3.13 the Raman spectra of Zn/AC-850, Zn/AC-600 and Cu/AC-850 samples are reported in the spectral region 1100-1800 cm<sup>-1</sup>, where carbon and its disorder degree can be identified. The Zn-based sample pyrolyzed at 600 °C shows more intense bands and all spectra show the typical D and G bands at 1340 and 1590 cm<sup>-1</sup>, assigned to the presence of amorphous and graphitic

carbon respectively (Cuesta et al., 1994). The disorder degree is generally referred to the ratio between the intensities of D and G peaks. Ordered carbon materials, such as graphite, show a narrow and intense G band and a wide weak D band, whereas a comparable intensity of D and G band indicates quite a high disorder degree. All the values of ratio between the intensity of the two peaks ( $I(D)/I(G)$ ) are very close to 1 for both samples pyrolyzed at 850 °C, except a value of 0.77 obtained for Zn/AC-600. This result suggests that the graphitic structure is partially destroyed by a higher pyrolysis temperature while it is preserved when the temperature is limited to 600 °C.

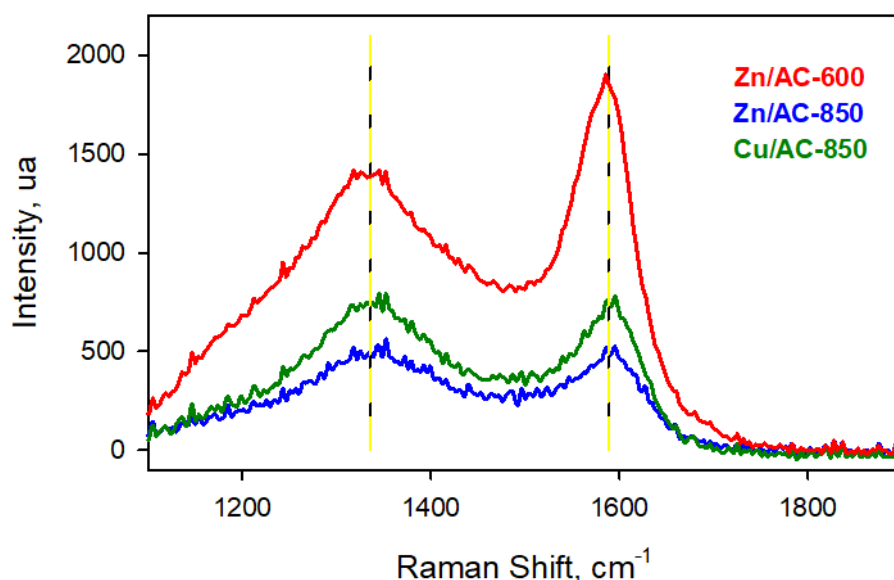


**Figure 3. 10** Raman spectra of Zn/AC-850, Zn/AC-600 and Cu/AC-850

The textural properties of the AC materials were preliminarily investigated through  $N_2$  physisorption at 77 K. The investigation was limited to the standard analysis for mesoporous materials as all the attempts to explore the  $10^{-7}$ - $10^{-5}$  bar of relative pressure ( $p/p^0$ ) range for the micropore analysis failed. In Figure 3.14 the adsorption/desorption isotherms are reported for all the samples pyrolyzed under pure helium (a) and for the corresponding samples pyrolyzed under  $O_2/He$  mixture (b). All samples show Type I isotherms, as expected for microporous materials, with a quite well-defined plateau, suggesting a small

contribution of the external surface area to the adsorption. A lower temperature of pyrolysis reflects in a much higher porosity of Zn-based AC. Nevertheless, an unusual behaviour was observed for all samples except for Zn/AC-600, i.e., adsorption and desorption branches do not converge to form a closed hysteresis, at least in the range of relative pressure explored, in contrast to what observed by Cesano et al. (2012). This effect is even more pronounced when oxygen traces are added in the pyrolysis gas.

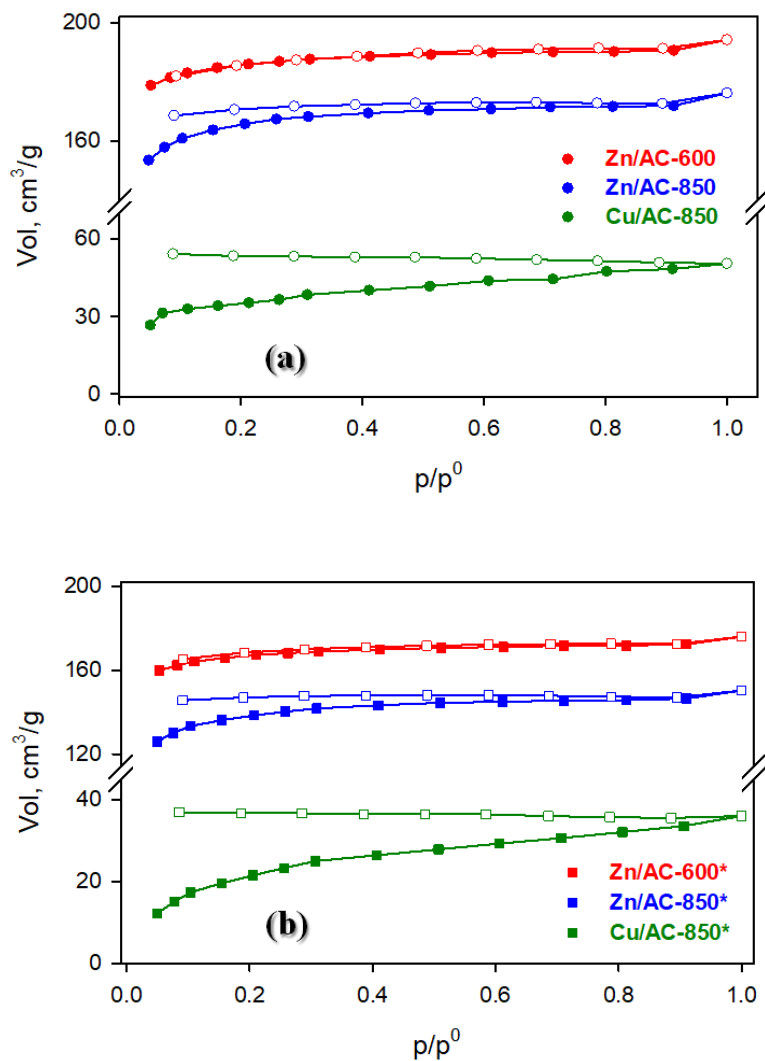


**Figure 3. 11** N<sub>2</sub> physisorption isotherms at 77 K for activated carbons pyrolyzed under pure helium (a) and under O<sub>2</sub>/He mixture (b) (closed symbols for adsorption branch, open symbols for desorption branch)

In literature, it is reported that this phenomenon is typically associated with the presence of narrow micropores (width  $< 10 \text{ \AA}$ ) and/or to pores with “bottle neck” structure (Gargiulo et al, 2018; Gargiulo et al., 2011; Morishige et al., 2006) and that PFA-derived carbons show bottle-like nano- and micropores with narrow openings connected to larger voids (Cesano et al., 2008).

Hysteresis phenomena in pore networks consisting of ink-bottle type pores are quite complex and two basic mechanisms of desorption in these pore networks are known, i.e., pore blocking and cavitation. The desorption from the pore body can occur only after emptying of its neck in the case of pore blocking. Thus, desorption from the neck triggers evaporation in the blocked pore and the vapor pressure of desorption from the pore body depends on the neck size and network connectivity. Furthermore, assumed that the diffusion at 77 K of  $\text{N}_2$  molecules in very small pores (i.e.  $< 7 \text{ \AA}$ ) is inherently limited, the presence of narrow micropores represents an obstacle to the analysis of the texture by adsorption of  $\text{N}_2$  at 77 K. For these reasons, the BET- $\text{N}_2$  area generally does not have the physical meaning of an effective area if the carbon is ultra-microporous (Rouquerol et al., 2013; Gargiulo et al., 2018). According to Morishige et al. (2006), closure of the hysteresis loop takes place at lower relative pressure when the diameter of the pore neck is  $< 50 \text{ \AA}$ , whereas when the diameter of the neck is  $> 50 \text{ \AA}$ , the hysteresis loop closes at higher values. As a consequence, since the hysteresis loop did not close at relative  $p/p^0$  pressure as low as 0.1, the presence of pores with a size well below  $50 \text{ \AA}$  can be supposed for our carbons.

Figure 3.15 reports the effect of the composition of the pyrolysis gas on the PSD, evaluated by DFT method using a slit/cylindrical pores model, in the last part of the microporosity and mesoporosity regions. For Zn-modified sorbents pyrolyzed up to  $600^\circ\text{C}$ , the introduction of small amounts of  $\text{O}_2$  in pyrolysis gas flow just results in an increase of the amount of pores centered at about  $14 \text{ \AA}$ . If the temperature is increased at  $850^\circ\text{C}$ , a wide size distribution is observed compared to  $T=600^\circ\text{C}$  but negligible differences in the structure when oxygen

is present in the feed occur. For Cu-modified sorbents, the presences of O<sub>2</sub> lead to a decrease of pores centered at 14 and 20 Å respectively.

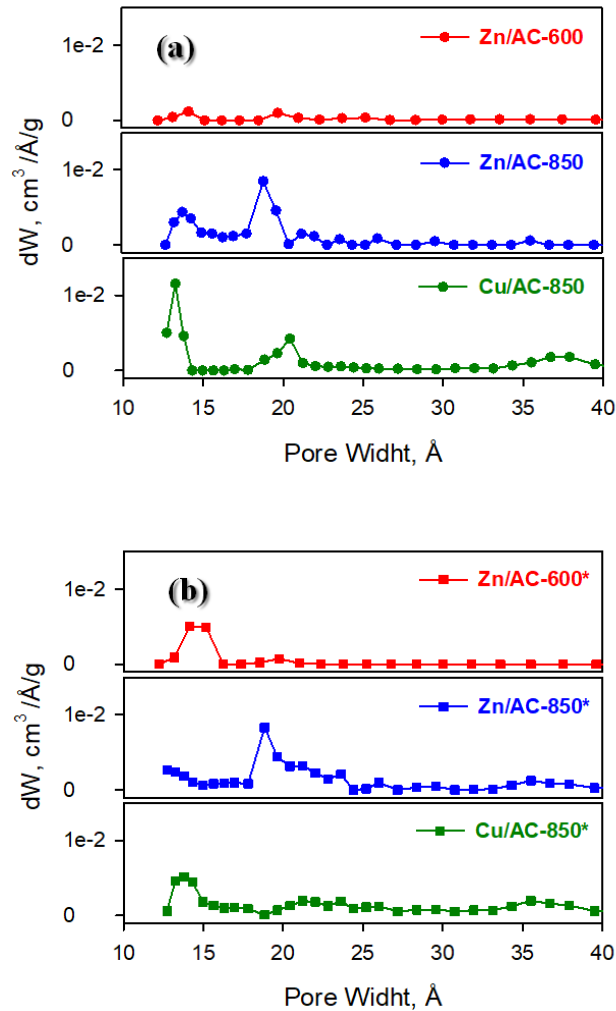


**Figure 3. 12.** The effect of the composition of the pyrolysis gas on the PSD in the micro/mesopores region Compared to N<sub>2</sub> adsorption at 77 K, the adsorption of CO<sub>2</sub> as probe molecule at 273 K has a higher kinetic energy that allows it to enter the narrowest pores, overcoming the already mentioned diffusional problems (Lozano-Castelló et al., 2004; Gargiulo et al., 2011) and limitations related to bottleneck pores (Thommes, 2010). The  $p/p^0$  range is limited to  $<0.03$  at sub-atmospheric pressures as at 273 K the CO<sub>2</sub> saturation pressure is quite high. This means that

the initial part of the adsorption isotherm can then be determined with much greater accuracy than using N<sub>2</sub> at 77 K. Furthermore, information provided by both N<sub>2</sub> and CO<sub>2</sub> adsorption are complementary.

For this reason, Figure 3.16 shows CO<sub>2</sub> adsorption isotherms at 273 K on all synthesized AC materials together with the corresponding N<sub>2</sub> adsorption isotherms at 77 K.

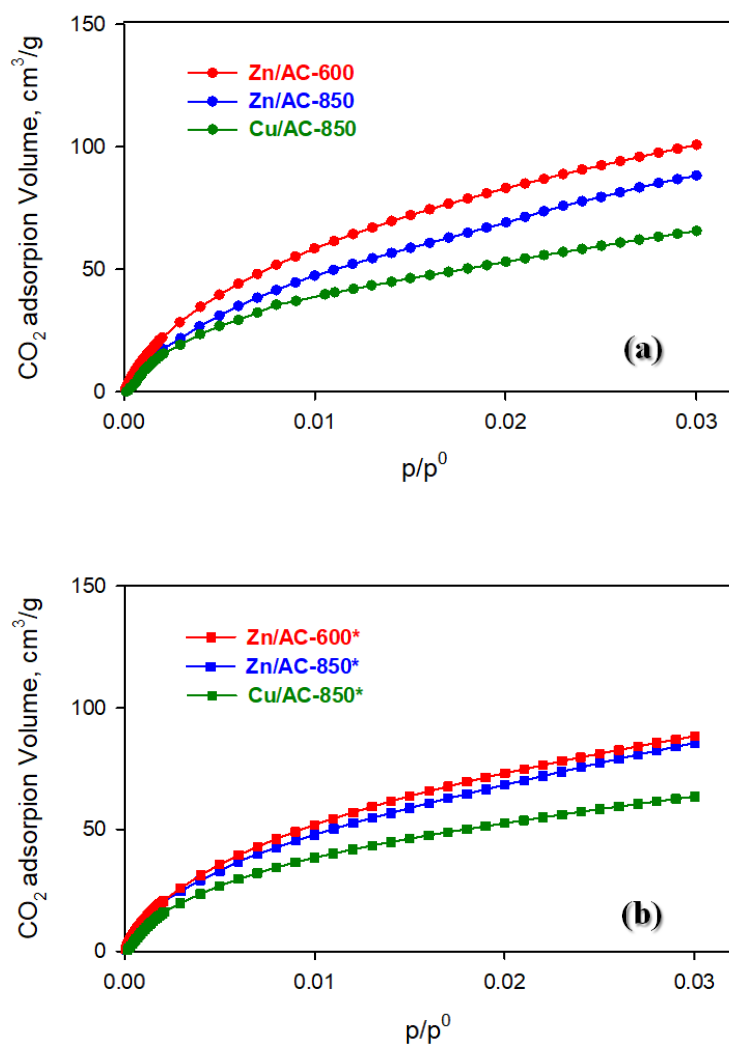


**Figure 3. 13** CO<sub>2</sub> physisorption isotherms at 273 K for activated carbons pyrolyzed under pure helium (a) and under O<sub>2</sub>/He mixture (b)

Even if limitations in the absolute pressure bearable by the adsorption instrument make it possible to reach only CO<sub>2</sub> relative pressures < 0.03, this kind of data can usually be modelled with the Dubinin–Radushkevich (DR) equation (Tascón et al., 2005; Echeverría et al., 2010). Indeed, the DR model allows the extrapolation (as model parameter) of the total micropore volume of the adsorbents, as reported in Table 3.4.

**Table 3. 4** Textural properties of activated carbons evaluated according to BET, DFT and DR models

<b>Sample</b>	<b>BET Area [m<sup>2</sup>/g, N<sub>2</sub> ads.]</b>	<b>DFT Area [m<sup>2</sup>/g, N<sub>2</sub> ads.]</b>	<b>Total Pore Volume [cm<sup>3</sup>/g, N<sub>2</sub> ads.]</b>	<b>Cumulative DFT Volume [cm<sup>3</sup>/g, N<sub>2</sub> ads.]</b>	<b>DR Micropore Volume [cm<sup>3</sup>/g, CO<sub>2</sub> ads.]</b>	<b>DR Effective Area [m<sup>2</sup>/g, CO<sub>2</sub> ads.]</b>	<b>Mean equivalent radius [Å, CO<sub>2</sub> ads.]</b>
<b>Zn/AC -600</b>	652	698	0.296	0.268	0.368	986	7.46
<b>Zn/AC -850</b>	622	664	0.266	0.254	0.343	904	7.60
<b>Zn/AC -600*</b>	618	639	0.267	0.243	0.313	843	7.41
<b>Zn/AC -850*</b>	475	493	0.219	0.209	0.296	798	7.41
<b>Cu/AC -850</b>	123	112	0.075	0.073	0.238	638	7.46
<b>Cu/AC -850*</b>	87	58	0.052	0.052	0.226	609	7.41

Table 3.4 shows the effective surface area (Medek, 1997), the values of the pore volume and the average equivalent radius calculated starting from the values of the micropore volume and those of the characteristic adsorption energy (another parameter of the model DR). Furthermore, the surface area values evaluated for the N<sub>2</sub> adsorption branch according to both the BET and DFT models (slit/cylindrical pores model) together with the total pore volume,

estimated at  $p/p^0 = 0.98$ , and the cumulative pore volume calculated by the DFT are reported.

Regardless of the pyrolysis conditions reported in Table 3.2, all Zn-containing samples show textural parameters that are higher than those reported for similar materials with the same Zn content (Cesano et al., 2008). As mentioned above, as these materials were first formulated in this work, no comparison with literature data can be given for Cu-containing samples.

The values of the BET and DFT surface area and the total pore volume are fairly close for each sample, while they are smaller than area and pore volume estimated using the DR model, although this model was only used to evaluate the volume of micropores. Jordà-Beneyto et al. (2007) also observed that pitch-based carbon fibers adsorbed  $\text{CO}_2$  at 273 K but did not adsorb  $\text{N}_2$  at 77 K, and this suggests that  $\text{CO}_2$  adsorption at 273 K makes it possible to also detect pores not accessible through  $\text{N}_2$  adsorption at 77 K. Moreover, this supports the choice of the DR model, which is a model suitable for these samples, which are basically microporous with an almost total absence of mesopores.

Nevertheless, although different models were used to estimate the textural parameters of the activated carbons, a unique trend was found for all samples. The results show that Zn-activated PFA derived carbons have a surface area definitively higher than Cu-activated samples, likely due to the quick exothermal polymerization occurring in a few seconds with formation of empty cavities generated by the fast water evaporation. Moreover, surface area increases with both lower pyrolysis temperature and absence of  $\text{O}_2$  traces in the pyrolysis gas. Therefore, the expected widening of porosity due to the limited burning of carbon did not occur or, if it did occur, it created macropores not evaluated by gas adsorption, likely at the expense of meso and micropores.

Cu-activated carbon shows a much lower surface area and pore volume evaluated according to BET or DFT model, further decreased when oxygen traces are present in the pyrolysis gas, compared to the corresponding Zn-activated samples. Nevertheless, the very large difference observed for both

surface area and pore volume using BET or DFT model using N<sub>2</sub> physisorption at 77 K between Zn- and Cu-activated carbons is strongly reduced when the surface area and volume are estimated according to the DR model applied to data from CO<sub>2</sub> physisorption at 273 K.

This is a reasonable indication of the great contribution of narrow micropores in these samples. Indeed, CO<sub>2</sub> is able to identify micropores that are completely undetectable using N<sub>2</sub> as adsorbent at 77 K, thus incorrectly identifying Cu-activated carbons as materials with a low porosity.

The latter result is in very good agreement with what was observed by Gargiulo et al. (2018), who found that the pore volume evaluated by N<sub>2</sub> adsorption for bio-chars was lower than that evaluated by CO<sub>2</sub> adsorption, suggesting that very narrow micro-pores were not accessible to N<sub>2</sub> due to diffusional limitation at 77 K. Furthermore, the value of mean average pore size of about 7.5 Å, estimated according to the DR model, confirms that the diameter of pores or of the pore neck is well below 50 Å, as reported by Morishige et al. (2006) and is also in agreement with results of Gargiulo et al. (2018), who found a pore size of around 6 Å for their ultra-microporous bio-chars.

In Figure 3.17, the effect of the pyrolysis gas composition on the PSD in the ultra microporosity region is reported. For Zn-based sorbents pyrolyzed up to 600 °C, the presence of O<sub>2</sub> in the feed gas stream does not bring many changes in the structure as previously seen for the micro-mesoporous region (Figure 3.15) where just an increase of the amount of pores of same size occurred. On the contrary, if the temperature increases to 850 °C, the introduction of oxygen leads to a growth of pores centered at 3.5 Å with the disappearance of those at 4.2 Å. Moreover, the structure of Zn/AC-600\* and Zn/AC-850\* is quite similar. For Cu-modified adsorbents, the trace of O<sub>2</sub> in the feed gas leads to the formation of smaller pores of about 3.5 Å.

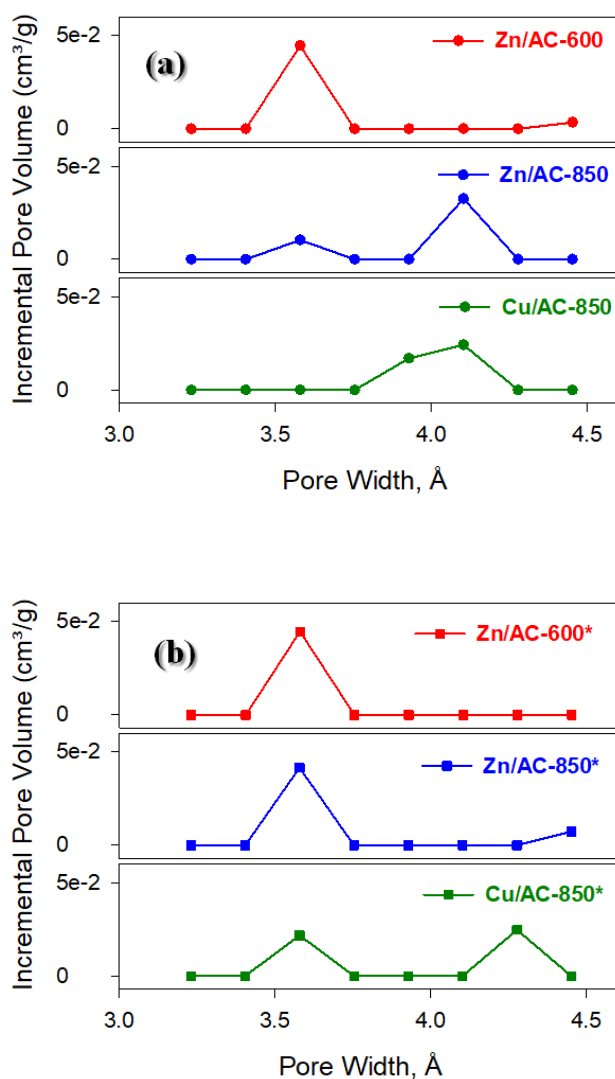


**Figure 3. 14.** The effect of the composition of the pyrolysis gas on the PSD in the ultra-micropore region

In conclusion, the porosimetric results suggest that the two different metal chloride activators lead to carbon materials with rather different textural properties: activated carbons with an almost total dominance of narrow micropores when copper is used as a Lewis acid activator, and activated carbons with meso and micropores in addition to micropores when zinc is used as a Lewis acid activator also leading to a higher surface area.

*List of figures*

<b>Figure 3. 1</b> Evolution of the carbon structure deriving from the polymerization of FA (Wang and Yao, 2006) .....	98
<b>Figure 3. 2</b> Condensation Reaction Schemes between the OH of the Methylol Group of One Furan Ring and (a) the 5-Position of Another Furan Ring and (b) the Methylol Group of Another Furan Ring (Bertarione et al., 2008) .....	100
<b>Figure 3. 3</b> Scheme of reactions responsible of progressive darker colour of the solutions in which acid-catalyzed polycondensation of the FA occurs (Bertarione et al. 2008) .....	101
<b>Figure 3. 4</b> Scheme of amorphous carbon formation (Bertarione et al. 2008)	102
<b>Figure 3. 5</b> Foamy PFA obtained from Zn-activated polymerization of FA at 80 °C .....	104
<b>Figure 3. 6</b> Weight loss as a function of temperature of Zn- and Cu-activated PFA under N <sub>2</sub> flow.....	107
<b>Figure 3. 7</b> SEM images of Zn/AC-850 (a) and Cu/AC-850 (b) .....	109
<b>Figure 3. 8</b> SEM images of Cu/AC-850 (a) and Cu/AC-850* (b) .....	111
<b>Figure 3. 9</b> XRD patterns of Zn/AC-850*Zn/AC-600*and Cu/AC-850*. In the lower graph patterns of reference Zn (PDF 1-1244), ZnO (PDF 36-1451, Cu (PDF 4-836), Cu <sub>2</sub> O (PDF 5-667) and CuO (PDF 45-937) are reported .....	113
<b>Figure 3. 10</b> Raman spectra of Zn/AC-850, Zn/AC-600 and Cu/AC-850.....	114
<b>Figure 3. 11</b> N <sub>2</sub> physisorption isotherms at 77 K for activated carbons pyrolyzed under pure helium (a) and under O <sub>2</sub> /He mixture (b) (closed symbols for adsorption branch, open symbols for desorption branch) .....	115
<b>Figure 3. 12.</b> The effect of the composition of the pyrolysis gas on the PSD in the micro/mesopores region.....	117

**Figure 3. 13** CO<sub>2</sub> physisorption isotherms at 273 K for activated carbons pyrolyzed under pure helium (a) and under O<sub>2</sub>/He mixture (b)..... 118

**Figure 3. 14.** The effect of the composition of the pyrolysis gas on the PSD in the ultra-micropore region ..... 122

*List of tables*

<b>Table 3. 1</b> Effect of temperature of polymerization condition on polymer formation.....	105
<b>Table 3. 2</b> List of ACs with the preparation conditions .....	108
<b>Table 3. 3</b> Cu and Zn content in AC samples determined by ICP-MS analysis and nominal content of metals evaluated on the basis of metal chlorides introduced in FA for polymerization .....	111
<b>Table 3. 4</b> Textural properties of activated carbons evaluated according to BET, DFT and DR models .....	119

## References

- Balsamo, M., Cimino, S., De Falco, G., Erto, A., Lisi, L. (2016). ZnO-CuO supported on activated carbon for H<sub>2</sub>S removal at room temperature. *Chemical Engineering Journal*, 304, 399-407.
- Bertarione, S., Bonino, F., Cesano, F., Damin, A., Scarano, D., Zecchina, A. (2008). Furfuryl alcohol polymerization in H-Y confined spaces: reaction mechanism and structure of carbocationic intermediates. *The Journal of Physical Chemistry B*, 112(9), 2580-2589.
- Bertarione, S., Bonino, F., Cesano, F., Jain, S., Zanetti, M., Scarano, D., Zecchina, A. (2009). Micro-FTIR and micro-Raman studies of a carbon film prepared from furfuryl alcohol polymerization. *The Journal of Physical Chemistry B*, 113(31), 10571-10574.
- Boutillara, Y., Tombeur, J. L., De Weireld, G., Lodewyckx, P. (2019). In-situ copper impregnation by chemical activation with CuCl<sub>2</sub> and its application to SO<sub>2</sub> and H<sub>2</sub>S capture by activated carbons. *Chemical Engineering Journal*, 372, 631-637.
- Cesano, F., Scarano, D., Bertarione, S., Bonino, F., Damin, A., Bordiga, S., Prestipino, C., Lamberti, C., Zecchina, A. (2008). Synthesis of ZnO-carbon composites and imprinted carbon by the pyrolysis of ZnCl<sub>2</sub>-catalyzed furfuryl alcohol polymers. *Journal of Photochemistry and Photobiology A: Chemistry*, 196(2-3), 143-153.
- Cesano, F., Rahman, M. M., Bertarione, S., Vitillo, J. G., Scarano, D., Zecchina, A. (2012). Preparation and adsorption properties of activated porous carbons obtained using volatile zinc templating phases. *Carbon*, 50(5), 2047-2051.
- Choura, M., Belgacem, N. M., Gandini, A. (1996). Acid-catalyzed polycondensation of furfuryl alcohol: mechanisms of chromophore

- formation and cross-linking. *Macromolecules*, 29(11), 3839-3850.
- Cimino, S., Lisi, L., De Falco, G., Montagnaro, F., Balsamo, M., Erto, A. (2018). Highlighting the effect of the support during H<sub>2</sub>S adsorption at low temperature over composite Zn-Cu sorbents. *Fuel*, 221, 374-379.
- Cimino, S., Lisi, L., Erto, A., Deorsola, F. A., de Falco, G., Montagnaro, F., Balsamo, M. (2020). Role of H<sub>2</sub>O and O<sub>2</sub> during the reactive adsorption of H<sub>2</sub>S on CuO-ZnO/activated carbon at low temperature. *Microporous and Mesoporous Materials*, 295, 109949.
- Cuesta, A., Dhamelincourt, P., Laureyns, J., Martinez-Alonso, A., Tascón, J. D. (1994). Raman microprobe studies on carbon materials. *Carbon*, 32(8), 1523-1532.
- Dunlop, A. P., Peters, F. N. (1953). *The furans*, Reinhold Pub. Corp., New York, 398-399.
- Echeverría, J. C., Estella, J., Barbería, V., Musgo, J., Garrido, J. J. (2010). Synthesis and characterization of ultramicroporous silica xerogels. *Journal of Non-Crystalline Solids*, 356(6-8), 378-382.
- de Falco, G., Montagnaro, F., Balsamo, M., Erto, A., Deorsola, F. A., Lisi, L., Cimino, S. (2018). Synergic effect of Zn and Cu oxides dispersed on activated carbon during reactive adsorption of H<sub>2</sub>S at room temperature. *Microporous and Mesoporous Materials*, 257, 135-146.
- Gargiulo, N., Imperatore, M., Aprea, P., Caputo, D. (2011). Synthesis and characterization of a microporous copper triazolate as a water vapor adsorbent. *Microporous and Mesoporous Materials*, 145(1-3), 74-79.
- Gargiulo, V., Gomis-Berenguer, A., Giudicianni, P., Ania, C. O., Ragucci, R., Alfè, M. (2018). Assessing the potential of biochars prepared by steam-assisted slow pyrolysis for CO<sub>2</sub> adsorption and separation. *Energy & Fuels*, 32(10), 10218-10227.

- Grabda, M., Oleszek-Kudlak, S., Shibata, E., Nakamura, T. (2011). Vaporization of zinc during thermal treatment of ZnO with tetrabromobisphenol A (TBBPA). *Journal of Hazardous Materials*, 187(1-3), 473-479.
- Marsh, H., & Reinoso, F. R. (2006). *Activated carbon*. Elsevier.
- Medek, J. (1977). Possibility of micropore analysis of coal and coke from the carbon dioxide isotherm. *Fuel*, 56(2), 131-133.
- Morishige, K., Tateishi, M., Hirose, F., Aramaki, K. (2006). Change in desorption mechanism from pore blocking to cavitation with temperature for nitrogen in ordered silica with cage-like pores. *Langmuir*, 22(22), 9220-9224.
- Jordá-Beneyto, M., Suárez-García, F., Lozano-Castelló, D., Cazorla-Amorós, D., Linares-Solano, A. (2007). Hydrogen storage on chemically activated carbons and carbon nanomaterials at high pressures. *Carbon*, 45(2), 293-303.
- Landers, J., Gor, G. Y., Neimark, A. V. (2013). Density functional theory methods for characterization of porous materials. *Colloids and Surfaces A: Physicochemical and Engineering Aspects*, 437, 3-32.
- Liu, B., Gu, J., Zhou, J. (2016). High surface area rice husk-based activated carbon prepared by chemical activation with ZnCl<sub>2</sub>-CuCl<sub>2</sub> composite activator. *Environmental Progress & Sustainable Energy*, 35(1), 133-140.
- Lozano-Castelló, D., Cazorla-Amorós, D., Linares-Solano, A. (2004). Usefulness of CO<sub>2</sub> adsorption at 273 K for the characterization of porous carbons. *Carbon*, 42(7), 1233-1242.
- Medek, J. (1977). Possibility of micropore analysis of coal and coke from the carbon dioxide isotherm. *Fuel*, 56(2), 131-133.
- Morishige, K., Tateishi, M., Hirose, F., Aramaki, K. (2006). Change in

desorption mechanism from pore blocking to cavitation with temperature for nitrogen in ordered silica with cage-like pores. *Langmuir*, 22(22), 9220-9224.

Rouquerol, J., Rouquerol, F., Llewellyn, P., Maurin, G., Sing, K. S. (2013). *Adsorption by powders and porous solids: principles, methodology and applications*. Academic press.

Tascón, J. M. D. (2005). Nanoporous carbon fibres by pyrolysis of nomex polyaramid fibres. *Journal of Thermal Analysis and Calorimetry*, 79(3), 529-532

Thommes, M. (2010). Physical adsorption characterization of nanoporous materials. *Chemie Ingenieur Technik*, 82(7), 1059-1073.

Wang, H., Yao, J. (2006). Use of poly (furfuryl alcohol) in the fabrication of nanostructured carbons and nanocomposites. *Industrial & engineering chemistry research*, 45(19), 6393-6404.

Wei, X., Li, H., Li, Q., Chen, S. (2009). Preparation of nano-ZnO supported on porous carbon and the growth mechanism. *Microporous and Mesoporous Materials*, 118(1-3), 307-313.

Zhang, W., Tian, Y., Liu, D. C., Wang, F., Yang, B., Xu, B. Q. (2020). Experimental study on the thermal volatilization and condensation of zinc at 10 Pa and 200 Pa. *Journal of Materials Research and Technology*.

#### 4. Conclusions

This PhD thesis focus on activated carbons as structured sorbents for purification of natural gas or biogas from H<sub>2</sub>S.

The use of activated carbons as sorbent materials for H<sub>2</sub>S and other impurities is well known as well as the effect of the addition of suitable metals to improve the performance. Nevertheless, the open literature is limited to the study of powder carbons because of the scarce adhesion properties of this material that hinders the production of structured sorbents, necessary to avoid high pressure drop in practical applications.

The work was divided into two main sections. The first one focused on commercial activated carbon monoliths which suffer from a low carbon load and the presence of a binder to improve the adhesion. The addition of two different metals (Cu and Mg) with significantly different properties, to improve performances, was investigated. The different paths of the reactive H<sub>2</sub>S adsorption activated by copper and magnesium was deeply analyzed in the presence of O<sub>2</sub> and H<sub>2</sub>O, simulating a real biogas. A large variety of characterization techniques was used to determine the nature of the reactive adsorption of hydrogen sulphide.

The mechanism occurring on Cu- and Mg-promoted sorbents was provided and the evolution of sulphur species, occurring for Cu-promoted sorbents, also after the end of the adsorption test, was studied. Finally, the thermal regeneration of the metal promoted monoliths was investigated giving conditions to completely restore the capture capability of the materials which can be proposed as highly effective sorbents for purification from H<sub>2</sub>S which can be reversibly re-used after many capture cycles.

The second section of the thesis focused on the development of single step technique to produce three dimensional foamy activated carbons to be directly used as structured sorbents avoiding the complex multi-step procedures proposed up to now, involving a template synthesis using a ceramic replica

which is afterwards dissolved. The new procedure also allowed the simultaneous introduction of an active metal cation (Cu or Zn) which played the double role of activating the polymerization of furfuryl alcohol (the precursor of the activated carbon) and enhancing the H<sub>2</sub>S capture capacity of the produced activated carbon.

All parameters involved in the synthesis were explored providing indications about the properties which can be obtained. The study demonstrates that a three dimensional activated carbon with tailored features (type of porosity, metal load etc.) can be produced by suitably tuning the operating parameters, thus providing sorbents for the adsorption of different molecules. A large variety of characterization techniques, specially a deep porosimetric analysis, was used to define the unusual textural properties of these materials.

## Appendix

### Attended Courses/Summerschool

- Green Economy – prof. Zollo and prof. Iandoli
- Vibrational Spectroscopy – dr. Pellegrino Musto
- Catalysis Summerschool “ELITECAT” - Université Claude Bernard Lyon 1 – 1-5° July 2019

### Publications

- Cepollaro, E. M., Caputo, D., Cimino, S., Gargiulo, N., Lisi, L. (2020). Synthesis and Characterization of Activated Carbon Foam from Polymerization of Furfuryl Alcohol Activated by Zinc and Copper Chlorides. *C - Journal of Carbon Research*, 6(3), 45.

### Congress participations:

- Cimino S., Cepollaro E.M., Gargiulo N., Caputo D., Lisi L. *Role of H<sub>2</sub>O and O<sub>2</sub> during the reactive adsorption of H<sub>2</sub>S on MgO/AC at low temperature.*

Poster presented at AIZ 2019 Congress (XVI National Congress of Zeolites Science and Technology) joint with the 8th Czech-Italian-Spanish Conference on Molecular Sieves and Catalysis, and with the GIC 2019 Congress (XXI National Congress of Catalysis) – 11-14th June, 2019 in Amantea (CS), Italy.

- Cepollaro E. M., Caputo D., Cimino S., Gargiulo N., L. Lisi. *Cu- and Mg-modified activated carbon monoliths for H<sub>2</sub>S removal from biogas.*

Full paper accepted for Conference CIS-2021 Young Researchers (6-8th September 2021).